Modelling Pattern Formation in Reaction-Diffusion Systems

**An Investigation of
Turing's Theory of Morphogenesis
with special reference to
highly non-linear and bistable models.**

Robin Engelhardt

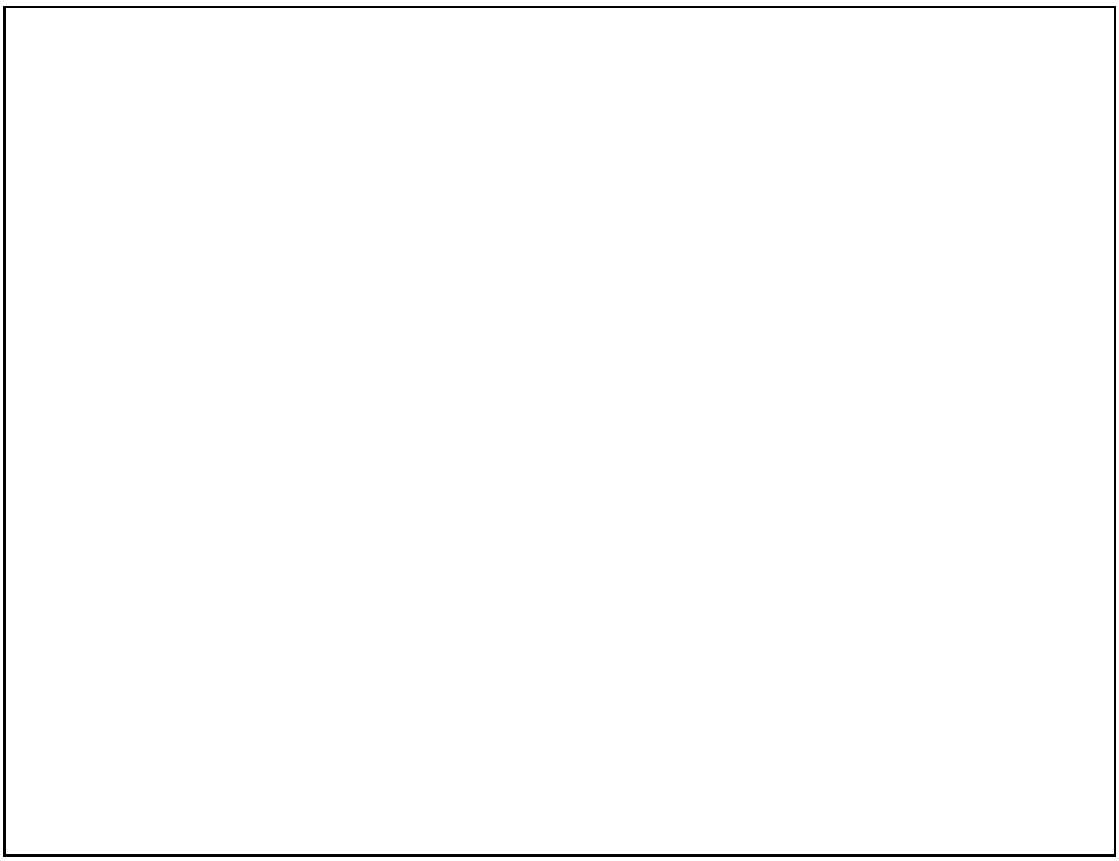

**Department of Chemistry
Laboratory III
H.C.Ørsted Institute
University of Copenhagen
Denmark**

June 1994

Contents

Chapter 1

Introduction

It was indeed a scientific revolution when Darwin proposed his theory of evolution. Today, the branching tree of life, based on simple principles as natural selection, adaptation and mutations, has become an inevitable acknowledgement for the natural sciences. The old vitalistic views for the creation of man have been replaced by the somewhat offending theory of heredity and genetics. But the darwinian theory is missing something. Darwin is mainly concerned with organisms which already exist, and not how they are created from their initially inorganic surroundings. It might be right that the most complex organisms which exist today are developed from very simple organisms long time ago, but how are these simple organisms created in the first place, and how is it possible to create such complex structures at all, if not because of some (transcendent) creational power? Then, the normal scientific approach conjectures: There must be some other mechanisms responsable for the emergence of spontaneous order within the system itself.

It is in this sense, this spirit, and with these motivations, the thesis presented here must be understood. Here we try to introduce the maybe even more offending theory of *morphogenesis* as an *self-organizing* phenomenon based on simple physical principles. The widely accepted founder of this theory was Alan Turing [1] who also said that his own motivations for the theory was the "defeat of the argument from design" [2]. The unification of of the theory of self- organizing dissipative structures and developmental biology, enables us to give some good suggestions for the occurrence of spatial order in inorganic systems and also for the fundamental processes of pattern and form in living organisms.

It is important to emphasize the word *introduce*, because the small masters thesis presented here can in no way be matched with the broader ideas and conceptual challenges within the field of developmental biology nor nonlinear dynamics. We will be restricted to a closer investigation of Turing structures, their modelling, their qualitative dynamics, parametric dependencies, and the connected pattern selection problems, all within the necessary mathematical framework.

From a biologist point of view, it is not enough to account for the spontaneous emergence of patterns in cells. There are some other concepts needed for the effectuation of differential processes in the cell. These concepts are mainly the idea of *positional information* and of *prepatterns* which can leed to spatially ordered arrangements in the cell. The Turing models are widely used to explain biological morphogenesis, cytokinesis and cell differentiation [3], [4]. The emergence of a concentration gradient of a chemical can be used as positional information for activation of specific genes in a cell, or as morphogenetic gradients for embryonic organization. In this context the word 'morphogen' is used for such a chemical because it effects morphogenesis. For a further discussion of the biological interpretations of Turing structures, the reader is referred to for instance [5, 6, 7, 8, 9].

From a chemist or physicist point of view, the theory of Turing structures is only one among many pattern forming mechanisms [11, 10], and this might give a clue to the fact that natural phenomena are highly complex with many competing mechanisms and principles. In this way the formulation and understanding of even only a very small part of this whole, requires enormous simplification and reductions, which again gives natural limitations for the interpretational power of our approach.

This thesis is mainly concerned with the modelling of Turing structures, and it is therefore important to think about the necessary requirement towards the model. Nature answers in very different ways, depending on the question we pose. In this sense, the modelling procedure is not objective but involves a series of decisions with respect to system definition, level of aggregation and evaluation of conflicting experimental data. The model is not true or false but useful to the extent that it helps further our understanding. Some of the principal requirements to our model are: i) that it represents a consistent hypothesis, ii) reproduces typical behaviour and, iii) is reasonable in the limits [12].

Therefore, one should not be surprised, when we make models of models of models in order to understand some specific phenomena (this is actually done in the 8'th chapter). The model is a generalization of existing experimental results, and it represents a strong simplification of the biological relations. Therefore, the model cannot be expected to reproduce specific data very accurately. Rather, it should reproduce general behaviour characteristics such as stability, amplitudes, phase relations and waveforms. And if it is a good model, it then should be able to predict system behaviour under conditions never previously experienced.

All this are rather general statements which regrettably only are captured very poorly in this thesis. Instead, we try, in the first three chapters, to give a general introduction of the now canonized theory of Turing, and in the last three chapters we present some new developments in the field of Turing structures. More explicit,

chapter 2 deals with the necessary chemical and biochemical background for the further formulation of our models. Chapter 3 introduces very shortly the necessary mathematical tools for the later analysis of the reaction-diffusion models. Chapter 4 goes through the Turing mechanism more explicitely, and some of the important results and equations are derived.

First in chapter 5 we start to look more closely on the subject with respect to the initial emergence of the spatial structures, exemplified by two different models. Chapter 6 introduces some new results for highly nonlinear systems as they are found in enzyme regulating processes.

Chapter 7 turns the subject to bistable chemical systems, where some new *secondary* Turing bifurcations are presented. Finally, chapter 8 goes, by an explicit example, through the history of a chemical reaction which recently has been shown to exhibit spatial structures, and the following modelling of these observed phenomena by a sequential process of simplifications, in order to capture the essence of the mechanisms responsible for the experimental obtained patterns.

Chapter 2

Reaction Kinetics

2.1 General Terminology

Normally many elementary reaction steps are needed to define a chemical or biochemical reaction. To describe the total dynamics of the net reaction, that is the time development of the species involved in the reaction, one has to build a realistic mechanism of elementary reactions, which seems plausible for the process under consideration. This first model still might be too complicated for our available tools for mathematical analysis, and then one has to find a simpler "model of the model" in order to reveal the qualitative features involved in the dynamics. This is always the first step in the understanding of complex chemical and biochemical behaviour, and we find that they mirror a large number of real reactions which again is helpful and essential when constructing models for more specific situations.

When we try to formulate chemical or biochemical elementary reactions within a mathematical framework, we express the stoichiometry between reactants and products by a *balanced reaction equation*:

$$aA + bB + ... \underset{k_{-1}}{\overset{k_1}{\rightleftharpoons}} ... + xX + yY \tag{2.1}$$

where a,b,x and y are the stoichiometric coefficients for the species A,B,X and Y. The arrows indicate the direction of an elementary reaction, and the k's are constant parameters associated with the rates of reaction defined below.

The time development of the extent of reaction is the *rate of conversion* which for a general rate equation is defined as:

$$\frac{d\xi}{dt} = -\frac{1}{a}\frac{dn_A}{dt} = -\frac{1}{b}\frac{dn_B}{dt} = \frac{1}{x}\frac{dn_X}{dt} = \frac{1}{y}\frac{dn_Y}{dt} \tag{2.2}$$

where n_A is the amount of substance of species A in units of moles. When reaction takes place within a constant volume, it is possible to rewrite this in terms of

concentrations and *reaction rates* v:

$$v = \frac{1}{V}\frac{d\xi}{dt} = -\frac{1}{aV}\frac{dn_a}{dt} = -\frac{1}{a}\frac{d[A]}{dt} \tag{2.3}$$

Here V is the volume of the reaction vessel and [ ] denotes concentration.

The *Law of Mass Action* says that the rate of a elementary reaction is proportional to the product of the concentrations of the reactants. In this way eq.(2.1) leads to one equation for each reactant an hence a system of reaction equations:

$$\begin{aligned} \frac{d[A]}{dt} &= a(k_{-1}[X]^x[Y]^y - k_1[A]^a[B]^b) \\ &\vdots \\ \frac{d[Y]}{dt} &= y(k_1[A]^a[B]^b - k_{-1}[X]^x[Y]^y) \end{aligned} \tag{2.4}$$

The *order* with respect to some component is defined as the power to which the concentration of that component is raised in the rate law. For example, the order of A in eq.(2.5) is a and the order of B is b. However, the overall order is the sum of the orders of all the components in the reaction. Generally the overall order of an elementary chemical reaction is within the range of $0-3$ simply because it is not very probable that too many reacting molecules hit each other at the same time. But when looking at overall biochemical reactions in living organisms, it is a well established fact [14] that the net order is highly increased by active gene control mechanisms resulting in highly nonlinear off-on control of the dynamics in a cell. This aspect will be treated in more detail in chapter 6.

Rate laws are experimentally determined, and thus one has to find a realistic mechanism for the subsequent elementary reaction which are compatible with the empirical rate law.

Thus, in conclusion, the dynamics of a reaction simply is expressed by an ordinary differential equation (ODE):

$$\dot{\mathbf{c}} = \mathbf{f}(\mathbf{c}) \tag{2.5}$$

where $\mathbf{c}$ is a vector representing the concentrations of the n dynamical species and $\mathbf{f}(\mathbf{c})$ a vector function containing the n rate law expressions for each species. By defining some additional initial conditions and conservation laws (when dealing with for instance an enzyme as a catalyst, see the next section) it is normally possible to reduce the number of dynamic variables, thus making the mathematical formulation and analysis of the resulting equation system more tractable.

2.2 Enzyme Kinetics

One of the most basic enzyme reactions is described by the *Michaelis-Menten mechanism*. It consists of the following elementary reaction steps:

$$E + S \underset{k_{-1}}{\overset{k_1}{\rightleftharpoons}} ES, \qquad\qquad ES \xrightarrow{k_2} P + E \tag{2.6}$$

where one substrate S reacts with an enzyme E forming a complex ES through a reversible process, which then by an irreversible reaction is converted into a product P plus the enzyme. The law of mass action applied to (2.6) results in four reaction equations:

$$\begin{aligned} \frac{d[S]}{dt} &= -k_1[E][S] + k_{-1}[ES], \\ \frac{d[E]}{dt} &= -k_1[E][S] + (k_{-1} + k_2)[ES] \\ \frac{d[ES]}{dt} &= k_1[E][S] - (k_{-1} + k_2)[ES] \\ \frac{d[P]}{dt} &= k_2[ES] \end{aligned} \tag{2.7}$$

We can introduce a conservation law by realizing that the addition of equation two and three in (2.7) results in a constant concentration of the free enzyme E and the bounded ES, that is:

$$\frac{d[E]}{dt} + \frac{d[ES]}{dt} = 0 \qquad \Rightarrow \qquad [E] + [ES] = e_0 \tag{2.8}$$

When substituting this into the rate equation for the complex ES, we obtain:

$$\frac{d[ES]}{dt} = k_1 e_0[S] - [ES](k_1[S] + k_{-1} + k_2) \tag{2.9}$$

Now, what is of biological interest is the overall *rate of reaction*, that is the formation of the product P. In experimental situations it is relevant to expect the enzymatic reaction for the complex ES to be very fast, and in this sense the rate equation is at a *steady state*, $\frac{d[ES]}{dt} \approx 0$, for all observable time scales. This is called the *pseudo-steady state hypothesis*.

It is possible to state this hypothesis in a more general way. When confronted with a large system which results in the dimensionless equations (for the explanation of non-dimensionalization of reaction equations see Appendix B)

$$\begin{aligned} \frac{du_i}{dt} &= f_i(u_1, ..., u_n), \qquad i = 1, 2 \\ \epsilon_i \frac{du_i}{dt} &= f_i(u_1, ..., u_n), \qquad i = 3, ..., n \\ 0 &< \epsilon_i \ll 1, \qquad i = 3, ..., n \end{aligned} \tag{2.10}$$

we can for all practical purposes assume a pseudo steady state for the equations $i = 3, ..., n$ if ϵ_i is sufficient small.

When dealing with biological processes where enzymes play the role of catalysts, or chemical reactions where some intermediate reaction steps are very fast, the pseudo-steady state hypothesis gives a good justification for reducing the order of species considerably, since it is the long time behaviour of mechanisms which dominates biological development.

In the case of (2.11) the number of dynamical species is reduced to two. This is a quite general possibility and thus explains the dominant role of two-species models in the literature when concerned with chemical or biological modelling. They are minimal models for a qualitative understanding of many different phenomena such as time oscillations, bifurcations and so on. In chapter 7.3 we have anyway tried to include a third equation for the general analysis of linear stability in Turing models in the hope of finding some unknown dynamic features under specific conditions which seem lost in the two-component description.

Returning to the Michaelis-Menten mechanism, we can obtain the rate equation for the production of P by inserting in the last equation in (2.7)

$$v = \frac{d[P]}{dt} = -\frac{d[S]}{dt} = \frac{k_2 e_0 [S]}{[S] + K_m} \tag{2.11}$$

where K_m is the *Michaelis-Menten constant* $K_m = \frac{k_{-1}+k_2}{k_1}$. The maximum rate of production is $Q = k_2 e_0$ and the reaction for k_2 is called the *rate limiting step*. Fig. 2.1 shows the typical Michaelis-Menten rate of uptake of product P at different initial concentrations of substrate S.

2.3 Cooperative Behaviour

When an enzyme has more than one binding site to which a substrate molecule can be bounded it is described as *cooperative*. When the binding of one molecule at one site on the enzyme can affect the activity of binding other substrate molecules on other sites (by for instance a spatial reorganization of the enzyme), we call this an *allosteric effect* and the enzyme an *allosteric enzyme*. If the substrate increases the binding activity it is called an *activator*; if it decreases an *inhibitor*. These are

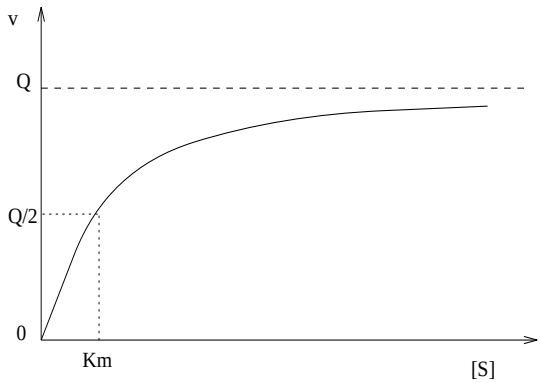

Figure 2.1: Schematical plot of the velocity of appearance of P at different initial concentrations of S. $Q = k_2 e_0$ is the maximum rate velocity. For large S the rate of production saturates.

very common phenomena in biology and suggest that there are many sophisticated control mechanisms working at the protein and genetic level. We will now show that the enzymatic control of the reaction rate can significantly be increased when the number of binding sites on an enzyme is increased.

In the simplest case we can look at an enzyme with 2 binding sites. Then the reaction mechanism looks like this:

$$\begin{aligned} \mathrm{S} + \mathrm{E} &\underset{k_{-1}}{\overset{k_1}{\rightleftharpoons}} \mathrm{ES} \xrightarrow{k_2} \mathrm{E} + \mathrm{P} \\ \mathrm{S} + \mathrm{ES} &\underset{k_{-3}}{\overset{k_3}{\rightleftharpoons}} \mathrm{ESS} \xrightarrow{k_4} \mathrm{ES} + \mathrm{P} \end{aligned} \tag{2.12}$$

When performing the same analysis as before and using the steady state approximation for both the concentrations of the complexes ES and ESS (see [4], p.119), we obtain the overall reaction rate

$$v = \frac{e_0[S](k_2 K_m^{'} + k_4[S])}{K_m K_m^{'} + K_m^{'}[S] + [S]^2} \tag{2.13}$$

Fig. (2.2) shows the difference. When $k_2 = 0$, that is, the substrate S activates further binding instead of converting into the product plus the free enzyme, the mechanism shows better "off-on" control due to the inflection of the curve. The Michaelis-Menten form for only one binding site is also shown in comparison.

Substrate inhibition occurs when $k_4 = 0$, that is, when the substrate S inhibits the complex ES to dissociate to the free enzyme E and the product P. This is shown in fig. (2.3).

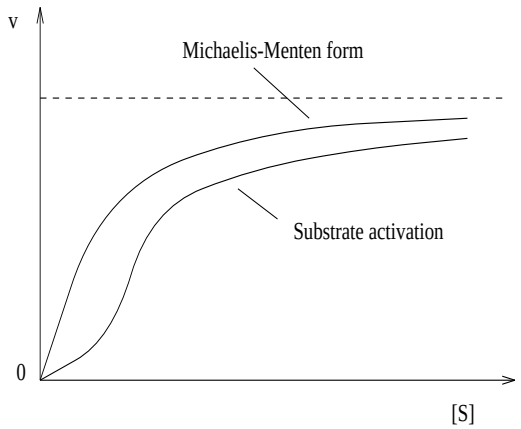

Figure 2.2: Velocity of appearance of P at different initial concentrations of S for one and two binding sites. For $k_2 = 0$ we have *substrate activation*.

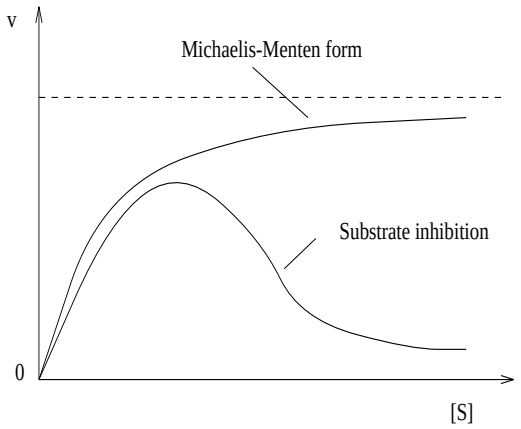

Figure 2.3: For $k_4 = 0$ we have *substrate inhibition*. Only for some definite values of [S] we have a large production of the product P.

When there is strong positive cooperation the assumption is that the underlying reaction velocity is

$$v = \frac{Q[S]^\gamma}{K_m + [S]^\gamma} \tag{2.14}$$

where $\gamma > 1$ is the *Hill coefficient*. For growing γ the system gradually approaches off-on control of the reaction rate with sensitive dependence on the concentration of $[S]$. In genetic control systems or in other enzyme regulation processes in the cytoplasm, cell membrane, etc. it is common to have large Hill numbers, often apparently in excess of 8. In respect to facilitating pattern formation the properties of large Hill constants will be investigated in chapter 6.

2.4 Autocatalysis

One of the most important concepts in the field of mathematical biology is the notion of *autocatalysis*. This is achieved when a chemical is involved in its own production by a feedback mechanism. Most commonly autocatalysis is achieved by a mechanism of double inhibition: Imagine a substrate S which by a normal enzyme process is converted to a product P. But in the solution there is a inhibitor I which inhibits this conversion. Anyway, P might be able to combine with I to form an inert complex IP. So, P inhibits I which inhibits S, and in this way P becomes a self-activator by breaking down the blockade of its own production.

Only due to some kind of autocatalytic process it is possible to incorporate

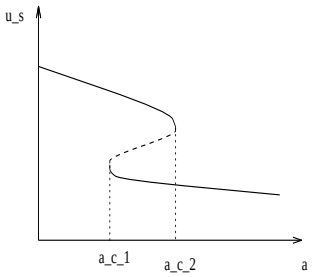

Figure 2.4: Bistable system with a hysteresis loop. By changing a through a_{c_1} and a_{c_2} makes u_s jump between the two stable branches.

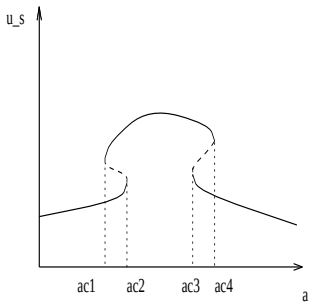

Figure 2.5: A mushroom has a more complicated solution. Here there are two hysteresis loops: one for a_{c_1} and a_{c_2} and another for a_{c_3} and a_{c_4}.

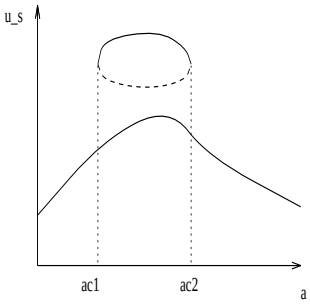

Figure 2.6: An isola has no hysteresis loop, but a finite amplitude perturbation of the steady state u_s makes it possible to hit the isolated stable branch.

one-component nonlinearities in the reaction equations, which enables the system to exhibit complex time-space behaviour. As an example, the corresponding differential equation of the most simple autocatalytic reaction

$$A + X \underset{k_{-1}}{\overset{k_1}{\rightleftharpoons}} 2X \tag{2.15}$$

is the chemical equivalent to the logistic map which can show time oscillations, period doubling bifurcations etc.. Spatial pattern formation (when diffusion is included) is only possible by autocatalysis because of the nonlinearities triggering self-enhancing growth.

2.5 Multiple Steady State Systems

In a system of linear differential equations it is possible only to have one asymptotic stable steady state. The introduction of nonlinearity gives rise to more and more complex solutions as the appearance of multiple steady states. Fig (2.4) shows a typical bistable system. An appropriate control parameter a in the system can pass through a bifurcation value a_c making a transitions from one steady state to three steady states, due to a saddle-node bifurcation (see next chapter). Linear stability analysis tells us that the middle branch (dotted line) is unstable while the other two are linear stable. Then, the transition from the exterior to the interior of the bistable area through a_{c_1} and a_{c_2} and back again results in a so-called *hysteresis loop*: an abrupt change in stability of the steady state u_s by changing parameter a.

It is also possible to have other scenarios like *mushrooms* (fig. (2.5) or *isolas*, fig.(2.6). These complex solution behaviours are not only mathematical constructions, but have been observed in several practical situations including chemical reactions like the iodate-arsenous acid reaction [13].

In the simplified models we can qualitatively observe many of these phenomena and thereby obtain a partial understanding of what mechanism is responsible for a given solution behaviour. So, in modelling biological or chemical processes we are able to incorporate such known qualitative behaviours as shown in the previous sections, and thereby unravel the basic underlying mechanisms responsible for many problems in the field of nonlinear dynamics.

Our concern is the modelling of pattern formation in the various kinds of reaction systems shown here. In the later chapters we will especially investigate the effect of high Hill coefficients on the control and size regulating properties of the model; and the possibility of spatial symmetry breaking instabilities occurring on the unstable branch of bistable systems, enabling the possible formation of other unknown structures.

Chapter 3

Mathematical Tools

In this chapter we shortly introduce some of the mathematical tools necessary for the understanding of the more specific mathematical problems in the later chapters. The theory of morphogenesis as proposed by Turing is deeply connected to the broader scientific discipline of nonlinear dynamics, and here one mainly is working with differential equations of different classes. The theory of bifurcations and stability are also some aspects which needs to be mentioned. All this will be rather short and cursory, and for more detailed introductions the reader is referred to the books of *Guckenheimer and Holmes* [15], *Hirsch and Smale* [16] or *Prigogine and Nicolis* [17].

3.1 Linear Differential Equations

A linear differential equation is in general written as

$$\frac{d\mathbf{c}}{dt} = \dot{\mathbf{c}} = \mathbf{A}\mathbf{c}, \qquad \mathbf{c} \in \mathbf{R}^n \tag{3.1}$$

where $\mathbf{A}$ is a n x n matrix with constant coefficients. A solution of (3.1) means a vector $\mathbf{c}(\mathbf{c_o}, t)$ which depends on the initial condition $\mathbf{c}(0) = \mathbf{c_o}$. A general solution of (3.1) is

$$\mathbf{c}(t) = e^{\mathbf{A}t}\mathbf{c_o} \tag{3.2}$$

The system (3.1) has n eigenvalues $\lambda_1, ..., \lambda_n$ connected to $\mathbf{A}$, and n eigenvectors $e_1, ..., e_n$, which either can be real or complex. More specific, a general solution to (3.1) can then be obtained by a linear superposition of the linear independent solutions determined by an exponential motion along the real eigenvectors and a spiralling motion in a plane spanned by the real and imaginary parts of the complex eigenvectors [16].

The stability properties of the system are then defined by the signs of the real parts of the eigenvalues.

(*i*) if all real parts are negative, then the solution is asymptotically stable, and the motion will converge towards the origin.

(*ii*) if at least one real part is positive, then the solution is unstable, and will diverge.

(*iii*) if the eigenvalues are distinct and if their real part is zero, then the solution is marginally stable (not asymptotic stable).

(3.3)

3.2 Nonlinear Differential Equations

In the proceeding chapter we saw that the dynamics of a chemical reaction could be expressed by an ODE. As soon as the rate law for a component exceeds first order kinetics, the vector function $\mathbf{f}(\mathbf{c})$ consists of nonlinear terms. In the case of chemical kinetics we therefore typically need to investigate a first order autonomous nonlinear ODE's defined as

$$\dot{\mathbf{c}} = \mathbf{f}(\mathbf{c}), \qquad \mathbf{c} \in \mathbf{R}^n \tag{3.4}$$

where $\mathbf{f}(\mathbf{c})$ normally are nonlinear functions of polynomial type.

In the case of nonlinear differential equations one has only very general statements for their solution behaviour. The best way to start is the determination of possible *fixed points*, which are stationary solutions to (3.4), that is

$$\mathbf{f}(\mathbf{c}) = 0 \tag{3.5}$$

Even this can sometimes be a complicated task, but when done so, we can use the principle of *linearized stability* which enables us to characterize the behaviour of the system near this point. The time evolution of a small perturbation ξ around a fixed point $\mathbf{c_o}$ is

$$\begin{aligned} \xi &= \mathbf{c} - \mathbf{c_o} \\ \dot{\xi} &= \dot{\mathbf{c}} \\ &= \mathbf{f}(\mathbf{c}) \\ &\simeq \mathbf{f}(\mathbf{c}) + \mathbf{J}(\mathbf{c} - \mathbf{c_o}) \\ &= \mathbf{J}\xi \end{aligned} \tag{3.6}$$

where a first order Taylor expansion of $\mathbf{f}(\mathbf{c})$ is used to obtain a linear approximation of $\dot{\xi}$. The matrix $\mathbf{J}$ is equal to

$$J_{ij} = \frac{\partial f_i}{\partial c_j} \tag{3.7}$$

and is called *the Jacobian matrix*. This determines the local behaviour of the solutions around the origin if

$$\xi = \left| \frac{c_i}{c_{oi}} \right| \ll 1 \tag{3.8}$$

The enormous advantage of the linearized system is that we know its solution, given by (3.2), and that this local behaviour turns out also to provide extremely significant information about the behaviour of the complete nonlinear system, since the linearized case is tangent to the nonlinear case (Center Manifold Theorem, see [15] p.13). The stability properties of the linearized behaviour around the fixed points are analogue to the previous section, and for the cases (i) and (ii) there exists a topological equivalence between the linearized system (3.6) and the full nonlinear system (3.4). That is, if $\mathbf{J}$ has no eigenvalues with zero real parts, the stability is determined by the linearization. If any of the eigenvalues has zero real part, then the stability cannot be determined by the linearization. This critical point (referred to as marginally stable or Lyapunov stable) is structurally unstable, since its properties are likely to change qualitatively on the action of an arbitrarily small disturbance. Necessarily, this is a branching point, or *point of bifurcation*.

3.3 Bifurcation Theory

We can write our nonlinear ODE in a way that it depends on a parameter μ

$$\dot{\mathbf{c}} = \mathbf{f}(\mathbf{c}, \mu), \qquad \mu \in \mathbf{R} \tag{3.9}$$

One can say that as long as all eigenvalues λ_i of $\mathbf{J}$ satisfy $Re\ \lambda_i \neq 0$, the fixed point $\mathbf{c_o}$ will be a smooth function of μ (Implicit Function Theorem). But as soon as at least one eigenvalue λ_i satisfies $Re\ \lambda_i = 0$ for some value of μ_c, we have the above mentioned point of bifurcation or singular point. In addition, the exchange of stability of $\mathbf{c_o}$ requires the criteria

$$\left. \frac{d\lambda_i}{d\mu} \right|_{\mu_c} \neq 0 \tag{3.10}$$

in order to be effectuated qualitatively in the dynamics. It is important to note that the very occurrence of bifurcations needs nonlinear kinetics, otherwise the equations would admit an unique solution.

We will concentrate on two important kinds of bifurcations: the *saddle-node bifurcation* and the *Hopf-bifurcation*, since these are two bifurcations which actually occur in physical systems.

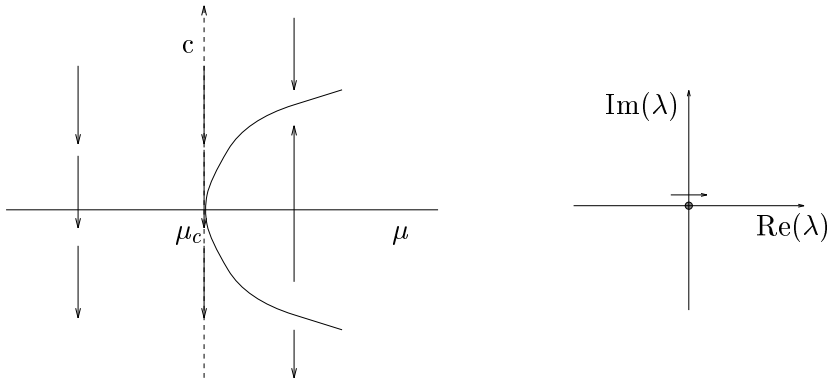

Figure 3.1: The saddle-node bifurcation. the indicated arrows in the left figure show the direction of the trajectories towards the stable branches.

3.3.1 Saddle-node Bifurcation

By use of the *Center Manifold Theorem* one can reduce the study of this kind of bifurcation problem to one in which **c** is only one-dimensional. The saddle-node bifurcation occurs when the following criteria are fulfilled:

$i)$ $\quad f(c_o, \mu_c) = 0$

$ii)$ $\quad$ A simple eigenvalue of the Jacobian with no imaginary part must satisfy$\lambda_i = 0$

$iii)$ $\quad \left.\dfrac{d\lambda_i}{d\mu}\right|_{\mu_c} \neq 0$

$iv)$ $\quad \left.\dfrac{\partial f_{\mu_o}}{\partial \mu}\right|_{c_o} \neq 0 \quad$ and $\quad \left.\dfrac{\partial^2 f_{\mu_o}}{dc^2}\right|_{c_o} \neq 0$

where the conditions (iv) are transversality conditions ruling out the possibility of a *transcritical-* or a *pitchfork bifurcation* The importance of the saddle-node bifurcation stems from the fact that all bifurcations of one-parameter families at an equilibrium with a zero eigenvalue can be perturbed to a saddle-node bifurcation (see [15] p.147). It is this property which makes the saddle-node bifurcation *a structurally stable* bifurcation in contrast to the transcritical- or pitchfork bifurcations which are structurally unstable. In fig.3.1 the saddle-node bifurcation is shown together with the conditions for the eigenvalues. There are two new states emerging at μ_c, of which the lower one is unstable.

For a homogeneous systems involving two variables the eigenvalues are given by

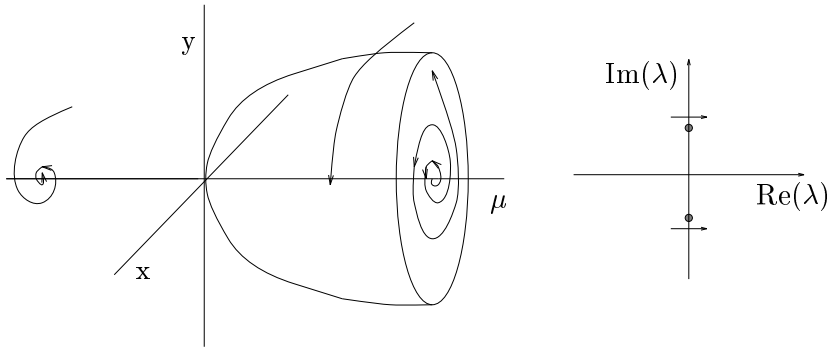

Figure 3.2: A supercritical Hopf bifurcation.

$$\lambda_{\pm} = \frac{Tr(\mathbf{J}) \pm \sqrt{Tr(\mathbf{J})^2 - 4Det(\mathbf{J})}}{2} \tag{3.11}$$

where $Tr\mathbf{J}$ and $Det\mathbf{J}$ is the trace and determinant of the Jacobian matrix evaluated at the fixed point (steady state). Thus, a saddle-node bifurcation requires that the determinant of the corresponding Jacobian matrix evaluated at the fixed point is zero.

3.3.2 Hopf Bifurcation

The Hopf bifurcation occurs when a fixed point exchanges its stability by the generation of a periodic limit cycle. The necessary criteria are

$$\begin{aligned}
&i) && \mathbf{f}(\mathbf{c_o}, \mu_c) = 0 \\
&ii) && \text{The Jacobian has a simple pair of pure imaginary eigenvalues} \\
& && \text{and no other eigenvalues with zero real part} \\
&iii) && \left.\frac{dRe\ \lambda_i}{d\mu}\right|_{\mu_c} \neq 0
\end{aligned} \tag{3.12}$$

In a homogeneous system involving two variables, the condition for a Hopf bifurcation point is given by $Tr(\mathbf{J}_o) = 0$.

A general classification of the singular points in phase space in a general two variable systems can be performed, see for instance [4]. For systems with more than two variables one needs to use the Routh-Hurwitz criteria (see appendix B) or other related criteria in order to find the conditions for stability.

3.4 Partial Differential Equations

When we want to outline a mechanism for spontaneous pattern formation we base our investigations on the phenomenon of bifurcations and branchings of solutions of nonlinear partial differential equations of the reaction diffusion type

$$\frac{\partial \mathbf{c}}{\partial t} = \mathbf{f}(\mathbf{c}) + \mathbf{D}\nabla^2\mathbf{c} \tag{3.13}$$

where the nonlinear function $\mathbf{f}(\mathbf{c})$ is the overall rate of production of $\mathbf{c}$ from the chemical reactions, and the second term is Fickian diffusion. Mathematically, this turns (3.13) into a system of nonlinear partial differential equations (PDE's).

The extraordinary richness in the behaviour of the solutions of these systems is accomplished by the fact that even a partial classification of the solutions is an extremely arduous task, primarily because of the nonlinear character of the rate functions.

3.4.1 Theory of Catastrophes

Anyhow, in 1972 Réne Thom developed a detailed theory in order to classify the phenomenon of pattern formation, based on an analysis of the structural stability of ODE's. These equations have no explicit dependence on diffusion, but the entire spatial dependence of the solutions is incorporated in a parameter μ

$$\frac{d\mathbf{c}}{dt} = \mathbf{f}(\mathbf{c}, \mu), \qquad \mu \equiv \mu(\mathbf{r}, t) \tag{3.14}$$

In this way the symmetry of the system is broken by an external action on the system μ instead of a spontaneous emergence of a pattern developing within the system itself. But, when we have a quantity to describe a biological function, it normally will depend both on space and time, and thus be governed by partial differential equations. The result is a mathematical problem involving an infinity of coupled degrees of freedom, for which Thom's classification no longer is applicable ([18]). This is a considerable drawback, if our aim is the understanding of biological processes.

An other important limitation of the theory of catastrophes is that the differential equations (3.14) describe *potential* systems with a finite number of degrees of freedom.

$$\frac{\partial \mathbf{c}}{\partial t} = -\frac{\partial V(\mathbf{c}, \mu)}{\partial \mathbf{c}}$$

$$= \quad \nabla_{\mathbf{c}} V(\mathbf{c}, \mu) = \mathbf{f}(\mathbf{c}, \mu)$$

called a gradient system, where V is a potential function.

The limitation consists in the fact that the dynamics of the kind of dissipative systems which we are interested in, are far away from the thermodynamic equilibrium. But only in very special cases such a system can be derived from a potential: a system involving only a single variable, or systems in the neighbourhood around the state of thermodynamic equilibrium. For instance is it impossible for a system like (3.15) to exhibit limit cycle behaviour. This can easily be seen from

$$\begin{aligned} \frac{\partial V}{\partial t} &= \frac{\partial V}{\partial \mathbf{c}} \frac{\partial \mathbf{c}}{\partial t} \\ &= -\left(\frac{\partial \mathbf{c}}{\partial t}\right)^2 \end{aligned}$$

integrating over a time interval T yields

$$\triangle V \equiv V(t+T) - V(t) = -\int_t^{t+T} \left(\frac{\partial \mathbf{c}}{\partial t}\right)^2 dt \leq 0 \tag{3.15}$$

which only can be consistent with our assumption of a periodic solution ($V(t+T) \equiv V(t)$ for T being the period), when $\frac{\partial \mathbf{c}}{\partial t}$ vanishes, but this is a set of points with measure zero.

As can be seen from the above investigations, the theory of catastrophes seems to be no appropriate candidate for the modeling of selforganizing phenomena in biological and chemical systems.

In contrast, the reaction-diffusion models given by eq. (3.13), are selforganizing and show temporal and spatial order in a definite region of parameter space. In the next chapter we will investigate the Turing models and show that it is in fact possible for a simple autocatalytic chemical systems to generate stable spatial patterns if the initial homogeneous distribution of the reactants is perturbed by for instance a random fluctuation. The system will then develop towards a new concentration distribution which is inhomogeneous and yet stable.

One must admit that at this time there exists no classification of the solutions of partial differential equations comparable in generality to Thom's theory of ordinary differential equations. However, by performing bifurcation analysis as in the previous section, one can construct explicit forms of the solutions in the neighbourhood of the bifurcation points and in this way obtain a preliminary classification of these solutions [18].

Chapter 4

The Turing Mechanism

Chemical reaction-diffusion systems are known to exhibit spatial or temporal patterns if they are kept far away from the thermodynamic equilibrium by a constant supply of fresh reactants. These thermodynamically open systems were, as outlined before, first described by Alan Turing [1] forty years ago. Here in this chapter we want to examine the mathematical basis for the Turing structures to emerge, and perform a *linear stability analysis* which investigates the stability of the system and of the possibility of self-organizing spatial patterns emerging from a close neighbourhood of the stable uniform state.

Such a system is mathematically described by eq.(3.13):

$$\frac{\partial \mathbf{c}}{\partial t} = \mathbf{f}(\mathbf{c}) + \mathbf{D}\nabla^2\mathbf{c} \tag{4.1}$$

From a mathematical examination of system (4.1) it is found that Turing systems, of which there are two main types, are mathematically equivalent, in the sense that they need to fulfil the same conditions in the linear expansions of the steady-state. Shortly, for a two component system, one component has to be self-activating (autocatalytic) and the other self-inhibiting, while the cross-activations/inhibitions of the two morphogenes need to be of opposite sign. If one component activates the other, this other component has to inhibit the first (or vice-versa).

In the second section we will look at the important *dispersion relation* which gives information for the most interesting dynamic features of the reaction diffusion system. There we also derive a relation for the constrains of the ratio of the diffusion coefficients necessary to obtain spatial patterns in the system.

In the third section of this chapter we will examine the two types of Turing systems, of which one is called an 'activator-inhibitor model' and the other 'activator substrate-depletion model', and try to arrive at some conclusions about their mutual differences especially in the range of early inhomogeneous growth of the spontaneously developing spatial patterns.

Finally a gel-reactor is introduced which effectively allows the observation of Turing structures in chemical reactions in the laboratory.

4.1 Linear Stability Analysis for Two-Component Systems

As mentioned in the previous chapter, the main interest from our point of view is restricted to models consisting of only two species. Such a system is described by:

$$\begin{aligned} \frac{dX}{dt} &= f(X,Y) + D_x \nabla^2 X \\ \frac{dY}{dt} &= g(X,Y) + D_y \nabla^2 Y \end{aligned} \tag{4.2}$$

where X and Y describes two different concentrations of either chemical species or morphogenes in a reaction diffusion system.

To make a well defined mathematical formulation of the problem it is necessary to formulate some boundary conditions specific to the system. Here we require zero-flux boundary conditions

$$(\mathbf{n} \cdot \nabla) \begin{pmatrix} x \\ y \end{pmatrix} = 0, \qquad \text{on} \qquad \partial B \tag{4.3}$$

where ∂B is the boundary of the domain B. Physically this means that there is no external input of chemical reactants in the system. We also require the initial conditions $X(\mathbf{r}, 0),\ Y(\mathbf{r}, 0)$ to be given.

4.1.1 The Homogeneous System

Let us first analyse the homogeneous system without diffusion:

$$\frac{dX}{dt} = f(X,Y), \qquad \frac{dY}{dt} = g(X,Y) \tag{4.4}$$

The state in which there is no change in concentration of the two morphogenes, the steady-state $f(X_0, Y_0) = g(X_0, Y_0) = 0$, will be regarded as a reference state from where small local perturbations

$$x(\mathbf{r},t) = X(\mathbf{r},t) - X_0(\mathbf{r},t) \tag{4.5}$$

(expressed by ξ in the previous chapter) either will cause the system to tend to move away from the steady state, or the steady state is stable and initial perturbations or fluctuations will die and have no effect on the system.

For the emergence of Turing structures a reaction-diffusion system exhibits diffusion-driven instabilities if the homogeneous steady state is stable to small perturbations in the absence of diffusion; but unstable to small spatial perturbations when diffusion is present. So, in the homogeneous case, we need to find conditions where the steady state is stable in the evolution of time.

A first order Taylor expansion around the steady state is valid as long $\left|\frac{x}{X_0}\right| \ll 1$:

$$f(X) = f(X_0) + \left(\frac{\partial f}{\partial X}\right)_{X_0} \cdot x \tag{4.6}$$

Repeating the above step with respect to Y and inserting in (4.4) one obtains the *linearized system*:

$$\begin{pmatrix} \frac{\partial x}{\partial t} \\ \frac{\partial y}{\partial t} \end{pmatrix} = \begin{pmatrix} \frac{\partial f}{\partial x} & \frac{\partial f}{\partial y} \\ \frac{\partial g}{\partial x} & \frac{\partial g}{\partial y} \end{pmatrix} \begin{pmatrix} x \\ y \end{pmatrix} \tag{4.7}$$

where

$$\mathbf{J_0} = \begin{pmatrix} \frac{\partial f}{\partial x} & \frac{\partial f}{\partial y} \\ \frac{\partial g}{\partial x} & \frac{\partial g}{\partial y} \end{pmatrix}_{X_0,Y_0} = \begin{pmatrix} f_x & f_y \\ g_x & g_y \end{pmatrix} \tag{4.8}$$

is the Jacobian matrix evaluated at the reference state. If we now look at a solution of the form $\mathbf{w} \propto \mathbf{w}_0 e^{\lambda t}$ where $\mathbf{w} = \begin{pmatrix} x \\ y \end{pmatrix}$ the system will retain its steady state, and hence be stable if $\mathbf{Re}(\lambda_i) < 0$. Inserting that solution in the linearized system:

$$\frac{\partial \mathbf{w}_0 e^{\lambda t}}{\partial t} = \mathbf{J_0}\mathbf{w}_0 e^{\lambda t} \tag{4.9}$$

one obtains by differentiation

$$\lambda \mathbf{w} = \mathbf{J_0}\mathbf{w} \tag{4.10}$$

Non-trivial solutions of $\mathbf{w}$ can then be found from:

$$|\mathbf{J_0} - \lambda \mathbf{I}| = 0 \tag{4.11}$$

which results in a second order polynomial in λ

$$\lambda^2 - Tr\lambda + Det = 0 \tag{4.12}$$

known as *the characteristic equation*. The trace Tr is given as:

$$Tr(\mathbf{J_0}) = f_x + f_y = \left(\frac{\partial f}{\partial x}\right)_0 + \left(\frac{\partial g}{\partial y}\right)_0 \tag{4.13}$$

and the determinant Det of $\mathbf{J_0}$ as:

$$Det(\mathbf{J_0}) = f_x g_y - f_y g_x = \left(\frac{\partial f}{\partial x}\right)_0 \left(\frac{\partial g}{\partial y}\right)_0 - \left(\frac{\partial f}{\partial y}\right)_0 \left(\frac{\partial g}{\partial x}\right)_0 \tag{4.14}$$

This determines the eigenvalues λ to be solutions of

$$\lambda_{\pm} = \frac{1}{2}\left[Tr \pm \sqrt{Tr^2 - 4Det}\right] \tag{4.15}$$

The necessary conditions for the homogeneous system to be linear stable are then:

$$Tr = f_x + f_y < 0, \quad \text{and} \quad Det = f_x g_y - f_y g_x > 0 \tag{4.16}$$

4.1.2 The Reaction-Diffusion System

Now consider the full reaction-diffusion system described by (4.2) and linearize about the steady state again

$$\frac{\partial \mathbf{w}}{\partial t} = \mathbf{J_0 w} + \mathbf{D}\nabla^2 \mathbf{w}, \qquad \mathbf{D} = \begin{pmatrix} D_x & 0 \\ 0 & D_y \end{pmatrix} \tag{4.17}$$

To solve this equation it is necessary to define a time-independent solution $\phi(\mathbf{r})$ of the Laplace operator, ∇^2:

$$\nabla^2\phi_{nml}(\mathbf{r}) = -\kappa^2\phi_{nml}(\mathbf{r}), \quad (\mathbf{n}\cdot\nabla)\phi_{nml}(\mathbf{r}) = 0 \quad \mathbf{r} \text{ on } \partial B \tag{4.18}$$

Here again $\mathbf{n}$ is the unit vector normal to the closed boundary ∂B of the reaction-diffusion domain B. The eigenfunctions and eigenvalues will then depend on the geometry, dimensionality and boundary conditions. This means that all the spatial dependencies of the linearized equation (4.17) are conditioned by the properties of the Laplace operator.

Let us look at one example. If eq. (4.18) is solved in one dimension satisfying zero-flux boundary conditions on a line of length L; $0 \leq r \leq L$, then the typical eigenfunction is:

$$\phi_n(\mathbf{r}) \quad \propto \quad cos\left(\frac{n\pi r}{L}\right) \tag{4.19}$$

for $r = 0$ and $r = L$ leading to $\phi_n(\mathbf{r}) = \pm 1$; $(\mathbf{n}\cdot\nabla)\phi_n(\mathbf{r}) = 0$. The eigenvalue

$$\kappa = \frac{n\pi}{L} \tag{4.20}$$

is called the *wavenumber* and is inversely proportional to the wavelength

$$\omega = \frac{2\pi}{\kappa} \tag{4.21}$$

This means that in a system with a constraint on the boundary conditions there exists a discrete set of possible wavenumbers, and to every wavenumber belongs exactly one eigenfunction. The computer simulations in the next sections are all solved for one dimension and zero-flux boundary conditions and therefore correspond to these results.

If we had boundary conditions stipulating the vanishing of φ_n at $r = 0$ and $r = L$ the typical eigenfunction would become: $\phi_n(\mathbf{r}) \propto sin\,(\frac{n\pi r}{L})$. If eq.(4.18) is solved on a two dimensional circular layer, $\phi_n(\mathbf{r})$ will be given by the product of Bessel functions and trigonometric functions [19].

Let us return to (4.17). Because the problem is linear the solution $\mathbf{w}(\mathbf{r}, t)$ of eq.(4.17) can generally be described as a sum of the product functions

$$\mathbf{w}(\mathbf{r}, t) = \sum_{\kappa} c_\kappa e^{\lambda t}\varphi_\kappa(\mathbf{r}) \tag{4.22}$$

and for the two variable system in one dimension

$$\begin{pmatrix} x \\ y \end{pmatrix} = \begin{pmatrix} c_1 \\ c_2 \end{pmatrix} e^{\lambda t} cos\left(\frac{n\pi r}{L}\right) \tag{4.23}$$

Now, inserting this in (4.17) the λ's are determined by the roots of the characteristic polynomial

$$\left|\mathbf{J_0} - \mathbf{D}\kappa^2 - \lambda\mathbf{I}\right| = 0 \tag{4.24}$$

leading to *the dispersion relation*

$$\lambda^2 - \lambda\left[Tr - \kappa^2(D_x + D_y)\right] + P(\kappa^2) = 0 \tag{4.25}$$

where

$$P(\kappa^2) = Det - \kappa^2(f_x D_y + g_y D_x) + \kappa^4 D_x D_y \tag{4.26}$$

Here again Tr is the trace and Det the determinant of the Jacobian matrix (4.8) evaluated at the steady state.

As said before, if we want to find symmetry-breaking patterns, we seek for a solution where the system becomes unstable. Because $Tr < 0$, $P(\kappa^2)$ in eq.(4.25) has to be negative in order to destabilize the system. Otherwise the polynomial could not have any roots with positive real part. Thus, a necessary condition is

$$f_x D_y + g_y D_x > 0 \tag{4.27}$$

and since $Tr = f_x + g_y < 0$

$$D_x \neq D_y \tag{4.28}$$

This result shows that Turing instabilities in general can occur only if the diffusion coefficients of the two species are not equal. This is a necessary but not a sufficient restriction and it has also for many years been the main obstacle for the experimental working scientist to observe Turing patterns. Biological experimentalists have difficulties in pinning down one mechanism responsible for morphogenesis, and chemical experimentalists mainly work in aqueous solution where the diffusion rates normally are of the same order of magnitude.

4.2 The Dispersion Relation and the Diffusion Ratio

We can define a critical ratio between the two diffusion coefficients D_x and D_y as

$$d_c = \left(\frac{D_x}{D_y}\right)_{crit} \tag{4.29}$$

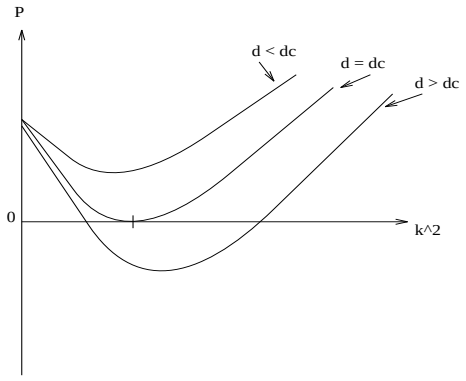

Figure 4.1: $P(\kappa^2)$ as a function of κ^2. Only when the diffusion ratio d is larger than d_c it is possible to destabilize the system.

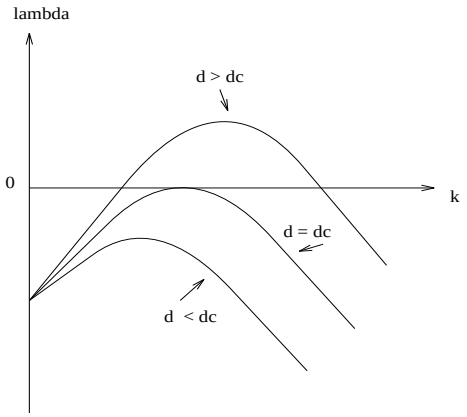

Figure 4.2: Schematical plot of the largest eigenvalue $\lambda(\kappa^2)$ as a function of κ. When $d > d_c$ a finite range of wavenumbers are linearly unstable.

for which it is possible to obtain the desired diffusion induced instabilities, so that the function $P(\kappa^2)$ becomes negative for a finite range of wavenumbers κ^2 creating unstable modes where the real part of the largest eigenvalue becomes positive.

Fig. 4.1 and 4.2 shows this schematically. Especially fig. 4.2, which is called *the dispersion plot* is very informative when characterizing the evolution of patterning since it immediately says which eigenfunctions, that is which spatial patterns, are linearly unstable and grow exponentially with time. The key assumption is that the linearly unstable eigenfunctions not will grow infinitely, but instead will be bounded by the nonlinear terms in the rate equations. Thus, a new steady state of spatially inhomogeneous solution should emerge.

Since it is the diffusion ratio which causes the main drawback in the theory of pattern formation for Turing structures, many ideas and improvements have been suggested in order to at least diminish this requirement. We will explore some different mechanisms where the ratio d_c comes close to unity, and where the Turing domain in parameter space is increased.

Let us find an explicit expression for the diffusion coefficient ratio d in terms of the parameters in the system. To do so, we start with equation (4.26).

$$P(\kappa^2) = Det - \kappa^2(f_x D_y + g_y D_x) + \kappa^4 D_x D_y \tag{4.30}$$

The extremum of this polynomial obtains for

$$\kappa^2 = \frac{f_x D_y + g_y D_x}{2 D_x D_y} \tag{4.31}$$

inserting in (4.30) one finds the fastest growing mode κ^4 going like

$$\kappa^4 = \frac{Det}{D_x D_y} \tag{4.32}$$

and a standard inequality obeying the demand $P(\kappa^2) < 0)$ and $Det > 0$

$$0 < Det < \frac{(f_x D_y + g_y D_x)^2}{4 D_x D_y} \tag{4.33}$$

Now we want to find an explicit inequality for $d = \frac{D_x}{D_y}$. Rearranging (4.33) we get

$$g_y^2 d^2 - d(2 f_x g_y - 4 f_y g_x) + f_x^2 > 0 \tag{4.34}$$

which has two roots

$$d_{1,2} = \frac{(Det - f_y g_x) \pm 2\sqrt{-f_y g_x Det}}{g_y^2} \tag{4.35}$$

Only one of these applies though: From eq. (4.27) we have

$$g_y d > -f_x \tag{4.36}$$

but from eq.(4.35)

$$g_y d = \frac{(Det - f_y g_x) \pm 2\sqrt{-f_y g_x Det}}{g_y} \tag{4.37}$$

So, for the negative root we get

$$\begin{aligned} g_y d + f_x &= \frac{(Det - f_y g_x) - 2\sqrt{-f_y g_x Det}}{g_y} + f_x \\ &= \frac{Det}{2} \frac{\sqrt{Det} - \sqrt{-f_y g_x}}{g_y} \end{aligned}$$

Since $f_x g_y < 0$ we can say that $f_x g_y - f_y g_x < f_y g_x$ and thus

$$\frac{\sqrt{Det} - \sqrt{-f_y g_x}}{g_y} < 0 \tag{4.38}$$

when g_y is positive.

As said before, when $g_y > 0$ then $f_x < 0$ and by investigating inequality (4.36) one sees that the negative root for d does not apply. The other root then yields

$$d = \frac{D_-}{D_+} > \frac{(Det - f_y g_x) + 2\sqrt{-f_y g_x Det}}{g_y^2} \tag{4.39}$$

where D_- is the diffusion coefficient for the self-inhibitor and D_+ the diffusion coefficient for the self-activator. This inequality holds for Turing matrices with positive g_y, that is for the matrices

$$\begin{pmatrix} - & + \\ - & + \end{pmatrix} \quad (A2) \quad \text{and} \quad \begin{pmatrix} - & - \\ + & + \end{pmatrix} \quad (S2) \tag{4.40}$$

The two remaining Turing matrices where f_x is positive obey the same inequality when interchanging x and y, that is for the Turing matrices

$$\begin{pmatrix} + & - \\ + & - \end{pmatrix} \quad (A1) \quad \text{and} \quad \begin{pmatrix} + & + \\ - & - \end{pmatrix} \quad (S1) \tag{4.41}$$

we have an inequality of the form

$$\frac{D_-}{D_+} > \frac{(Det - f_y g_x) + 2\sqrt{-f_y g_x Det}}{f_x^2} \tag{4.42}$$

here $D_- = D_y$ and $D_+ = D_x$ in contrast to before.

In the following chapters we will use these particular inequalities for the ratio of diffusion coefficients to show that the diffusion constants may become almost equal in magnitude when the cooperativity of the defining kinetics becomes as high as is seen in genetic control systems (chapter 6). When concerned with a Turing bifurcation from an unstable branch in a bistable system, it is also possible to obtain a similar inequality. This will be one of the subjects in chapter 7.

4.3 Activation-Inhibition and Activation Substrate-Depletion

The inequalities (4.39) and (4.42) show that the diffusion coefficient of the activator must be smaller than the diffusion coefficient of the inhibitor (normally about a factor of ten) if spontaneous patterns are to occur. This is why one speaks of 'short range activation' and 'long range inhibition'. But there are problems with this explanation; x and y both develop into patterns at the onset of instability with the *same* wavelength. This means that there is no fast diffusing inhibitor, which traps a slow diffusing activator into patterns.
For the systems:

$$\begin{pmatrix} + & - \\ + & - \end{pmatrix} \quad (A1) \quad \text{and} \quad \begin{pmatrix} - & + \\ - & + \end{pmatrix} \quad (A2) \tag{4.43}$$

one has the notion of a 'real activator-inhibitor model'. One component activates itself and the other, while the second component inhibits itself and the first. The

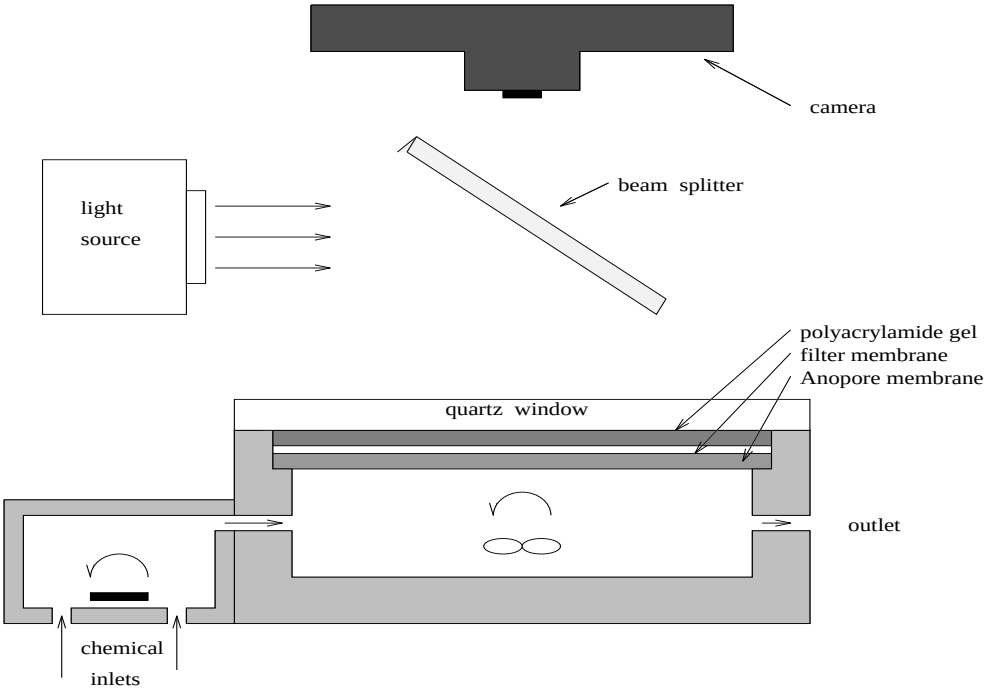

Figure 4.3: Schematic diagram of a gel reactor. This particular gel reactor was used for the iodate-ferrocyanide-sulfite reaction studied by Lee et. al.

inhibitory effect is not only due to the fact that the inhibitor inhibits the activator directly, but also because the activator produces its own inhibitor. But this structure of the Jacobian matrix cannot be used to develop the common qualitative picture of inhibitors and activators trapping or catching each other, because, as we later will see more clearly, the concentrations of both the two components always have high concentration in the same region in space and thus are in phase. In contrast, the so called 'activator-substrate depleted' systems:

$$\begin{pmatrix} + & + \\ - & - \end{pmatrix} \quad (S1) \quad \text{and} \quad \begin{pmatrix} - & - \\ + & + \end{pmatrix} \quad (S2) \tag{4.44}$$

are characterized by opposite signs of the cross-couplings resulting in a spatial distribution out of phase. That is: one is high where the other is low. We will investigate this qualitative difference more closely in the next chapter.

4.4 The Gel-Reactor

The fact that almost all chemical species have nearly equal diffusion coefficients in aqueous solutions, has been the major problem for obtaining diffusion induced

Figure 4.4: Experimentally obtained Turing structures in the EOE-reaction.

Figure 4.5: Experimentally obtained Turing structures in the CIMA-reaction.

instabilities in chemical reactions analysed in the laboratories. Several authors have pointed out that this difficulty can be overcome if the activator reacts with an immobilized substrate to form an immobile complex [22],[23].

Now gel-filled reactors are widely used for the study of sustained patterns arising from the interplay of diffusion and chemical kinetics, and many chemical reactions have been investigated since then. But still it seems rare to find Turing structures and the only exception within the last three years is the bistable iodate-ferrocyanide-sulfite reaction, known as the EOE-reaction. It is based on the classical iodate-sulphite clock reaction by Landolt [24]. We will investigate this reaction and its many new pattern features more deeply in chapter 8.

Figure 4.3 shows a typical gel disc reactor. A thin polyacrylamide gel layer is fed diffusively by a continuously refreshed reservoir of chemicals. The gel is sufficiently thin so that the patterns can be considered approximately two-dimensional. There are two thin membranes between the polyacrylamide gel and the stirred reservoir, one Anopore disk that provides structural rigidity for the thin gel layer and another that provides a white backing for visualization of the patterns. The chemicals are premixed before entering the reactor reservoir and both are vigorously stirred to ensure homogeneity.

Figure (4.4) shows some typical two-dimensional structures obtained experimentally for the EOE-reaction. Fig.(4.5) shows experimentally obtained hexagons in the CIMA-reaction.

Chapter 5

Initial Growth and Damping

In this chapter we will try to examine the initial pattern growth in some particular models in order to reach a closer understanding of the role of the two species interacting cooperatively. The mode selection of the system as a function of different kind of perturbations is also an interesting point on which we focus. The dependence of boundary conditions, length of the system and initial conditions is investigated by computer simulations in one space dimension.

First the Lengyel-Epstein model is considered as a representative of the 'activator-inhibitor' systems (with an $A1$-structure in the Jacobian), and as an opponent the Sel'kov model is investigated, since it is an 'activation substrate-depletion' model ($S2$-type).

The simulations on the computer where carried out with a C-program consisting of 98 coupled differential equations simulating the coupled nonlinear partial differential equations in one spatial coordinate and time, and solved with a stiff-integrator (for further interest in the computer program, the reader may communicate with the author).

5.1 The Lengyel-Epstein Model

The first clear experimental verification of the stationary concentration patterns predicted by Turing was made by a group in Bordeaux in 1990 [25]. They used a Clorite-Iodide-Malonic Acid-Starch reaction (CIMA-reaction) for which a two variable model was proposed by Lengyel and Epstein [23]. The starch has the effect that the effective ratio between the diffusion coefficients is enlarged, thus allowing Turing structures to occur. The activator-ions (I^-) are for a small period of time trapped in a medium of gel-bound (I_2, I_3^-) and starch thereby diminishing the diffusion through the gel. The Bordeaux-group found by numerical studies that only $[ClO_2^-]$ and $[I^-]$ would vary significantly during an oscillation. A reasonable two-variable model is therefore

$$\frac{\partial x}{\partial t} = k_1 - k_2 x - 4k_3 \frac{xy}{u + x^2} + D_x \nabla^2 x \tag{5.1}$$

$$\frac{\partial y}{\partial t} = k_2 x - k_3 \frac{xy}{u + x^2} + D_y \nabla^2 y \tag{5.2}$$

The steady state is:

$$x_0 = \frac{k_1}{5k_2}, \quad y_0 = \frac{k_2 u}{k_3} + \frac{k_1^2}{25 k_2 k_3} \tag{5.3}$$

From eq.(4.8) the Jacobian becomes:

$$\mathbf{J_0} = \begin{pmatrix} -k_2 + 4k_3 y_0 \left[\frac{x_0^2 - u}{(x_0^2+u)^2}\right] & -4k_3 \frac{x_0}{x_0^2+u} \\ \\ k_2 + k_3 y_0 \left[\frac{x_0^2 - u}{(x_0^2+u)^2}\right] & -k_3 \frac{x_0}{x_0^2+u} \end{pmatrix} \tag{5.4}$$

In order to fulfil the required structure of signs, $\mathbf{J_0} = \begin{pmatrix} + & - \\ + & - \end{pmatrix}$, it is necessary that

$$f_x = \frac{\partial f}{\partial x} = -k_2 + 4k_3 y_0 \left[\frac{x_0^2 - u}{(x_0^2 + u)^2}\right] > 0 \tag{5.5}$$

which leads to the condition

$$x_0 > \left(\frac{5u}{3}\right)^{\frac{1}{2}} \tag{5.6}$$

Performing the same analysis as in eq.(4.17) – (4.26) requires that $P(\kappa^2)$ takes the explicit form:

$$P(\kappa^2) = \kappa^4 D_x D_y - \kappa^2 \left(-k_2 D_y + 4k_3 D_y y_0 \left[\frac{x_0^2 - u}{(x_0^2 + u)^2}\right] - k_3 D_x \frac{x_0}{x_0^2 + u}\right) + \frac{k_1 k_3}{x_0^2 + u} \tag{5.7}$$

with x_0, y_0 as in (5.3) and $\kappa^2 = \frac{n^2\pi^2}{l^2}$.

We can plot $P(\kappa^2)$ against the length-scale $\frac{D_x}{l^2}$, and obtain the *critical curve* (see fig.5.1). The point where $P(\kappa^2)$ vanishes is a possible onset of instability,

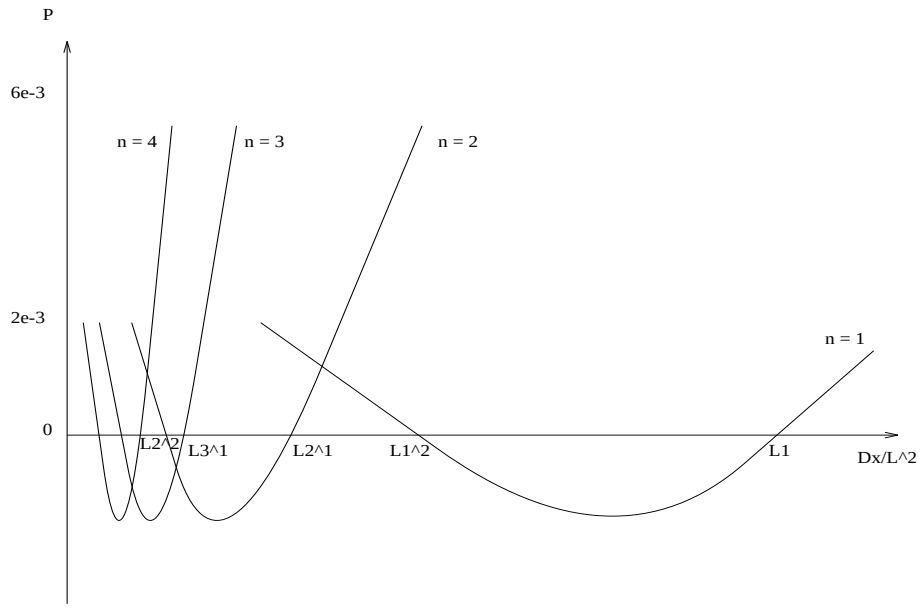

Figure 5.1: Dependence of the characteristic polynomial in κ^2 versus the length-scale $\frac{D_x}{l^2}$ for different values of the wave number n. Areas with $P(\kappa^2) < 0$ can give rise to spatial patterns.$D_y = 0.02, k_1 = 0.01, k_2 = 2e^{-3}, k_3 = 6e^{-3}$ and $u = 6.94e^{-3}$

which means that at least one of the eigenvalues in eq.(4.25) becomes positive, corresponding to a destabilization of the steady state as $t \to \infty$.

It is possible to understand fig.(5.1) in two ways. One can either study $P(\kappa^2)$ in terms of the length l of the system, or inversely in terms of the diffusion-coefficient of the activator D_x, by setting the length to 1. If the total length of the system is less than L_1^1 (or D_x higher than L_1^1) the homogeneous state of the system remains stable, and there is no possibility for the generation of patterns. If the length is increased beyond L_1^1, there is a possibility for spontaneous pattern formation due to the instability of the homogeneous state; see fig.5.2.

Decreasing the diffusion coefficient D_x below L_1^2 the steady state is again stable and no pattern will arise (see fig.5.3) until the point L_2^1, where one may obtain a spatial structure with two high concentration points. Moreover, performing the perturbations with only a small difference of their location, creates an bifurcation between the two possibilities in this area. It depends on the direction and place of the perturbation. In the first figure (5.4) the activator is perturbated upwards at the point $l = 73$, resulting in a maximum in the middle. In the second (5.5) the perturbation is placed at the point $l = 75$, resulting in the reversed picture.

Moving into the space between L_3^1 and L_2^2 of fig.(5.1), two possibilities arise due to the overlapping of various n-values. Structures with two high concentration points and one low, and structures with two high and two low concentration points may appear (periods π and $\frac{3\pi}{2}$ respectively). These are shown in fig. 5.6 and fig.

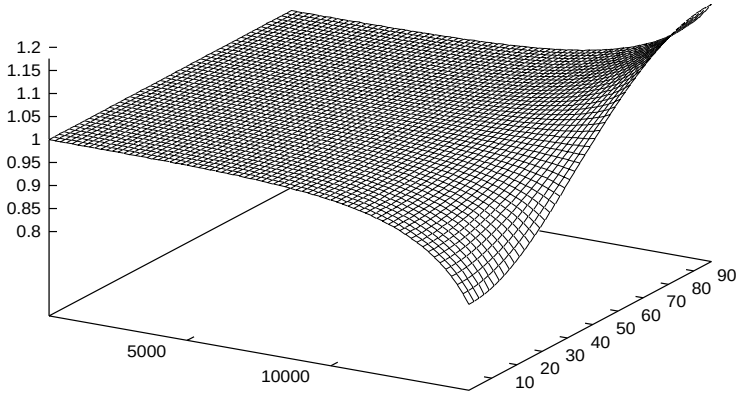

Figure 5.2: Three-dimensional plot for the development of a Turing structure in space and time. Here the Epstein model in the area between L_1^1 and L_1^2, creating one high and one low concentration point: $k_1 = 0.01, k_2 = 0.002, k_3 = 0.006, u = \frac{1}{144}, D_x = 0.00049$ and $D_y = 0.02$. Perturbation of the activator x at $l = 95$.

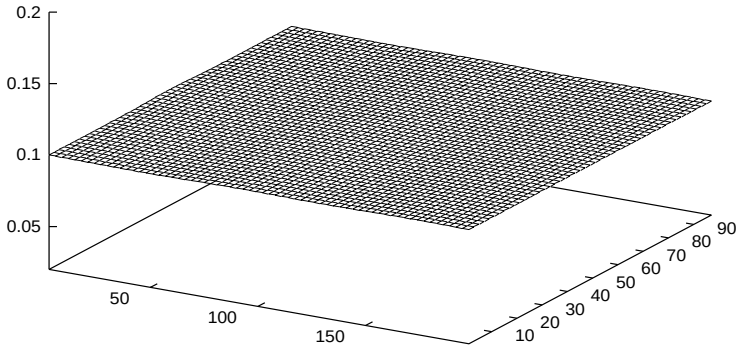

Figure 5.3: In the area between L_1^2 and L_2^1, where the homogeneous reference state is stable, with $k_1 = 0.01, k_2 = 0.02, k_3 = 0.006, u = \frac{1}{14400}, D_x = 0.0012$ and $D_y = 0.01$. Perturbed at $l = 49$.

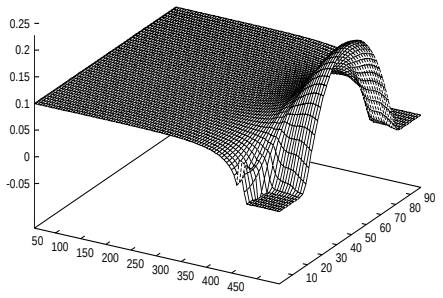

Figure 5.4: The area between L_2^1 and L_3^1. Two possibilities of pattern formation. Which of these is obtained depends on the bias in the initial conditions.

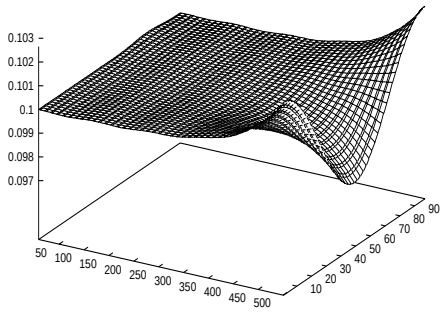

Figure 5.5: This one is perturbed at $l = 75$. The other parameters are $k_1 = 0.01, k_2 = 0.02, k_3 = 0.006, u = \frac{1}{14400}, D_x = 0.00056$ and $D_y = 0.01$. Perturbed at $l = 73$.

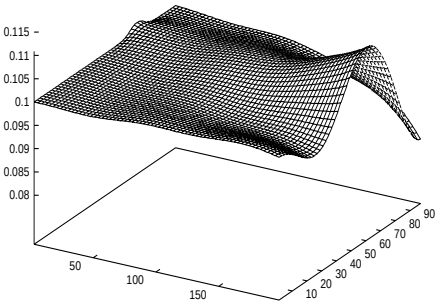

Figure 5.6: In the area between L_3^1 and L_2^2, The parameters used: $k_1 = 0.01, k_2 = 0.02, k_3 = 0.006, u = \frac{1}{14400}, D_x = 0.00037$ and $D_y = 0.01$. Perturbed at $l = 71$.

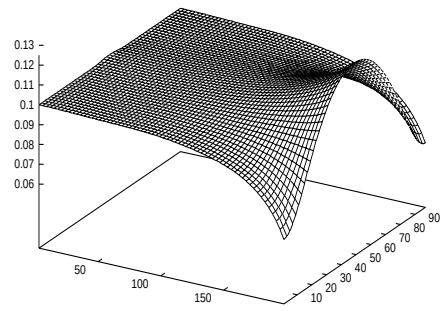

Figure 5.7: Perturbed at $l = 49$. These figures show bistability depending on the location of the perturbation.

5.7 respectively.

Decreasing D_x further leads to an introduction of higher n-values and their overlapping create multistable and more complex patterns. Thus, the form of the final pattern is a function of the magnitude of the initial perturbations and their location in the system [17].

5.2 Couplings and Amplifications

We can make a short mathematical investigation of the initial amplitude evolution at the onset of instability. In this sense we analyse the solutions of the system, where the eigenvalues of the time dependent part of equation (4.22) just become zero, so that a root of the characteristic equation (4.25) moves from negative values to a positive value, i.e. the cross-over point where the homogeneous state becomes unstable and patterns start to grow. At that point the full Jacobian is:

$$\mathbf{J} = \mathbf{J_0} - \kappa^2 \mathbf{D} \tag{5.8}$$

$$\begin{vmatrix} f_x - \kappa^2 D_x & f_y \\ g_x & g_y - \kappa^2 D_y \end{vmatrix} = 0 \tag{5.9}$$

To obtain a qualitative picture of the development of a small perturbation at the bifurcation point, we introduce a small perturbation ξ:

$$\mathbf{J}\xi = 0 \tag{5.10}$$

where

$$\xi = \begin{pmatrix} \delta_x \\ \delta_y \end{pmatrix} \phi_n \tag{5.11}$$

we obtain the two linear equations:

$$(f_x - \kappa^2 D_x)\delta_x + f_y \delta_y = 0 \tag{5.12}$$

$$g_x \delta_x + (g_y - \kappa^2 D_y)\delta y = 0 \tag{5.13}$$

We can use an appropriate expression for κ^2 from eq.(4.31) Inserting this in for instance (5.13) and setting $\delta_y = 1$ we get

$$\delta_x = \frac{f_x D_y - g_y D_x}{2 D_x g_x} \tag{5.14}$$

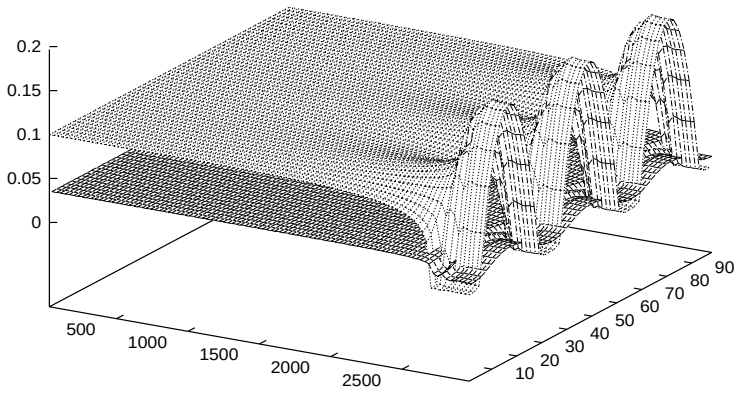

Figure 5.8: Turing structure in the Epstein model with $k_1 = 0.01, k_2 = 0.02, k_3 = 0.006, u = \frac{1}{14400}, D_x = 9.3 \cdot 10^{-5}$ and $D_y = 1 \cdot 10^{-3}$. Perturbed at $l = 49$. The activator and inhibitor has maximum in the same space region. The activator has a much higher amplitude.

As f_x is positive and g_y negative, one obtains a positive term in the numerator. The denominator is positive and so the entire expression becomes positive. From now on it is evident that for a Jacobian, with the structure in (4.43), that is the forms $A1$ and $A2$, the perturbation δ_y has the same sign as δ_x. Consequently component x and y will both have maxima (or minima) in the *same* space regions. The concentration pattern of the activator and the inhibitor will therefore be in phase.

The Jacobian for the Selkov model on the other hand has a $(S2)$-structure and here the analysis of eq.(5.14) results in opposite direction of the growth in concentration for each of the two components. The δ_x is *always* negative when δ_y is positive, corresponding to a spatial concentration distribution out of phase (see figures next section).

The common understanding of the activator and inhibitor competition is challenged by this analysis. Generally it is meant hereby that if the activator initially increases its own concentration locally (and simultaneously generates the inhibitor) and the inhibitor diffuses faster than the activator - then there will be created an island of high activator concentration surrounded by high inhibitor concentration [26]. The usual analogy drawn to give an intuitive notion of the activator-inhibitor mechanism is that of "fire and firefighters" [27]. A fire (the activator) starts in a forest and the firefighters, who had been dispersed throughout the forest, start to

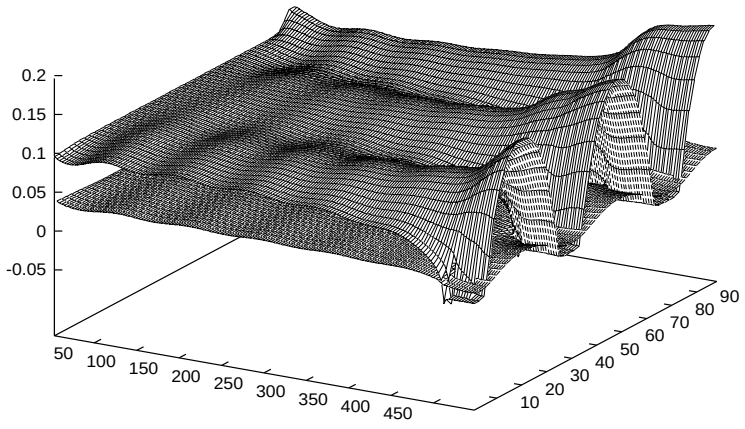

Figure 5.9: Here the inhibitor is perturbed upwards at $l = 4$, but it reacts downwards (see most left corner); resonant with the perturbation of the activator at $l = 95$.

react against the activator by spraying fire-resistant chemicals (with helicopters) on the not yet burning trees. The result of this scenario should be an area with patches of burned trees interspersed with patches of green, unburned trees.

The problem with this analogy is that in a 'real activator-inhibitor' system, both morphogenes have a maximal concentration in the same space regions, which should suggest that the trees with most fire-resistant chemicals will burn the best! (see fig. 5.8) This is unsatisfactory, and we have to find another analogy to explain the phenomena of pattern formation in reaction-diffusion systems. It may not even be possible to find a complete and satisfactory analogy, because the cross-couplings and nonlinear terms in the equation create too complicated interactions.

Another interesting point is the dominant role of the activator in the initial pattern growth. Looking at fig.(5.9) and (5.10), we see (apart from small time-dependent waves arising from small interactions with a Hopf bifurcation) two striking things: a) when the activator is perturbed upwards, it will remain at high concentration there (and the inhibitor will also have high concentration there), but when perturbing the inhibitor upwards it will in contrast decrease its own concentration at this place (and the activator decreases also). b) the perturbation of the activator is much more 'effective' in the sense that when both x and y are perturbed with an equal amount, the activator will determine the structure of the pattern. In figure (5.9), the perturbation develops faster to the final pattern, because the inhibitor is perturbed 'in phase' with the perturbation of the activator x. Fig. 5.10 is slower in the development of the pattern, because the inhibitor is perturbed out of phase, but

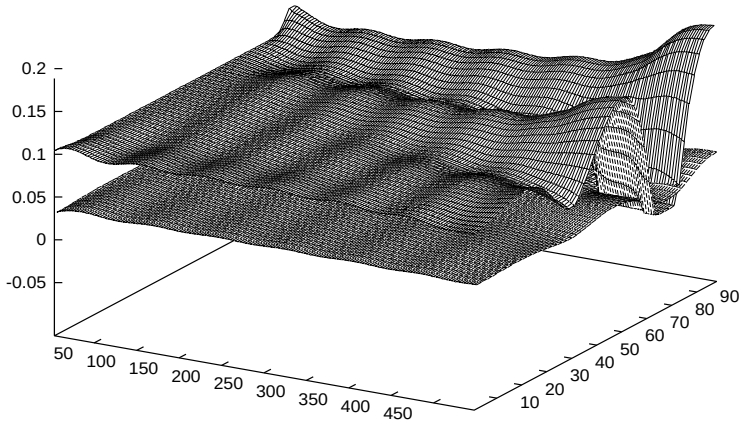

Figure 5.10: Here the inhibitor is perturbed downwards at the same point.

anyway, the activator still wins the race.

To make sure, I have also simulated the Gierer-Meinhardt model on the computer. It consists of the equations:

$$\frac{\partial x}{\partial t} = k_1 - k_2 x + \frac{k_3 x^2}{y} + D_x \nabla^2 x \tag{5.15}$$

$$\frac{\partial y}{\partial t} = k_4 x^2 - k_5 y + D_y \nabla^2 y \tag{5.16}$$

with a $(A1)$-Jacobian form. As shown in fig.(5.11) this gives rise to the same qualitative picture as for the Epstein model. The activator has a larger amplitude and determines the structure of the pattern.

5.3 The Selkov Model

The Selkov model consists of the equations:

$$\frac{\partial x}{\partial t} = \nu - \frac{k_1 x y^\gamma}{1 + K y^\gamma} + D_1 \nabla^2 x \tag{5.17}$$

$$\frac{\partial y}{\partial t} = \frac{k_1 x y^\gamma}{1 + K y^\gamma} - k_2 y + D_2 \nabla^2 y \tag{5.18}$$

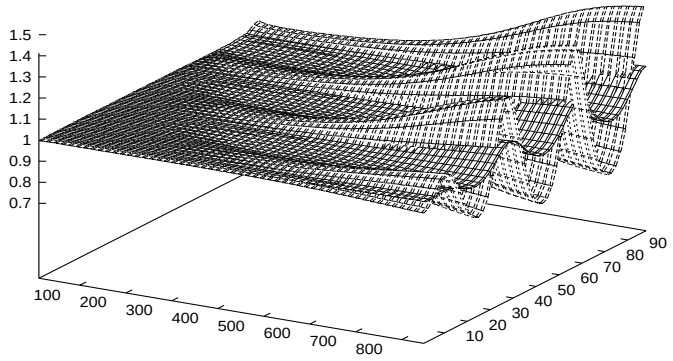

Figure 5.11: Three dimensional plot of a Turing structure in the Gierer-Meinhardt model The components are in phase. $k_1 = 0.1, k_2 = 0.3, k_3 = 0.2, k_4 = 0.6, k_5 = 0.6, D_x = 0.0001$ and $D_y = 0.01$. The inhibitor is perturbed upwards at $l = 4$ and the activator upwards at $l = 95$. x and y are in phase with a much larger amplitude for x.

Here component one is generated by a constant uniform rate ν and transformed into component two by Hill type kinetics. Component two is created by the same rate and decomposed by first order kinetics. Usually the denominator is neglected and the equations renormalized to the form

$$\frac{\partial x}{\partial t} = 1 - xy^{\gamma} + D_1 \nabla^2 x \tag{5.19}$$

$$\frac{\partial y}{\partial t} = \alpha x y^{\gamma} - \alpha y + D_2 \nabla^2 y \tag{5.20}$$

The Jacobian matrix has a $(S2)$-form, and the steady-state is $x_0 = y_0 = 1$. Here the activator (or at least self-activator) is the y component, and the self-inhibitor is the x component and the Hill-coefficient γ is known from chapter 2.
The full Jacobian $\mathbf{J}$ is:

$$\mathbf{J} = \begin{pmatrix} -1 - \kappa^2 D_x & -\gamma \\ \alpha & \alpha(\gamma - 1) - \kappa^2 D_y \end{pmatrix} \tag{5.21}$$

In appendix A the amplitude formalism for the Hopf-bifurcation is used to obtain the Ginzburg-Landau parameters for the Selkov model. In this way it is possible to

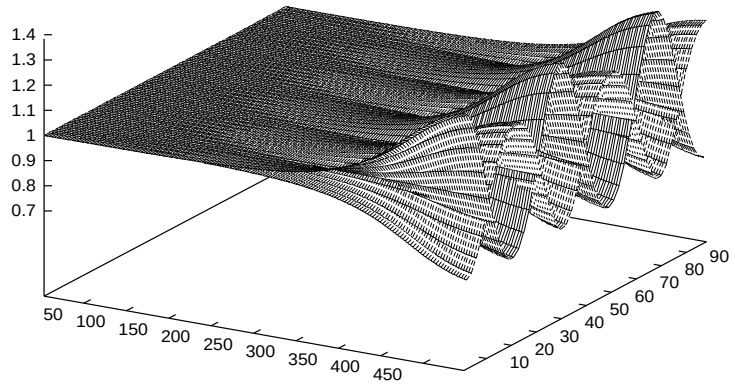

Figure 5.12: Three dimensional plot of a Turing structure in the Selkov model. The components are out of phase with a factor π. Here the inhibitor has a larger amplitude than the activator. $\alpha = 0.3, \gamma = 3, D_x = 0.005, D_y = 0.00075$. Perturbed at $l = 95$ and $l = 94$.

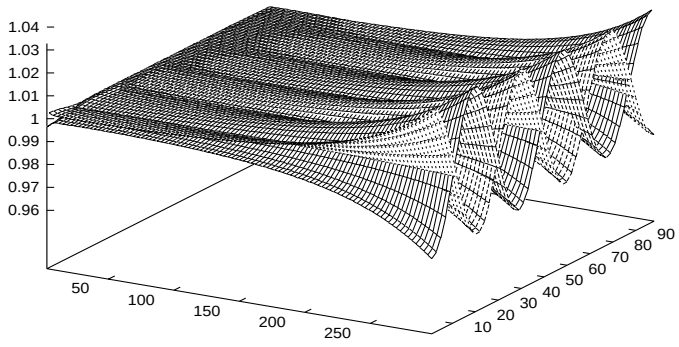

Figure 5.13: The activator y is perturbed upwards at $l = 4$ and the inhibitor upwards at $l = 95$. One can see the same effect as in the Epstein model: The inhibitor-perturbation is damped and the activator determines the structure of the pattern; $\alpha = 0.3, \gamma = 3, D_x = 0.005, D_y = 0.00077$.

find out, whether the Hopf-bifurcation is super- or subcritical for a given value of the parameter γ; α was used as the critical Hopf bifurcation parameter. But here we will look at the amplitude of the emerging pattern, and try to find out how the spatial amplitudes are related between the two morphogenes.

Because of the nice scaling in the Selkov model we can go further with the bifurcation analysis from chapter 4.
The Jacobian for the homogeneous case is:

$$\mathbf{J_0} = \begin{pmatrix} -1 & -\gamma \\ \alpha & \alpha(\gamma - 1) \end{pmatrix} \tag{5.22}$$

Inserting these values in eq.(5.14), one obtains for a small perturbation δ_x:

$$\delta_x = -\frac{D_y}{2D_x\alpha} - \frac{(\gamma - 1)}{2} \tag{5.23}$$

As in the section before δ_y was set to 1; and we see that δ_x always is negative (corresponding to a concentration pattern out of phase). If we set $\delta_x = -1$, we can find an expression where the initial growth rate of the two patterns is equally strong; that means we want to find a critical value where the amplitudes of the two morphogenes is equal. Now, at the bifurcation point, the fraction $\frac{D_x}{D_y}$ is precisely equal to the condition (4.33):

$$\frac{D_x}{D_y} = \frac{1 + \gamma + 2(\gamma)^{\frac{1}{2}}}{\alpha(\gamma - 1)^2} \tag{5.24}$$

Inserting this in (5.23) we get:

$$\delta_x = -\frac{(\gamma - 1)}{2} - \frac{(\gamma - 1)^2}{2 + 2\gamma + 4(\gamma)^{\frac{1}{2}}} = -1 \tag{5.25}$$

After some manipulations one finds a polynomial in γ

$$\gamma^2 + \gamma^{\frac{3}{2}} - 2\gamma - 3\gamma^{\frac{1}{2}} - 1 = 0 \tag{5.26}$$

where the only positive root is:

$$\gamma = \frac{1}{g^2} \simeq 2.618 \tag{5.27}$$

where g is the golden number. So, when $\gamma > \frac{1}{g^2}$ the inhibitor x has a larger amplitude than the activator y, and when $\gamma < \frac{1}{g^2}$ the activator has a larger amplitude than the inhibitor. This somewhat funny result might suggest that we have used some symmetric assumptions as condition for the analysis at the bifurcation point. Later in chapter 6 we will investigate the effect of larger values for the Hill constant γ. In this case it can already be stated that the amplitude of one component growths while the amplitude of the other component drops to very low values.

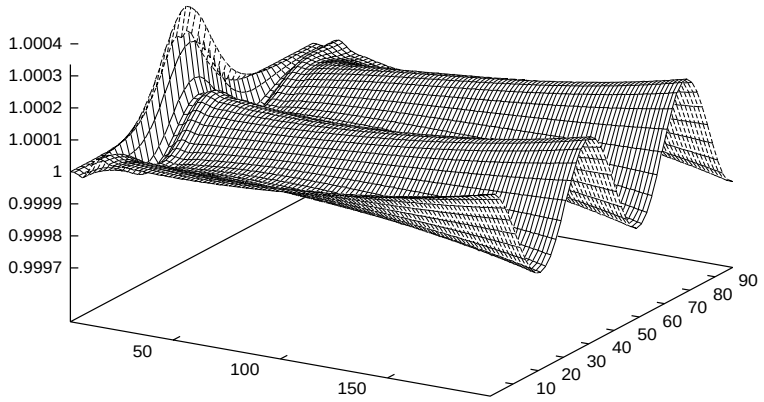

Figure 5.14: The Selkov model. Note the fast coupling throughout the system, and also the initial damping of the perturbation, which repeatedly has been observed. Only the inhibitor is shown.

5.4 Concluding Remarks

As seen from fig.5.14 the coupling throughout the system is very fast and the pattern first starts to grow after an initial damping of the perturbation. If the parameters are chosen outside the Turing space (as in fig. 5.15), the initial perturbation flattens out and the steady state becomes stable.

It is an interesting feature that there has to exist a minimal system size below which spatial patterns cannot occur. It can be explained as follows [19]: In the spatially distributed reactive system, chemical reactions and diffusion cooperate in a symmetry-breaking manner. The chemical kinetics can give rise to a runaway phenomenon by amplifying the effect of a small perturbation. The diffusion tends to smear out the inhomogeneities caused by this, but it does not quite succeed in erasing them. Therefore, the result is a space pattern whose characteristic length reflects the average distance over which a group of reactive molecules can diffuse before a reaction takes place. If the system is small, the effective diffusion rate (which is proportional to $\frac{D}{l^2}$) is tremendously enhanced and so the homogenizing feature of the diffusion rate dominates the entire system, corresponding to no pattern formation.

The terminology of activators and inhibitors is indeed questionable, especially if it is used to give a simple picture of the generation of patterns. The reason for the understanding of reaction-diffusion system as a competition between an activa-

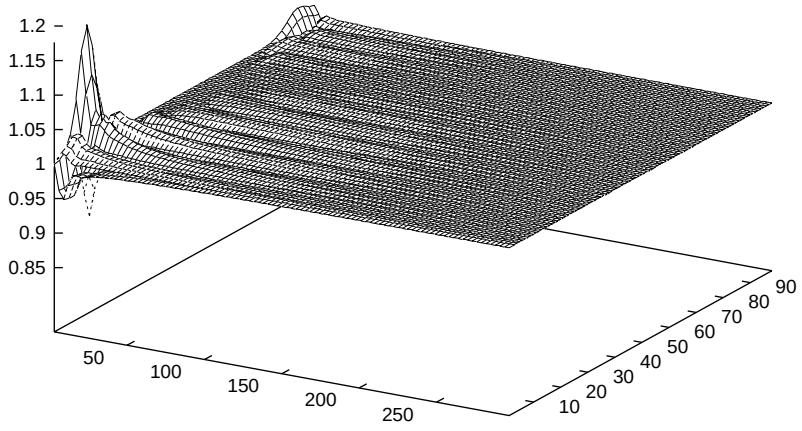

Figure 5.15: The Selkov model. Here the inhibitor is perturbed at $l = 95$ and the activator at $l = 4$ with the same amount. Even though the inhibitor diffuses faster, the activator produces the structure more effectively with a much broader range. The parameters used are: $\alpha = 0.3, \gamma = 3, D_x = 0.001, D_y = 0.000166$.

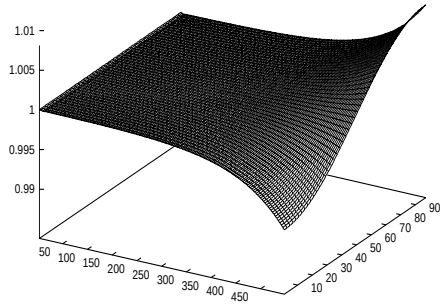

Figure 5.16: Downward perturbation of the inhibitor at $l = 95$ with $n = 1$. This plot has parametric conditions near the border of the Turing space: $\alpha = 0.3, \gamma = 3, D_x = 0.15, D_y = 0.023$.

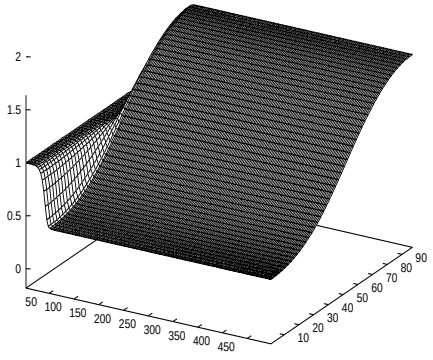

Figure 5.17: This plot has been taken deep inside Turing space. The coupling through the system becomes much stronger and the final stable pattern is reached almost at once. The parameters are: $\alpha = 0.5, \gamma = 3, D_x = 0.15, D_y = 0.023$.

tor and an inhibitor migth be found in the fact that the only models analysed are two-component models, creating a dialectical distinction between them. Surely it is possible to obtain pattern formation in a three-component system, and here it is not so easy to talk about activators and inhibitors any longer (it is actually possible to have a three-component Turing system, where all components are self-inhibitory). The reason for these symmetry-breaking phenomena is due to the interaction between chemical kinetics and diffusion, and not because of a competition of activators/inhibitors. Of course, there has to be an autocatalytic step involved (often due to double-inhibition), but only for the reason that at least one of the morphogenes can create itself; i.e. it must be autocatalytic.

Another interesting observation, also due to Murray [28] is the much greater sensitivity towards parameter variations in the Epstein model, than is the case in the Selkov model. Generally, the models given by (4.44) (*substrate depletion-* systems), are more stable against variations than the *activation-inhibition* models.

In our investigation of the importance of initial conditions and magnitude of perturbations we found that many different patterns can come into existence even with the same parametric conditions (se figures 5.6 and 5.7). In this case, one might object that several solution behaviours of pattern formation could possess some conceptual difficulties from a developmental biology point of view. But development, however, is a sequential process and so a previous stage generally cues the next.

Chapter 6

Cooperative Systems

In chapter 2 we mentioned the inclination towards high cooperativity in genetic control systems and other enzyme regulating processes in the cell. There, the allostery of enzymes was shown (already with only two binding sites) to give better "on-off" control of the reaction rate, since the enzyme complex activates further binding instead of only converting the substrate into a product. Why should enzymes want to do so, if not because the biochemical regulation processes become more stable and controllable? In aqueous chemical complexation mechanisms, such as the copper-ammonium system (fig. 6.1) the reaction constants *decrease* with increasing binding of more ligands to the copper(II)-ion.

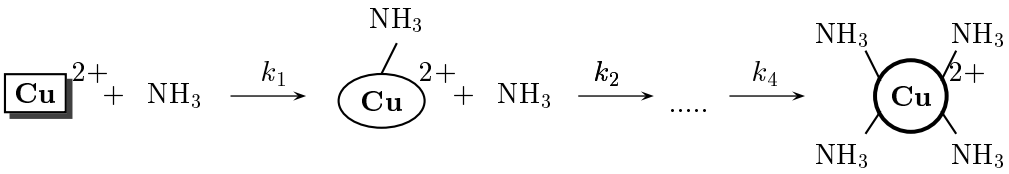

Figure 6.1: In this normal complexation mechanism the successive reaction constants k_i are ordered with decreasing value $k_1 > k_2 > .. > k_4$. A square symbolizes an active state, whereas a circle symbolizes an inactive state, which facilitates no further binding. The ellipse symbolizes an intermediate state.

For allosteric enzymes the reverse is true. Here a binding of a substrate S to an enzyme E facilitates further uptake (if the substrate is an activator for the enzyme), and the enzyme becomes in effect an on-off switch for the rate of reaction. Fig. 6.2 shows this schematically. The four initially inactive states convert into active states all together if one substrate S binds to one of the states. The rearranged enzyme works thus as a catalyst.

The overall reaction rate v for this strong positive cooperation is expected to be approximatively expressed by eq. 2.14:

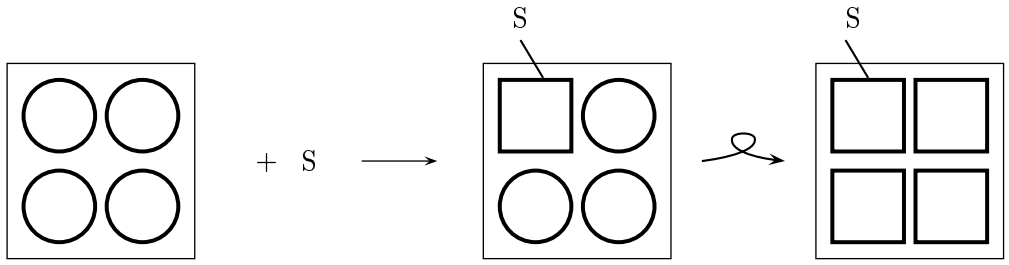

Figure 6.2: The enzyme with four inactive binding sites will, after a binding with an activating substrate S, undergo a transformation (normally a spatial rearrangement of the molecule) and become active. This is the normal effect producing enzyme control.

$$v = \frac{QS^{\gamma}}{K_m + S} \tag{6.1}$$

where $\gamma > 1$ is the Hill coefficient. With increasing γ the system approaches off-on control in the reaction rate, as shown in fig. i 6.3.

If the concentration of S is sufficient small, the denominator in eq. 6.1 can be neglected, leading to $v \propto k_1 S^{\gamma}$, so that S is an activator for the rate of reaction. On the contrary, if v can be approximated by $v \simeq \frac{f(S)k_1}{k_2+S^{\gamma}}$, provided $f(S)$ is of order less than S, the substrate is an inhibitor, and the rate of reaction declines when γ becomes larger - in the same way as it increases for S being an activator, as in fig. 6.3.

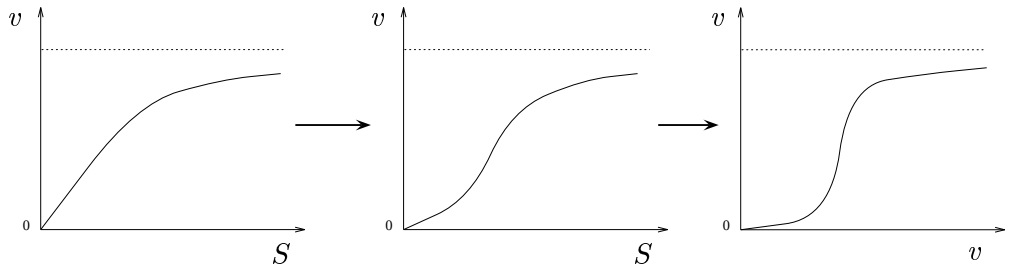

Figure 6.3: As γ increases the inflection of the curve becomes more dominant, and for sufficiently large γ the reaction rate is controlled by a virtual "on-off" switch sensitive to the concentration of S.

The properties of such coupled biochemical networks with allosteric enzymes

become very quickly complex. The modelling of such connected highly nonlinear systems is of course not too realistic, since the underlying assumption for eq.(6.1) is that E + nS combine to form a complex in one step. This is not very probable if $n > 2$, and often n is not even an integer. Normally one obtains two polynomials in S, $v = \frac{f(S)}{g(S)}$, but when we combine several reactions, and neglect fast intermediary reactions, the approximation by Hill type kinetics (eq. 6.1) can anyway be very useful for a qualitative understanding of the behaviour of the system, and reflect the experimental observations remarkably good.

6.1 Turings Mechanism with High Hill Numbers

A recent development in the understanding of these higly nonlinear control systems [14], is the recognition that a system gradually approaching off-on control, becomes increasingly prone to create phenomena known from the study of nonlinear dynamics, such as chemical oscillations and trigger waves, controlled pattern formation by Turings mechanism, as well as multistable systems.

We will limit our self to demonstrating that high cooperativity greatly facilitates pattern formation by Turings mechanism. Usually effective Hill numbers in such studies have been taken to be less than approximatively 3, as this equals the actual values measured for enzyme regulation in the cytoplasm. In genetic control systems, it is however common to have substantially larger Hill numbers, often apparently in excess of 8.

In particular, we will use the previous derived relations for the diffusion ratio to show that the diffusion constants may become almost equal in magnitude when the cooperativity of the defining kinetics becomes as high as is seen in genetic control systems. We shall demonstrate this for a number of particular models.

6.1.1 The Selkov Model

First consider the Selkov model in the renormalized form

$$\frac{\partial x}{\partial t} = 1 - xy^{\gamma} + D_1 \nabla^2 x \tag{6.2}$$

$$\frac{\partial y}{\partial t} = \alpha x y^{\gamma} - \alpha y + D_2 \nabla^2 y \tag{6.3}$$

which has the stationary solution $x_0 = y_0 = 1$. The Jacobian elements become $f_x = -1$, $f_y = -\gamma$, $g_x = \alpha$ and $g_y = \alpha(\gamma - 1)$.
Stability towards homogeneous oscillations are provided by

$$Tr = \alpha(\gamma - 1) - 1 < 0 \tag{6.4}$$

and det $= \alpha$. Thus an increasing cooperativity, measured by Hill constant γ, make the system more prone to autonomous oscillations, which is a well known result. For

$\gamma > 1$ the Jacobian becomes a Turing matrix of the form $(S2)$. The ratio between diffusion constants, inequality (4.39), evaluates to

$$\frac{D_-}{D_+} > \frac{1+\gamma+2\sqrt{\gamma}}{\alpha(\gamma-1)^2} > \frac{1+\gamma+2\sqrt{\gamma}}{\gamma-1} \tag{6.5}$$

where we have used inequality (6.4). Inequality (6.5) may be rewritten

$$\frac{D_-}{D_+} > \frac{\sqrt{\gamma}+1}{\sqrt{\gamma}-1} \tag{6.6}$$

For increasing cooperativity γ the ratio between diffusion constants approaches one.

In the following we shall demonstrate that the same may be shown for a number of other mechanisms. Whenever the effective Hill constant increases the critical ratio of diffusion constants approaches one. Thus Turing instabilities are greatly facilitated by high nonlinearity in the kinetics.

6.1.2 The Brusselator

To show this for an extension of the Brusselator scheme, consider the generalized kinetics

$$\frac{\partial x}{\partial t} = Ax^\gamma y - (B+1)x + 1 \tag{6.7}$$

$$\frac{\partial y}{\partial t} = -Ax^\gamma y + Bx \tag{6.8}$$

Usually γ is set to 2. Here we consider higher values. The stationary solutions are $x_0 = 1$, $y_0 = B/A$. With $w = B(\gamma-1)$, the Jacobian elements evaluate to $f_x = w - 1$, $f_y = A$, $g_x = -w$ and $g_y = -A$. Thus to have a Turing matrix we must have $w - 1 > 0$. The inequality (4.13) becomes

$$(w-1) - A < 0 \tag{6.9}$$

and det $= A$. Thus the ratio of diffusion constants must satisfy inequality (4.42) which evaluates to

$$\frac{D_-}{D_+} > \frac{A(1+w+2\sqrt{w})}{(w-1)^2} \tag{6.10}$$

$$> \frac{\sqrt{w}+1}{\sqrt{w}-1} \tag{6.11}$$

where we again have used the condition for the trace, inequality (6.9). Since $w = B(\gamma-1)$, increasing cooperativity again results in a ratio of diffusion constants approaching one.

Note however, that an increase in γ now may be compensated by a lower value of the effective rate constant B. However, if the other kinetics is unchanged, but the system has its cooperativity increased, then the system becomes increasingly a Turing system.

6.1.3 The Schnakenberg Model

We shall pursue with yet another mechanism, a generalized Schnakenberg model

$$\frac{\partial x}{\partial t} = A - x + x^{\gamma} y \tag{6.12}$$

$$\frac{\partial y}{\partial t} = -x^{\gamma} y + B \tag{6.13}$$

With the temporary abbreviation

$$w_1 = A + B \tag{6.14}$$

the stationary state evaluates to

$$x_0 = w_1 \tag{6.15}$$

$$y_0 = \frac{B}{(w_1)^{\gamma}} \tag{6.16}$$

and the Jacobian becomes

$$J = \begin{pmatrix} \frac{B\gamma}{w_1} - 1 & w_1^{\gamma} \\ -\frac{B\gamma}{w_1} & -w_1^{\gamma} \end{pmatrix} \tag{6.17}$$

This is a Turing matrix of type $S1$, Eq.(4.8) if matrix element $a > 0$ that is

$$\frac{B\gamma}{w_1} - 1 > 0 \tag{6.18}$$

The determinant is w_1^{γ} and the trace inequality (4.13) is

$$Tr = \frac{B\gamma}{w_1} - 1 - w_1^{\gamma} < 0 \tag{6.19}$$

The ratio of the diffusion constants, inequality (4.42), evaluates to

$$\frac{D_-}{D_+} > (w_1)^{\gamma} \frac{1 + \frac{B\gamma}{w_1} + 2\sqrt{\frac{B\gamma}{w_1}}}{(\frac{B\gamma}{w_1} - 1)^2} \tag{6.20}$$

From inequality (6.19)

$$(w_1)^\gamma > \frac{B\gamma}{w_1} - 1 \tag{6.21}$$

and thus (6.20) becomes,

$$\frac{D_-}{D_+} > \frac{w-1}{(\sqrt{w}-1)^2} = \frac{\sqrt{w}+1}{\sqrt{w}-1} \tag{6.22}$$

with

$$w = \frac{B\gamma}{w_1} = \frac{B\gamma}{A+B} \tag{6.23}$$

Again the ratio of diffusion constants approaches one when γ increases as w is proportional to the Hill constant γ.

6.1.4 The Gierer-Meinhardt Model

We proceed with a generalized version of a classic explicit activation-inhibition model, as proposed by Gierer and Meinhardt.

$$\frac{\partial x}{\partial t} = A - Bx + \frac{x^\gamma}{y} \tag{6.24}$$

$$\frac{\partial y}{\partial t} = x^\gamma - y \tag{6.25}$$

Observe that the term with high nonlinearity is not taken to be the same in the two rates, contrary to our earlier models. With

$$w_1 = \frac{B}{A+1} \tag{6.26}$$

the stationary concentrations are

$$x_0 = \frac{1}{w_1} \tag{6.27}$$

$$y_0 = \frac{1}{w_1^\gamma} \tag{6.28}$$

The Jacobian elements become $f_x = w_1\gamma - B$, $f_y = -w_1^\gamma$, $g_x = \gamma w_1^{-\gamma+1}$ and $g_y = -1$ respectively. This is a Turing matrix of type $A1$ in Eq.(4.8) provided $w_1\gamma - B > 0$. The trace and determinant evaluate to

$$Tr = w_1\gamma - B - 1 < 0 \tag{6.29}$$

$$\det = B > 0 \tag{6.30}$$

The ratio of diffusion constants is evaluated from inequality (4.42) to yield

$$\frac{D_-}{D_+} > \frac{B+\gamma w_1+2\sqrt{\gamma B w_1}}{(w_1\gamma - B)^2} \tag{6.31}$$

It is convenient to change to variable

$$w_2 = \frac{\gamma}{A+1} \tag{6.32}$$

and thus $\gamma w_1 = B w_2$. Using the trace inequality (6.29) $B(w_2-1) < 1$ inequality (6.31) becomes

$$\frac{D_-}{D_+} > \frac{1+w_2+2\sqrt{w_2}}{B(w_2-1)^2} \tag{6.33}$$

$$> \frac{1+w_2+2\sqrt{w_2}}{w_2-1} \tag{6.34}$$

$$= \frac{\sqrt{w_2}+1}{\sqrt{w_2}-1} \tag{6.35}$$

As w_2 is proportional to the Hill coefficient γ, we again find that for increasing cooperativity the ratio between diffusion coefficients converges to one.

6.1.5 The Lengyel-Epstein Model

Finally we consider a generalized Lengyel-Epstein model of the form

$$\frac{\partial x}{\partial t} = A - x - \frac{Cxy}{1+x^\gamma} \tag{6.36}$$

$$\frac{\partial y}{\partial t} = B\left(x - \frac{xy}{1+x^\gamma}\right) \tag{6.37}$$

Here the nonlinearity is only inhibitory, whereas our former examples were cooperative activation. With the abbreviation

$$w_1 = \frac{A}{C+1} \tag{6.38}$$

the stationary concentrations evaluate to

$$x_0 = w_1 \tag{6.39}$$

$$y_0 = 1 + w_1^\gamma \tag{6.40}$$

and the Jacobian matrix elements become

$$f_x = -1 - C + \frac{C\gamma w_1^\gamma}{1+w_1^\gamma} \quad , \qquad f_y = -\frac{Cw_1}{1+w_1^\gamma} \tag{6.41}$$

$$g_x = \frac{B\gamma w_1^\gamma}{1+w_1^\gamma} \quad , \qquad g_y = -\frac{Bw_1}{1+w_1^\gamma} \tag{6.42}$$

This is a Turing matrix of type $A1$ in Eq.(4.8) provided $f_x > 0$ that is

$$-1 - C + \frac{C\gamma w_1^\gamma}{1+w_1^\gamma} > 0 \tag{6.43}$$

The condition for the trace becomes

$$Tr = -1 - C + \frac{C\gamma w_1^\gamma - Bw_1}{1+w_1^\gamma} = -(C+1) + \frac{C\gamma(w_2-1) - Bw_1}{w_2} < 0 \tag{6.44}$$

where we have introduced another temporary abbreviation

$$w_2 = 1 + w_1^\gamma \tag{6.45}$$

The determinant is

$$\det = (C+1)\frac{Bw_1}{w_2} \tag{6.46}$$

and the ratio between diffusion constants, inequality (4.42) evaluate to

$$\frac{D_-}{D_+} \quad > \quad \frac{Bw_1}{w_2} \frac{(C+1) + \frac{C\gamma(w_2-1)}{w_2} + 2\sqrt{(C+1)C\gamma\frac{(w_2-1)}{w_2}}}{(\frac{C\gamma(w_2-1)}{w_2} - (C+1))^2} \tag{6.47}$$

Using inequality (6.44) in the form

$$\frac{Bw_1}{w_2} > \frac{C\gamma(w_2-1)}{w_2} - (C+1) \tag{6.48}$$

inequality (6.47) may be written

$$\frac{D_-}{D_+} \quad > \quad \frac{(C+1) + \frac{C\gamma(w_2-1)}{w_2} + 2\sqrt{(C+1)C\gamma\frac{(w_2-1)}{w_2}}}{(\frac{C\gamma(w_2-1)}{w_2} - (C+1))} \tag{6.49}$$

$$= \quad \frac{1+z+2\sqrt{z}}{z-1} \tag{6.50}$$

$$= \quad \frac{\sqrt{z}+1}{\sqrt{z}-1} \tag{6.51}$$

where we have finally introduced variable z by

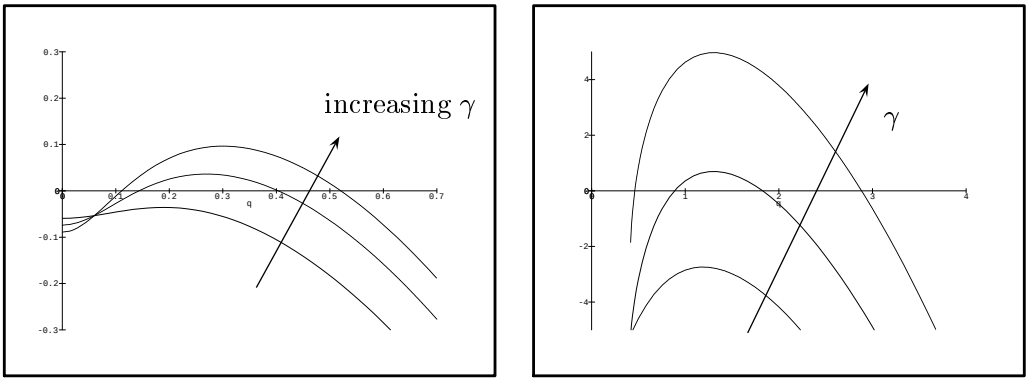

Figure 6.4: Pattern formation by Turings mechanism is facilitated by increasing cooperativity and thus high effective Hill constants γ in the defining rates. The dispersion relation is plotted for the Selkov model (left) an for the Lengyel-Epstein model (right) for three different γ each.

$$z = \gamma(\frac{C}{C+1})\frac{w_2 - 1}{w_2} = \gamma(\frac{C}{C+1})\frac{(\frac{A}{C+1})^\gamma}{1+(\frac{A}{C+1})^\gamma} \tag{6.52}$$

If

$$\frac{(\frac{A}{C+1})^\gamma}{1+(\frac{A}{C+1})^\gamma} \to 1 \tag{6.53}$$

which is fulfilled by

$$\frac{A}{C+1} \gg 1 \tag{6.54}$$

variable z becomes proportional to γ and thus again; the high cooperativity facilitates Turing structures, as the ratio between diffusion coefficients converges to one. The condition (6.54) is the same as stating that the stationary concentration of x fulfils $x_0 \gg 1$ which again means that the system operates on the strongly inhibitory side of the term

$$\frac{Cxy}{1+x^\gamma} \tag{6.55}$$

in the defining rates.
In all the models investigated here, we obtain an expression of the form

$$\frac{D_-}{D_+} > \frac{\sqrt{z}+1}{\sqrt{z}-1} \tag{6.56}$$

where z is function of γ, usually a linear function at least for suitable parameter values, and thus z increases with increasing cooperativity γ.

We shall proceed by noting that the dispersion equation Eq.(4.25) yields an increasing Turing region with increasing Hill number. In Fig. 6.4 we have calculated the eigenvalue λ from Eq.(4.25) as a function of wave number κ as is usual, but with the extension of plotting a set of such curves for increasing values of the Hill constant γ.

It is tempting to suggest, as a conjecture, that this will always be true, but even with occasional exceptions to this rule the above results show that a substantial class of models become Turing systems with increasing cooperativity. Thus the usually stated requirement of having effective diffusion coefficients differ by almost an order of magnitude, which is often found in systems with small Hill constants, is relaxed in gene control systems where much larger effective Hill constants have been recorded. Cooperativity with effective γ in excess of 8 has been recorded experimentally for several different gene control systems. Such high Hill constants may have developed under evolutionary pressure, as they are necessary for accurate control in other contexts, even in single cells, but such control systems also become increasingly prone to create spontaneous pattern formation by Turing mechanisms.

Table 1

z	$\frac{D_-}{D_+}$
2	5.83
4	3.00
8	2.09
16	1.67

Table 6.1: Ratio of diffusion coefficients D_-/D_+ in a Turing system approaches one when effective Hill constant increases according to Eq.(6.56). In this equation z is a function of the effective Hill constant γ and for a number of mechanisms it has been shown here that $z \simeq \gamma$ at least for suitable parameter combinations.

Chapter 7

Bistable Systems

7.1 A New Pattern Forming Mechanism in Bistable Systems

The recent experimental observations of a new type of stationary concentration patterns in a gel reactor reported by *Lee et.al.* [20, 21] are based on the bistable iodate-ferrocyanide sulfite reaction. For some values of the ferrocyanide concentrations, the system makes a hysteresis loop between the two homogeneous steady states as the flow rate is varied. The observed patterns are for some values initiated by finite amplitude perturbations inside the bistable area rather than through spontaneous symmetry breaking. For other values of the feed concentration, the lamellar patterns emerge spontaneously from the high pH state.

A variant of the Gray-Scott model proposed by Pearson [29] is regarded as a qualitative skeleton model for these phenomena. However, some further analysis shows that the patterns in this model rather are normal Turing structures emerging from one of the two stable states [30]. The enormous variety of observed structures in this model seems also to be a result of the permanent interaction with a Hopf bifurcation close to the saddle-node. The experimental results from Lee *et.al.* show stable labyrinthic patterns and fronts propagating towards each other until a critical separation where they stop. These observations suggest that the mechanism involved is somewhat different than a normal Turing branch emerging sub- or supercritically out of a stable state.

The approach in this chapter is based on the idea that the unstable steady state, enclosed by two stable steady states, can undergo a kind of Turing bifurcation or rather a secondary diffusion driven instability, where a spatial mode different from zero can be selected and form these reported pattern phenomena. With this pure Turing bifurcation from the unstable branch the patterns are markedly different by being irregular and pinned. When starting from the unstable branch any small perturbation breaks the symmetry and the two stable states catch or hold the pattern, and it does not seem possible for one specific mode to determine the global picture alone. In the next chapter we will also show that a front, starting the system from

one of the stable steady states, grows and spreads to fill space in the same way as observed in the experiment.

One of the important points in this scenario is again the required restriction of the ratio of the diffusion coefficients when a secondary Turing bifurcation emerges out of the unstable branch, and the comparison of the same restriction in a normal Turing bifurcation. The actual value of the required ratio of the diffusion coefficients is of course model dependent, but our hope is that the general picture for this new mechanism shows much less restrictive conditions for the emergence of stable spatial patterns than is the case with the previous ones.

In the next chapter we will first give a short review of the history of this reaction an thereafter derive a caricature model of the EOE model based on the reduction of the empirical rate-law model proposed by Gáspár and Showalter [32]. In many respects this simple model shows the same qualitative features as the experimental results by Lee *et al.* and it has the above discussed form. We will see that in some region of parameter space the ratio of the diffusion coefficients only needs to be slightly larger than one, and the patterns formed are highly irregular as is the case with the experimental results. In this chapter we will explore the general mechanism and discuss the importance of this from a more theoretical point of view. Some of the patterns formed from the model in the next chapter will anyway be shown here.

7.2 General Mechanism

Many of the models that have been developed to study diffusion-driven instabilities only exhibit a single homogeneous steady state as is the case for instance in the Brusselator and the Lengyel-Epstein model. This steady state can then, as we have seen, undergo a Turing instability leading to more or less regular structures. Recapitulating shortly; a normal two-component reaction-diffusion system

$$\begin{aligned} \frac{dx}{dt} &= f(x,y) + D_1\nabla^2 x \\ \frac{dy}{dt} &= g(x,y) + D_2\nabla^2 y \end{aligned} \tag{7.1}$$

has, after the normal linear expansion and introduction of a small perturbation, eigenvalues determined by the characteristic polynomial:

$$\lambda^2 - \lambda\left[Tr - \kappa^2(D_1 + D_2)\right] + P(\kappa^2) = 0 \tag{7.2}$$

At the critical point which is given by

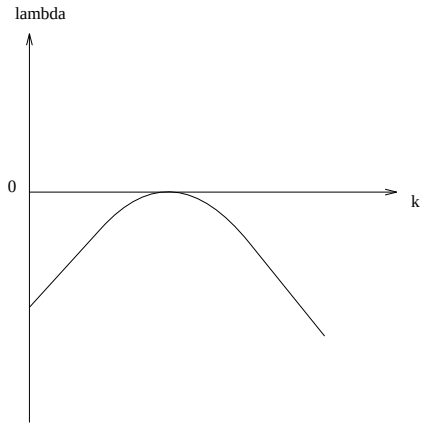

Figure 7.1: Schematical plot of the real part of the eigenvalue as a function of the spatial mode κ in a normal monostable model.

$$\frac{dP(\kappa)}{d\kappa} = 0 \qquad at \qquad \lambda(\kappa) = 0 \tag{7.3}$$

where

$$P(\kappa^2) = \kappa^4 D_1 D_2 - \kappa^2 (f_1 D_2 + g_2 D_1) + Det \tag{7.4}$$

the dispersion plot looks like fig.7.1: Only when $Re(\lambda) > 0$ for some $\kappa \neq 0$ we can have a growth of an instability to form spatial patterns.

When we perform the same analysis for a bistable system, which contains multiple steady states, eq.(7.2) becomes a threefold equation for each steady-state. The transition from a situation with one steady state to three occurs when a parameter a in the model passes through a bifurcation value. Fig.7.2 (left) is a (x_s, a) graph with a hysteresis loop and we expect the steady state in the middle to be linearly unstable. For simplicity we here confine our self to the case of a simple hysteresis loop, disregarding other multiple steady state systems like mushrooms and isolas. The dispersion relation looks schematically like fig. 7.2 (right).
For the stable steady-states s_1 and s_2 to bifurcate we require

$$\frac{dP(\kappa)}{d\kappa} = 0 \qquad at \qquad \lambda_s(\kappa) = 0 \tag{7.5}$$

But for the unstable branch to have a pattern selection different from the zero mode, an approximative requirement is

$$\frac{d^2 \lambda_u(\kappa)}{d\kappa^2} > 0 \qquad at \qquad \kappa = 0 \tag{7.6}$$

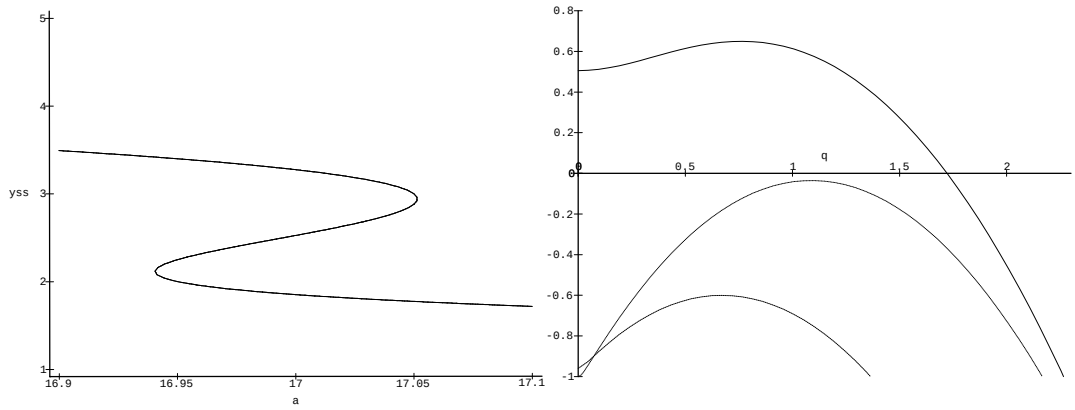

Figure 7.2: The left figure shows a normal bistable system with a hysteresis loop. By changing an appropriate control parameter, the system enters the bistable region. The right figure shows a schematical plot of the real part of the eigenvalue as a function of the spatial mode κ in a bistable system. s_1 and s_2 are the two stable steady-states surrounding the unstable steady-state u.

This requirement presumes that the only minima is located at $\kappa = 0$, and that there are no other local minima for $\kappa \neq 0$. This is in principle a wrong assumption, but there doesn't seem to be any physical example known, where this other type of bifurcation occurs (see [31], p.169). So, in effect, when a $\lambda_u(\kappa \neq 0) > \lambda_u(\kappa = 0)$ we can have a pattern selected, which is different than the pattern selected when the zero mode has the maximum growth.

7.2.1 The Diffusion Ratio in Bistable Systems

Here again we are interested in the ratio between the two diffusion coefficients. In chapter 4 we obtained the important relation (4.39) and (4.42) which gave us the necessary requirement for the diffusion coefficients. We saw that the self-inhibitor in general needs to diffuse 5 to 10 times faster than the self-activator. Here we find generally (by a numerical investigations of different bistable systems) that *this restrictive condition is relaxed in the case of bistable systems.* We can even obtain a similar expression as in section 4.3. When solving eq.(7.6) we obtain after some manipulations:

$$-D_1 - D_2 + \frac{-4TrD_1 - 4TrD_2 + 8f_1D_2 + g_2D_1}{4\sqrt{Tr^2 - 4Det}} < 0 \qquad (7.7)$$

Rearranging in order to get an expression for the ratio of the diffusion coefficients, we get:

$$\left(\frac{D_-}{D_+}\right)_u > -\frac{\sqrt{Tr^2-4Det}+Tr-2f_1}{\sqrt{Tr^2-4Det}+Tr-2g_2} \tag{7.8}$$

for systems with a Jacobian $(A2)$ and $(S2)$. The subscript u denotes that this inequality only is applicable for the unstable branch. For systems with a Jacobian $(A1)$ and $(S1)$ the inequality becomes

$$\left(\frac{D_-}{D_+}\right)_u > -\frac{\sqrt{Tr^2-4Det}+Tr-2g_2}{\sqrt{Tr^2-4Det}+Tr-2f_1} \tag{7.9}$$

In the models we have investigated, eq. 7.8 and 7.9 always gives a lower value than the same equation (4.39) and (4.42) obtained from the normal monostable Turing models. To illustrate this, look at figure 7.3. For a $d = \frac{D_1}{D_2} = 2$ it is only the unstable branch which after the criteria from 7.6 can give rise to a spatial structure. When decreasing d (that is, going upwards in the figure) the selected mode is lower, and the pinning effect is larger. Decreasing d below the critical ratio $d_c|_u$, it is the zero mode which has the larges exponential growth, and a droplet is formed. For even lower d the homogeneous steady state becomes dominant.

When increasing d (that is: going down in the figure), another scenario appears. Close to the primary Turing bifurcation of one of the stable steady states, $d_c|_s$ the pinning disappears. Beyond the bifurcation a new mode emerges.

A typical Turing structure in 2D emerging spontaneously out of the unstable branch is visualized in fig.7.4 together with a section through the 2D plot showing the profile of the concentration distribution.

7.3 Three Component Systems and Turing-Saddle node Interaction

Here we will try to obtain the conditions for the linear stability and for the emergence of Turing structures in a three component system. After that we will go on and analyse the co-dimension 2 problem of the interaction between the Turing and saddle-node bifurcation. The motivation for this is the thought that one can omit the fact that for two-component systems, the fastest growing mode κ^4 (from eq. 4.32):

$$\kappa^4 = \frac{Det}{D_x D_y} \tag{7.10}$$

goes to zero, since $Det = 0$ at the saddle-node, which again implies that the wavelength $\omega_c = \frac{2\pi}{\kappa_c}$ at the critical point goes to infinity.

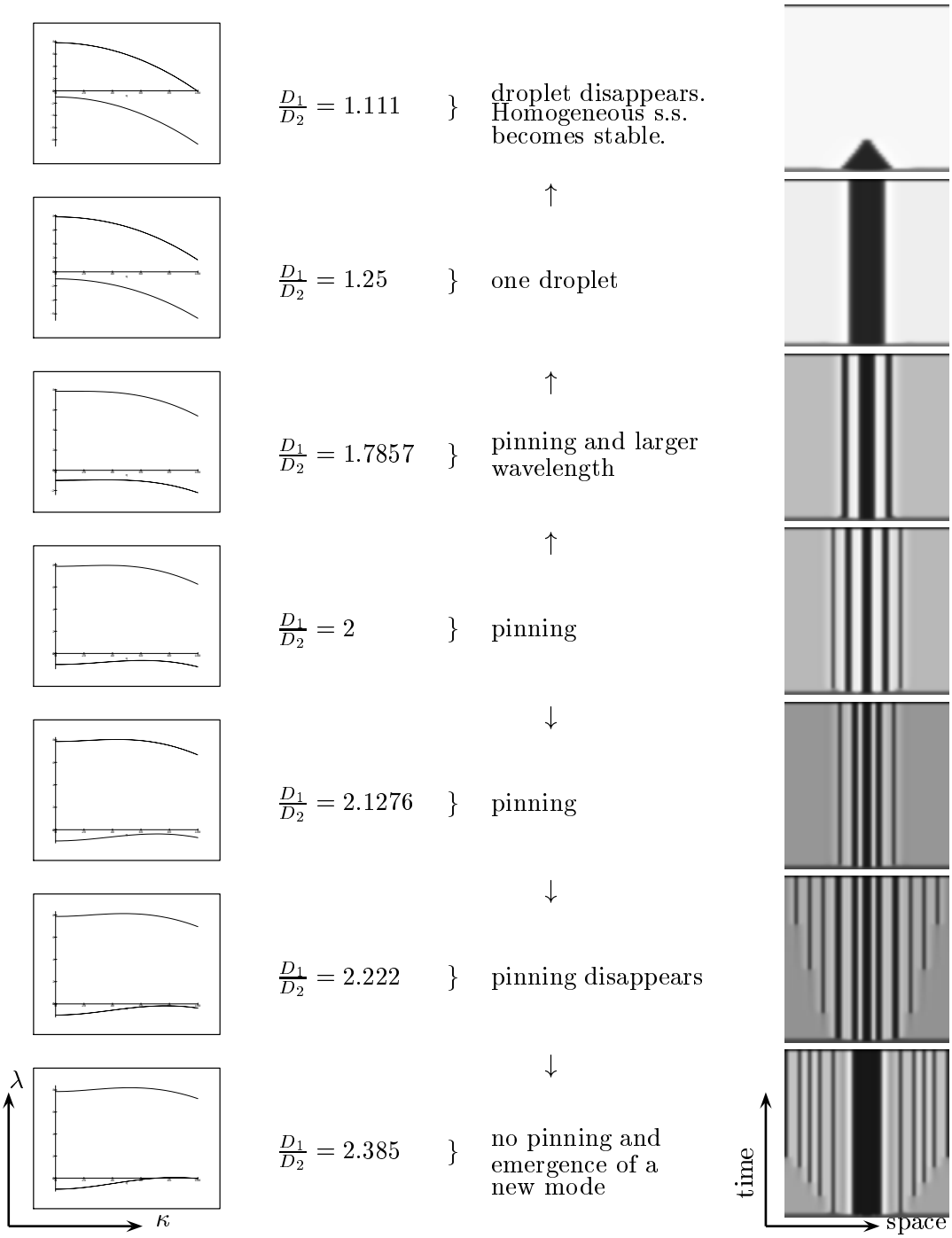

Figure 7.3: Space-time plots for 1D Turing structures and associated dispersion plots for the reduced EOE-model given in the next chapter. For the values $a = 30, b = 1, F = 11$ the critical diffusion ratio for the stable and unstable branch respectively has to be $d_c|_s = \left(\frac{D_1}{D_2}\right)_s = 2.30$ and $d_c|_u = \left(\frac{D_1}{D_2}\right)_u = 1.76$.

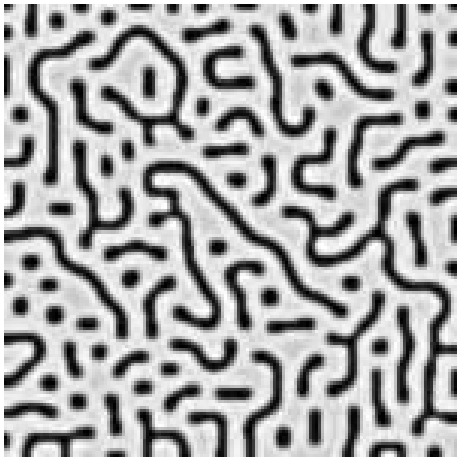

Figure 7.4: Turing bifurcation from the unstable branch only. The model is the reduced non-oscillatory EOE-model from chapter 8.

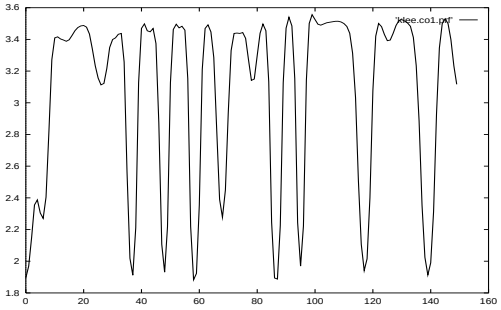

Figure 7.5: The corresponding profile plot for the y-component. The values are: $a = 17$, $b = 1$, $F = 7.65$, $\frac{D_-}{D_+} = 1.39$

$$\lim_{Det \to 0} \kappa_c^4 = 0 \qquad \Rightarrow \qquad \lim_{\kappa_c^4 \to 0} \omega_c \to \infty \tag{7.11}$$

In experiments one has never observed this. From the discussion in the first chapter, we of course aim to built models which are valid in the limits. So, this is one case where we have to admit a theoretical drawback of the model.

As an example, look at fig. (7.6) together with the dispersion plot (7.7). These figures are initiated very close to the co-dimension 2 point of a saddle-node and Turing bifurcation, started with noise from the unstable branch. Fig.(7.8) and (7.9) are initiated with the same parameters, but from the stable branch.

The patterns obtained should correspond to the analytical fact, that the wavelength of the pattern goes to infinity, since it is the zero-mode which is selected in the limit. But it is not clear from fig.(7.6) whether it has a large wavelength or not. Maybe it is not always the wavelength with the maximum exponential growth (eq. 7.10) that will be selected.

One might think that the reason for this incompatibility at the hysteresis point with the experiments is grounded in the fact, that we have confined our self to the study of two-variable models. So, this inconsistency might not exist for three-component systems. Therefore we will try to do the necessary linear analytical calculations for a general three-component Turing system, and derive an expression for the fastest growing mode κ_c^6.

First we can write down the three reaction-diffusion equations:

$$\frac{dx}{dt} = f(x, y, z) + D_x \nabla^2 x$$

Figure 7.6: The 2D-plot for the codim. 2 problem started from the unstable branch.

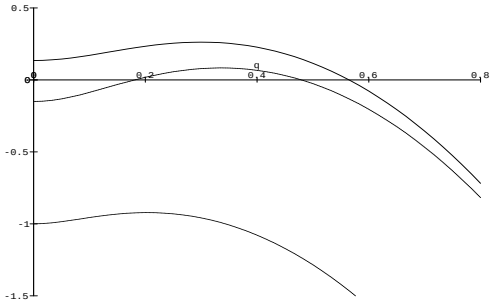

Figure 7.7: The dispertion plot close to the saddle node - Turing point. Both the stable and unstable branch bifurcate.

Figure 7.8: The 2D-plot for the codim. 2 problem started from the stable branch.

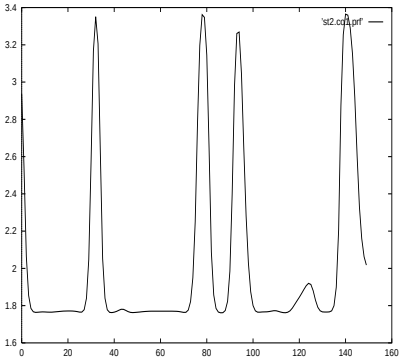

Figure 7.9: Shows the profile from the pattern from the unstable branch.

$$\begin{aligned} \frac{dy}{dt} &= g(x,y,z) + D_y\nabla^2 y \\ \frac{dz}{dt} &= h(x,y,z) + D_z\nabla^2 z \end{aligned} \tag{7.12}$$

Again, for the emergence of Turing structures a reaction-diffusion system exhibits diffusion-driven instabilities if the homogeneous steady-state is linear stable to small perturbations in the absence of diffusion but unstable to small perturbations when diffusion is present. Let us therefore start to look at the condition for the homogeneous case.

7.3.1 The Homogeneous Case

$$\begin{aligned} \frac{dx}{dt} &= f(x,y,z) \\ \frac{dy}{dt} &= g(x,y,z) \\ \frac{dz}{dt} &= h(x,y,z) \end{aligned} \tag{7.13}$$

A linear expansion after the introduction of a small perturbation gives the characteristic determinant:

$$\mathbf{M} = \begin{vmatrix} f_1 - \lambda & f_2 & f_3 \\ g_1 & g_2 - \lambda & g_3 \\ h_1 & h_2 & h_3 - \lambda \end{vmatrix} = 0 \tag{7.14}$$

obtaining the *characteristic equation*:

$$\lambda^3 - Tr(M)\lambda^2 + R(M)\lambda - Det(M) = 0 \tag{7.15}$$

where

$$Tr(M) = f_1 + g_2 + h_3 \tag{7.16}$$

$$R(M) = f_1g_2 - f_2g_1 + f_1h_3 - f_3h_1 + g_2h_3 - g_3h_2 \tag{7.17}$$

$$Det(M) = \begin{vmatrix} f_1 & f_2 & f_3 \\ g_1 & g_2 & g_3 \\ h_1 & h_2 & h_3 \end{vmatrix} \tag{7.18}$$

Applying the Routh-Hurwitz conditions (appendix B), we find that:

$$\triangle_1 = -Tr(M) > 0 \tag{7.19}$$
$$\triangle_2 = -Tr(M)R(M) + Det(M) > 0 \tag{7.20}$$
$$\triangle_3 = -Det(M)\triangle_2 > 0 \tag{7.21}$$

So, for the homogeneous system to be linear stable we require that

$$Tr(M) < 0, \qquad R(M) > 0 \quad and \quad Det(M) < 0 \tag{7.22}$$

7.3.2 The Reaction-Diffusion System

Now we progress with the full reaction-diffusion system. Again a linear expansion after the introduction of a small perturbation gives the full characteristic determinant:

$$\begin{vmatrix} f_1 - \kappa^2 D_1 - \lambda & f_2 & f_3 \\ g_1 & g_2 - \kappa^2 D_2 - \lambda & g_3 \\ h_1 & h_2 & h_3 - \kappa^2 D_3 - \lambda \end{vmatrix} = 0 \tag{7.23}$$

So we obtain the *characteristic equation*:

$$a_0\lambda^3 + a_1\lambda^2 + a_2\lambda + a_3 = 0 \tag{7.24}$$

where

$$\begin{aligned} a_0 &= 1 \\ a_1 &= -Tr(M) + \kappa^2(D_1 + D_2 + D_3) \\ a_2 &= R(M) + \kappa^4(D_1D_2 + D_1D_3 + D_2D_3) - \kappa^2(f_1(D_2 + D_3) \\ &\quad + g_2(D_1 + D_3) + h_3(D_1 + D_2)) \\ a_3 &= P(\kappa^2) \end{aligned}$$

The last term $P(\kappa^2)$ is the interesting one since it by changing sign from positive to negative may destabilize the system in order to give solutions of (7.24) with a positive real part. So the Turing instability may occurs when:

$$P(\kappa^2) = b_0\kappa^6 - b_1\kappa^4 + b_2\kappa^2 - Det(M) = 0 \tag{7.25}$$

where

$$\begin{aligned} b_0 &= D_1D_2D_3 \\ b_1 &= f_1D_2D_3 + g_2D_1D_3 + h_3D_1D_2 \\ b_2 &= D_1(g_2h_3 - g_3h_2) + D_2(f_1h_3 - f_3h_1) + D_3(f_1g_2 - f_2g_1) \end{aligned} \tag{7.26}$$

Setting $\lambda = 0$ and $\frac{dP(\kappa^2)}{d\kappa^2} = 0$ one obtains an expression for κ_c^2:

$$\kappa_c^2 = \frac{b_1 \pm \sqrt{b_1^2 - 3b_0b_2}}{3b_0} \tag{7.27}$$

In order to have κ^2 positive the requirements are:

$$b_1^2 - 3b_0b_2 > 0 \quad and \tag{7.28}$$

$$b_1 > 0 \qquad or \qquad b_2 < 0 \tag{7.29}$$

Now, if comparing $b_1 > 0$ with $Tr(M) < 0$ and $b_2 < 0$ with $R(M) > 0$ one reaches again to the restriction that:

$$D_1 \neq D_2 = D_3 \quad or \quad D_1 = D_2 \neq D_3 \tag{7.30}$$

As in the two-component system, Turing instabilities can occur only if the diffusion coefficients are unequal. Of course we must emphasize that the conditions derived here are necessary but not sufficient.

7.3.3 Turing-Saddle node Interaction

At the point of Turing bifurcation the critical mode goes like (7.27):

$$\kappa_c^2 = \frac{b_1 \pm \sqrt{b_1^2 - 3b_0b_2}}{3b_0} \tag{7.31}$$

We can try to isolate b_1 and b_2, obtaining:

$$b_1 = \frac{3}{2}b_0\kappa^2 + \frac{b_2}{2\kappa^2} \tag{7.32}$$
$$b_2 = -3b_0\kappa^4 + 2b_1\kappa^2 \tag{7.33}$$

Reinserting b_1 back in $P(\kappa)$ (7.25):

$$P(\kappa^2) = b_0\kappa^6 - \frac{3}{2}b_0\kappa^6 - \frac{1}{2}b_2\kappa^2 + b_2\kappa^2 - Det(M) \tag{7.34}$$
$$= -\frac{1}{2}b_0\kappa^6 + \frac{1}{2}b_2\kappa^2 - Det(M) = 0 \tag{7.35}$$

leading to:

$$\kappa^6 = \frac{Det(M) - \frac{1}{2}b_2\kappa^2}{-\frac{1}{2}b_0} \tag{7.36}$$

reinserting b_2 back in $P(\kappa)$

$$P(\kappa^2) = b_0\kappa^6 - b_1\kappa^4 - 3b_0\kappa^6 + 2b_1\kappa^4 - Det(M) \tag{7.37}$$
$$= -2b_0\kappa^6 + b_1\kappa^4 - Det(M) = 0 \tag{7.38}$$

leading to:

$$\kappa^6 = \frac{Det(M) - b_1\kappa^4}{-2b_0} \tag{7.39}$$

At the point of saddle-node bifurcation $Det(M) \to 0$ which means that $\kappa^4 \to \frac{b_2}{b_0}$, $\kappa^2 \to \frac{b_1}{2b_0}$ which again leads to:

$$\kappa^6 \to \frac{b_1 b_2}{2b_0^2} \tag{7.40}$$

Now we have to remember that one of the restrictions for a Turing instability was (7.29), which in means that either b_1 or b_2 must go through zero at the bifurcation point. So, here we again have the same result as from the two-component system, namely that $\kappa^6 \to 0$ at the point where the Turing and saddle-node intersects. Correspondingly the critical wavelength goes to infinity.

Our suggestion that the inconsistency between the model and experiments at the limit of hysteresis is due to the two-variable reduction, has not been verified. The same inconsistency is still existing for three variable models. Therefore, it might be necessary to use other analytical techiques at this singular point.

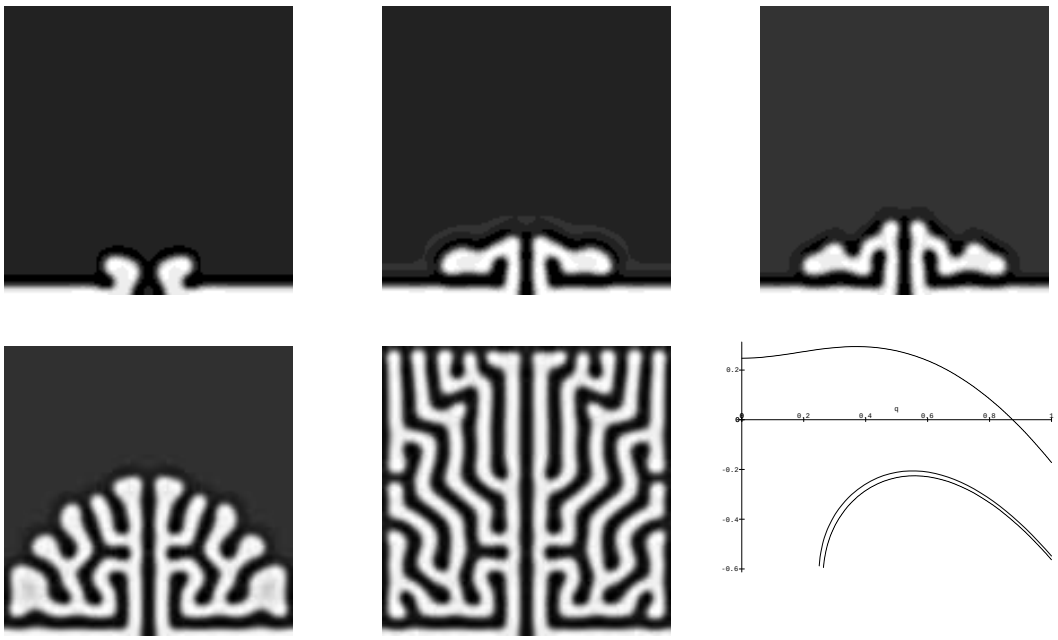

Figure 7.10: This simulation is made for an extension of the FHN-model: $\frac{du}{dt} = u + bu^2 - u^3 - v$; $\frac{dv}{dt} = eps(1 + a(u - v))$. The values of the constants are $a = 0.22, b = 1, eps = 2, \frac{D_-}{D_+} = 3$. The system was perturbed with $u = 0.5$ from the lower stable steady state $(u_s = 0, v_s = 0)$. The upper left picture shows the initial curvature of the front which gives a positive speed of these concave segments. This finally leads to a labyrinthic pattern. The dispersion curve for the chosen parameters is shown in the lower right picture. Only the linear unstable branch has a positive mode selection.

7.4 Labyrinthic Patterns

The recently observed patterns in bistable systems (in the Fitz-Hugh-Nagumo model [33] or experimentally in the Edblom-Orbán -Epstein reaction [20, 21] are markedly different in comparison with the normal obtained Turing structures. They are irregular and have typically a labyrinthic structure. Fig.(7.4) shows the development of two fronts approaching each other. The tip of the front destabilizes and at a critical distance the fronts stop instead of invading each other. But the edge of the front invades the whole space and produces a labyrinthic pattern. This scenario is investigated more closely in the next chapter, but it is interesting to note here that the labyrinthine structures observed in bistable systems are obtainable solely from a secondary diffusion driven instability emerging out of the middle unstable branch.

Chapter 8

The Edblom-Orbán-Epstein Reaction

8.1 The Ten- and Four Variable Models

In 1886 Landolt reported on his investigations of the iodate oxidation of sulfite. This so called classical *Landolt clock reaction* [24] is used in classroom demonstrations showing first a long period of slow reaction followed by a rapid conversion of reactants to products visualized by an indicator. His careful studies yielded an empirical expression for the complete consumption of sulfite as a function of reactant concentrations and temperature. This reaction and some variants, like the iodate-ferrocyanide reaction and the iodate-arsenous acid reaction, are interesting in their autocatalytic character, and the reaction with arsenite has served as a model system for the study of bistability [34].

Recently, Edblom, Orbán and Epstein [35] (EOE) found oscillatory behaviour in the iodate oxidation of sulfite in a CSTR when ferrocyanide was included as a reactant. A description of the reaction in terms of component processes and associated empirical rate laws was given by Gáspár and Showalter [36]. A detailed mechanism for these processes was proposed, and in result a ten-variable empirical rate-law (ERL) model reproduced the qualitative and even in some cases nearly quantitative dynamical behaviour of the system. The component processes for the 10-variable model are

$$\mathrm{IO_3^- + 8I^- + 6H^+ \rightleftharpoons 3I_3^- + 3H_2O} \qquad \text{(A)}$$

$$\mathrm{HSO_3^- + I_3^- + H_2O \rightleftharpoons HSO_4^- + 3I^- + 2H^+} \qquad \text{(B)}$$

$$\mathrm{2Fe(CN)_6^{4-} + I_3^- \rightleftharpoons 2Fe(CN)_6^{3-} + 3I^-} \qquad \text{(C)}$$

$$\mathrm{IO_3^- + 3HSO_3^- \rightleftharpoons I^- + 3HSO_4^-} \qquad \text{(D)}$$

$$\mathrm{H_2SO_3 \rightleftharpoons H^+ + HSO_3^-} \qquad \text{(E1)}$$

$$\mathrm{HSO_3^- \rightleftharpoons H^+ + SO_3^{2-}} \qquad \text{(E2)}$$

$$\mathrm{HSO_4^-} \rightleftharpoons \mathrm{H^+ + SO_4^{2-}} \qquad \text{(E3)}$$

The empirical rate law is then constructed by writing a differential equation for each of the variable species in the reaction equations. Eleven species result in a 10-variable dynamical system since the conservation of iron atoms allows elimination of one variable. A further reduction to eight independent variables could also be done when considering conservation relations between species containing sulfur atoms and species containing iodine atoms [36].

In a later paper [37] Gáspár and Showalter made a further reduction of the 10-variable ERL model to a four-variable model by considering the following simplifications:

1. Each process is expressed in terms of iodine with the triiodide equilibrium incorporated into the rate laws, thereby simplifying the stoichiometry.
2. Of the three acid equilibria involving the oxysulfur species, only the equilibrium between $\mathrm{HSO_3^-}$ and $\mathrm{SO_3^{2-}}$ is kept, since equilibria $E1$ and $E3$ are relatively unimportant over the pH range of a typical oscillation.
3. The concentrations of iodate, iodide, ferrocyanide and sulfate are in large excess, and therefore considered as constants.

After these simplifications we have reduced the dynamical system to a four-variable model consisting of the following symbolic reaction steps

$$\mathrm{A + Y} \underset{k_{-1}}{\overset{k_1}{\rightleftharpoons}} \mathrm{X} \qquad \text{(N1)}$$

$$\mathrm{X} \xrightarrow{k_2} \mathrm{Y} \qquad \text{(N2)}$$

$$\mathrm{2Y} \xrightarrow{k_3} \mathrm{Z} \qquad \text{(N3)}$$

$$\mathrm{Z + X} \xrightarrow{k_4} \mathrm{3Y} \qquad \text{(N4)}$$

$$\mathrm{Z} \xrightarrow{k_5} \qquad \text{(N5)}$$

where the corresponding species of the chemical reactions are $\mathrm{X = HSO_3^-}$, $\mathrm{Y = H^+}$, $\mathrm{A = SO_3^{2-}}$ and $\mathrm{Z = I_2}$.

The resulting ordinary diffrential equations for this system in a CSTR are then given by

$$\frac{dX}{dt} = k_1 AY - (k_{-1} + k_2 + k_4 Z + k_0)X \qquad (8.1)$$

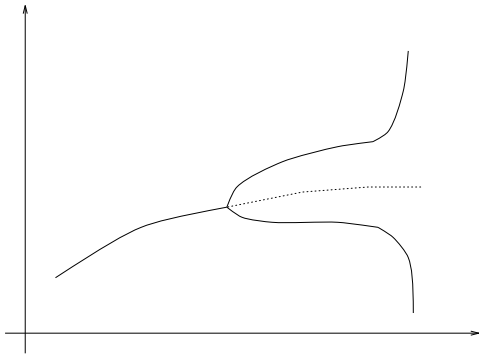

Figure 8.1: The amplitude of oscillations as the function of a parameter in the system showing a schematical canard bifurcation. Increasing a results in a normal supercritical Hopf-bifurcation, but at a certain point the amplitude of the oscillations growths much larger.

$$\frac{dY}{dt} = -k_1 AY + (k_{-1} + k_2 + 3k_4 Z)X - 2k_3 Y^2 + k_0(Y_0 - Y) \tag{8.2}$$

$$\frac{dZ}{dt} = k_3 Y^2 - k_4 ZX - k_5 Z - k_0 Z \tag{8.3}$$

$$\frac{dA}{dt} = -k_1 + k_{-1} X + k_0(A_0 - A) \tag{8.4}$$

where k_0 is the reciprocal residence time of the reactor. The last terms in the differential equations for Y and A are the CSTR terms for the in and out flow of hydrogen ion and sulfite.

This four-variable model shows most of the dynamical features from the ten-variable ERL-model and is also in quite good agreement with the experimentally observed behaviour. The oscillations in pH are qualitatively the same. When decreasing the inflow concentration of hydrogen ions (Y_0) the system undergoes a supercritical Hopf bifurcation revealing small-amplitude, high-frequency oscillations. Decreasing the Y_0 concentration further results in an abrupt change to large-amplitude, low-frequency oscillations, which suggests a canard [37, 38]. A *canard* is a false bifurcation in the sense that even though the quantitative behaviour undergoes a dramatic change, the qualitative, that is, the oscillatory behaviour, remains. Fig.8.1 shows this schematically. A similar canard is found in the 10-variable ERL-model [36].

8.2 Reduction to a Two-variable Model

A further reduction to a minimal two-variable model is of course a desirable goal, and in order to do so, one needs to find the species which are the fastest variables.

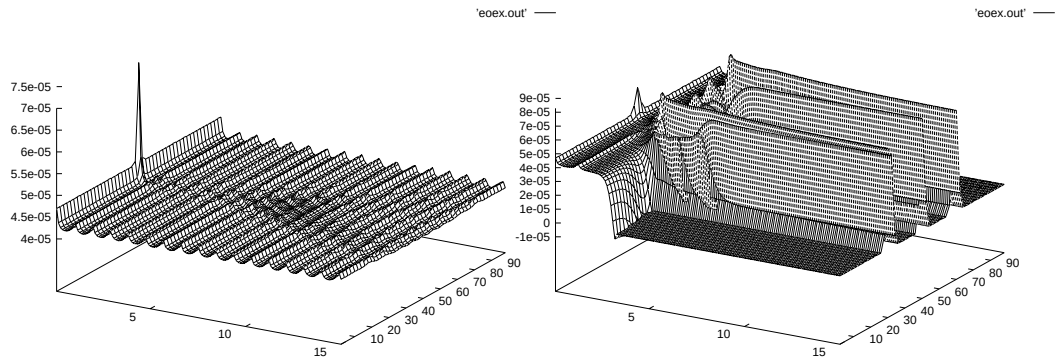

Figure 8.2: The left figure shows (for $Y_0 = 4.0e-3$) small-amplitude, high-frequency oscillations. For $Y_0 = 3.8e-3$ one obtains a Turing structure with $\frac{D_-}{D_+} = 10$ as shown in the right figure. The other values are $k_0 = 1.5e-3, k_1 = 5.0e+10, k_{-1} = 8.1e+3, k_2 = 6.0e-2, k_3 = 7.5e+4, k_4 = 2.3e+9, k_5 = 30, A_0 = 9.0e-2$.

They relax to their steady-state values much faster than the other species, and it is therefore possible to apply the pseudo steady state hypothesis as described in chapter 2. When examining the scaled equations and the resulting nondimensional parameters, it is seen that the variables A and Z are very fast in comparision with X and Y [37]. Thus, assuming $\frac{dA}{dt} = 0$ and $\frac{dZ}{dt} = 0$, we can find the steady-state values as

$$A_s = \frac{k_{-1}X + k_0 A_0}{k_1 Y + k_0}, \qquad Z_s = \frac{k_3 Y^2}{k_4 X + k_5 + k_0} \tag{8.5}$$

and then the two-variable model becomes

$$\begin{aligned} \frac{dX}{dt} &= k_1 A_s Y - (k_{-1} + k_2 + k_4 Z_s + k_0)X \\ \frac{dY}{dt} &= -k_1 A_s Y + (k_{-1} + k_2 + 3k_4 Z_s)X - 2k_3 Y^2 + k_0(Y_0 - Y) \end{aligned} \tag{8.6}$$

The variables A and Z are not really eliminated. They are rather "hidden variables" since they are expressed in terms of the other variables X and Y. This of course makes the resulting two-variable model more complex in the kinetic terms and much more intractable for the mathematical analysis.

It is remarkable that even this minimal two-variable model shows many of the experimental features as a hysteresis loop, a supercritical Hopf bifurcation and an

associated canard behaviour with large oscillations in pH. When adding diffusion to these equations, it is possible to obtain some Turing structures for the right experimental reaction constants by tuning the flow rate Y_0 as shown in fig. 8.2.

But these structures are always associated with a Hopf bifurcation and they are outside the bistable area. The bistable region itself is inside the canard. Consequently, the oscillations are so large and fast in this region that any numerical approach was more or less impossible. Because of the stiffness of the system, any two dimensional program simulating these equations broke down and only because of the very sensitive step length control in the 1D program used especially in chapter 5, it was possible to obtain these structures shown above.

The problem was then to try to find a good model which resembles the minimal EOE model qualitatively, and which makes analytical and numerical calculations practicable.

8.3 The Reduced Non-Oscillatory EOE-Model

It would of course be desirable to use the "real" empirical rate equations 8.7 instead of models with only partial qualitative resemblence, but the information content of the obtained dynamical behaviour in these "real" equations is very limited, since we only can have a vague knowledge of which mechanism corresponds to which phenomenon. When we want to examine dynamical features in space and time from a more theoretical point of view, it is very important to facilitate the analysis by using a simple model. Only in this way one can get a general understanding of the different mechanisms contributing to the complex behaviour of nonlinear dynamical systems in nature. The characterization of bifurcation points and pattern selection processes is then a matter of some few parameters contained in the caricature model.

The motivation for the development of a simple model was not the oscillatory behaviour of the EOE-reaction, but rather the possibility for Turing structures in the bistable region. The experimental observations by Lee et.al.[20] suggested that the interaction with a bistable state results in new, and highly irregular stationary patterns in contrast with the regular patterns such as hexagons, squares and stripes that have been observed in many nonequilibrium systems. The figures 8.3 and 8.4 are typical experimentally obtained structures for the idate oxidation of sulfite when ferrocyanide is added.

In the first approach we therefore restricted ourself to the study of Turing-saddle node interactions, and try to omit Hopf bifurcations.

A non-oscillatory simple variant of the EOE-reaction, based on parametric simplifications of the scaled two-variable EOE-model and other approximations, results in a two variable model given by reaction $M1 - M5$

$$\xrightarrow{k_1} \quad \mathrm{Y} \qquad \text{(M1)}$$

Figure 8.3: Experimentally obtained patterns for the EOE-reaction when ferrocyanide is included. A typical labyrinth pattern.

Figure 8.4: Fronts in the experiment propagate towards each other until they reach a critical distance where they stop.

$$\mathrm{A} + \mathrm{Y} \underset{k_{-2}}{\overset{k_2}{\rightleftharpoons}} \mathrm{X} \qquad \text{(M2)}$$

$$2\mathrm{Y} + \mathrm{X} \xrightarrow{k_3} 3\mathrm{Y} \qquad \text{(M3)}$$

$$\mathrm{X} \xrightarrow{k_4} \qquad \text{(M4)}$$

$$\mathrm{Y} \xrightarrow{k_5} \qquad \text{(M5)}$$

A short comparison with the four variable model (reaction steps $N1 - N5$) shows that

1. The two bimolecular reaction steps $N3$ and $N4$ are now replaced by the autocatalytic threemolecular reaction step $M3$ which is a reasonable approximation when the reaction constants k_3 and k_4 in $N3, N4$ are high (the experimental values are $k_3 = 7.5\text{x}10^4 m^{-1}s^{-1}, k_4 = 2.3\text{x}10^9 m^{-1}s^{-1}$.
2. The step $M4$ is new, and introduces an asymmetry in the system.
3. We expect A to be in excess, and therefore it is set to a constant which is different from expressing it as a hidden variable. The step $N2$ is then also accounted for in the revese step of $M2$. This simplification is the major difference and needs maybe some more investigation in order to be justified completely [40].

With this mechanism the rate law becomes:

$$\frac{dX}{dt} = -k_3 XY^2 + k_2 AY - (k_{-2} + k_4)X + D_x \nabla_\chi^2 X$$

$$\frac{dY}{dt} = k_3XY^2 - (k_5 + k_2A)Y + k_{-2}X + k_1 + D_y\nabla_\chi^2 Y \tag{8.7}$$

where we have included diffusion. After an appropriate non-dimensionalization (see appendix B) we get:

$$\begin{aligned} \frac{du}{d\tau} &= c\left[-uv^2 + av - (1+b)u\right] + D\nabla_s^2 u \\ \frac{dv}{d\tau} &= c^{-1}\left[uv^2 - (1+a)v + u + F\right] + \nabla_s^2 v \end{aligned} \tag{8.8}$$

where

$$\begin{aligned} &u = \tfrac{X}{X_0} \quad X_0 = \tfrac{k_5}{k_3 Y_0} \quad a = \tfrac{k_2 A}{k_5} \quad c = \tfrac{k_{-2}}{\sqrt{k_5 k_{-2}}} \\ &v = \tfrac{Y}{Y_0} \quad Y_0 = \sqrt{\tfrac{k_{-2}}{k_3}} \quad b = \tfrac{k_4}{k_{-2}} \quad F = \tfrac{k_1 k_3 Y_0}{k_5 k_{-2}} \\ &\tau = \tfrac{t}{t_0} \quad t_0 = \tfrac{\chi_0^2}{D_y} \quad D = \tfrac{D_x}{D_y} \\ &s = \tfrac{\chi}{\chi_0} \quad \chi_0^2 = \tfrac{D_y}{\sqrt{k_5 k_{-2}}} \end{aligned} \tag{8.9}$$

We will now try to make a linear stability analysis in order to find the different properties of this system. We will find the bistable region and the line of Turing bifurcation.

8.3.1 The Homogeneous System without Diffusion

In the following approach we will limit ourself to the case where $c = 1$. The steady states of the system are then for the first component given by

$$u_0 = \frac{av_0}{v_0^2 + 1 + b} \tag{8.10}$$

and the steady states of the second component are given by the cubic polynomial

$$v_0^3 - Fv_0^2 + (1 + b + ab)v_0 - F(1 + b) = 0 \tag{8.11}$$

Descartes' rule of signs (appendix B) tells us that there is a possibility for three positive real roots since the number of sign changes in the sequence of coefficients is three. Consequently, it should be possible to obtain three positive and real steady states (u_0, v_0) for a right choice of the parameters a, b and F. A numerically obtained example is given in fig.8.5.

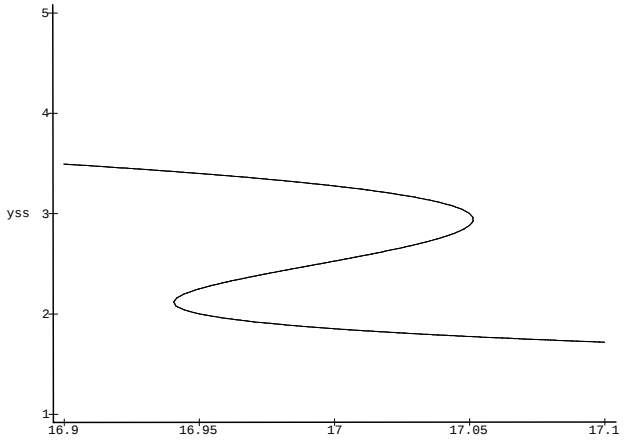

Figure 8.5: (v_s, a)- graph showing bistability. When changing a back and forth, one makes a hysteresis loop, since the middle line is an unstable steady state encapsulated by two stable steady states. The other constants are: $F = 7.65$ and $b = 1$.

The Jacobian matrix evaluated at a steady state is:

$$\mathbf{J_0} = \begin{pmatrix} -v_0^2 - 1 - b & a - \frac{2av_0^2}{v_0^2+1+b} \\ \\ v_0^2 + 1 & \frac{2av_0^2}{v_0^2+1+b} - 1 - a \end{pmatrix} \tag{8.12}$$

and for $v_0 > \sqrt{\frac{2(1+a)}{a-1}}$ we have:

$$\mathbf{J_0} = \begin{pmatrix} - & - \\ + & + \end{pmatrix} \tag{8.13}$$

which is a $(S2)$-form, allowing Turing instabilities to occur.

8.3.2 The Saddle-node Bifurcation

The criteria for a saddle-node bifurcation; i.e. the emergence of bistability is that the determinant of the jacobian goes from a positive to a negative value through zero:

$$Det(\mathbf{J}_0) = v_0^2 + 1 + b + ab - \frac{2abv_0^2}{v_0^2 + 1 + b} = 0 \tag{8.14}$$

Evaluating this equation for real solutions, this condition can only be achieved when:

$$a \geq 8 + \frac{8}{b} \tag{8.15}$$

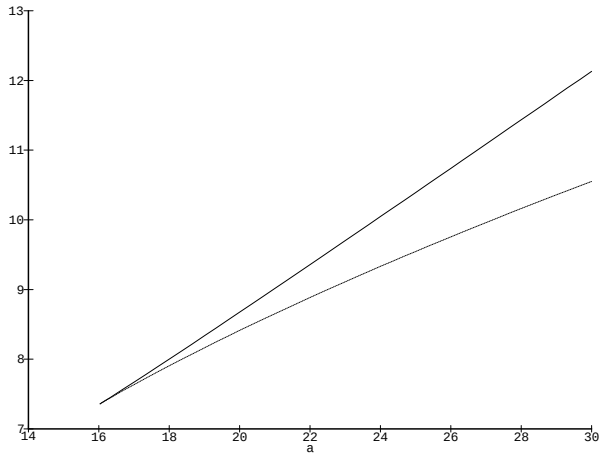

Figure 8.6: Phase-space plot of parameter F versus parameter a. Determines the bistable region for $b = 1$. The point where the two curves in phase-space meet is sometimes referred to as a *cusp*.

For $b = 1$ the hysteresis point is at $a = 16$, and for $a > 16$ we are in the bistable area. A function for the width of the bistable area in terms of parameter F is for the case of real solutions obtained by the explicit roots of the cubic polynomial (see for instance [4]), leading to

$$F_{border} = \frac{1}{3}\left[-\frac{2}{9}F^3 - (2 + 2b - ab)F\right]^2 - \frac{4}{3}\left[\frac{1}{3}F^2 - 1 - b - ab\right]^3 \tag{8.16}$$

For a given value of the parameters a and b, the parameter F has to be within the region shown in fig.8.6, determined by eq.(8.16) This determines the bistable region in phase space.

8.3.3 Patterns in the Bistable Region

Here we want to analyse some pattern selection mechanisms, when simulating the model with different initial conditions such as small noise around the Turing-destabilized branch, or different kinds and strenght of perturbations. We will also try to illustrate the front dynamics of the model. But from the position of parameters we will restrict ourself to the case of figure 8.5, and only analyse patterns that are related to different locations on this figure, i.e the parameters b and F will be fixed. In the pictures the white colour always corresponds to low pH, that is, to a high concentration of $v \equiv H^+$.

A normal 2D-Turing pattern emerging solely from the unstable branch has been shown in the previous chapter (fig. 7.4). When moving outwards to the border of bistability, say to $a = 17.04$, we obtain again a structure for the unstable branch, see fig. 8.7. But in this case, also a normal Turing bifurcation on the upper stable branch

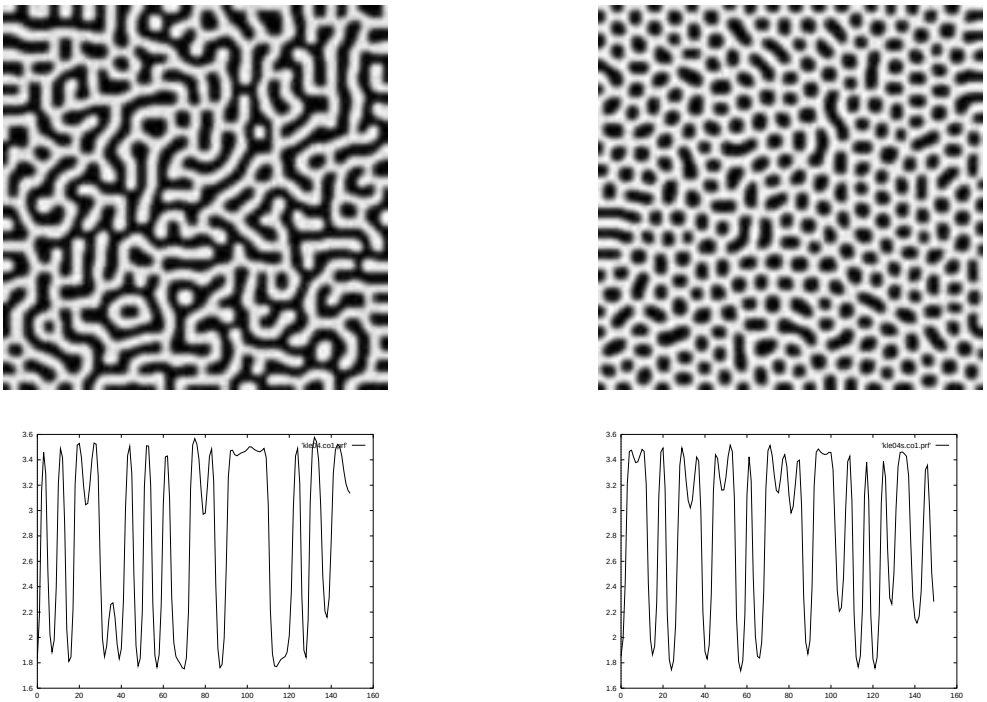

Figure 8.7: The pictures on the left hand side illustrate a Turing structure in 2D (top) appearing spontaneously from the unstable branch, and the corresponding profile plot (bottom) which is obtained by cutting through the middle of the grid. The right hand side shows a Turing structure appearing spontaneously from the upper stable branch. While the pattern from the unstable branch has an irregular labyrinthic structure, the pattern from the stable branch shows more "normal" hexagonal symmetry as has been seen in most mono-stable Turing models. The parameter values for both pictures are $a = 17.04, b = 1, F = 7.65, \frac{D_-}{D_+} = 1.39$, and both are induced with noise.

has appeared. A structure of hexagonal symmetry may then emerge spontaneously from this state.

The continuation of the stable stationary pattern from the normal Turing bifurcation (fig. 8.7) outside the bistable area to $a = 17.06$, still gives rise to patterns (see fig. 8.8), and a transition from hexagons to stripes is observed. The continuation of spatial structures towards the direction of marginal stability and further outside the bistable domain, has also recently been observed by Pearson in the Gray-Scott model. There the structures obtained emanate from a Turing instability on the upper stable branch of an isola appearing between the Hopf and Saddle node bifurcation.

It is interesting to see the qualitative differences between structures emerging out of the upper branch and structures emerging out of the unstable middle branch

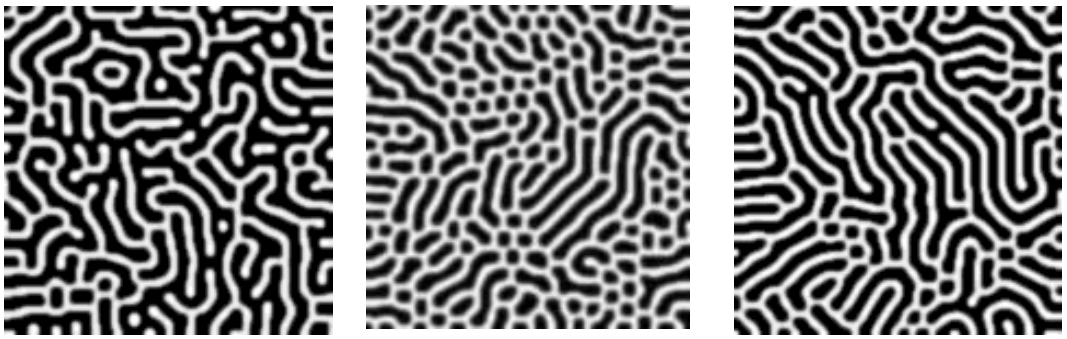

Figure 8.8: Here the left most figure shows a structure from the unstable branch continued outside the bistable domain ($a = 17.07$). In comparison with the previous figure, the lower stable branch (the only existing) is more dominant (the black region occupies more space). The figure in the middle is a continuation of the pattern from the stable branch (middle $a = 17.06$). The hexagonal symmetry dissolves into stripes. For $a = 17.07$ this effect is even more clear (in the figure on the right hand side).

(both outside the bistable domain). For $a = 17.07$ the figures in fig. 8.8 are obtained. In this parameter region only the lower steady state exists (black color) and becomes more dominant. The pattern from the middle unstable branch (most left) also has an other mode selection and is still more irregular.

8.3.4 Front Dynamics and Morphological Instabilities

In order to illustrate the dynamics of fronts in this system, the following simulations are performed. At the initial time, the system is prepared in the lower homogeneous steady state. A front with a concentration in between the middle and upper branch is then induced in the middle of the grid where one third of the front is displaced one pixel, as seen from the first left picture in fig. 8.9. For the chosen parameter values ($a = 17$) the upper state is dominant. This results in a invasion of the front, which finally fills the whole space (the final picture is not shown here). From the profile plot one can see that the concentration at the edge of the front is larger than behind. With a one pixel displacement of a part of the front, there is no significant morphological instability.

A different scenario appears when two fronts are induced for instance at the border on the lower boundary of fig. 8.10. Along the x-axis these fronts move towards each other, but the substrate v is deflected from the region between the two approaching fronts. This repulsion implies the slowing down of the progression of these waves. At a critical distance, the level of v is sufficiently low to completely block the propagation and thus give give rise to a stable domain of the initial lower state bounded by the other state. It is indeed known that nonvariational bistable models

Figure 8.9: The upper steady state invades the whole space with $a = 17$.

may exhibit intrinsic localized structures which coexist in the spatial juxtaposition of the various stable states [30]. As the front invades the teritory of the lower state in the y-direction, it traces a furrow of this state in the domain of the other (see fig. 8.10).

The front undergoes a morphological instability when $\delta = \frac{D_-}{D_+}$ is sufficiently large. This instability occurs when the effective diffusion coefficient $\nu(\delta)$ appearing in the eikonal expression [41] of the front velocity $v(k)$ goes to zero, i.e. when $\nu(\delta) = 0$), where

$$v(k) = v_n - \nu k \tag{8.17}$$

and v_n is the velocity of the planar front and k the curvature, which is positive for convex segments in the direction of propagation. As shown in fig. 8.10 $\nu < 0$ for $\delta = 1.39$. In agreement with eq. 8.17 the convex segments of the front move more slowly than the planar front, whereas the concave parts near the tip of the localized structure have a larger velocity. As the front continues to progress, the appearing convex segments act as nucleating centers for the formation of new stripes of the initial state embedded in the other one.

This simulation suggests that the formation of large amplitude labyrinthine structures results from the combination of two effects:

1. The morphological instability of the front connecting the two stable states.
2. The existence of stable motionless solitary waves of the lower state.

Both effects are favored by a large value of the ratio of the diffusion coefficients. There is indeed a striking resemblence in the patterns obtained by the above simulations and the experimentally obtained patterns in fig. 8.3 and 8.4. This strongly suggests that the outlined mechanism, which is new in the context of Turing structures, gives an important contribution to the theoretical understanding of experimentally observed spatial structures.

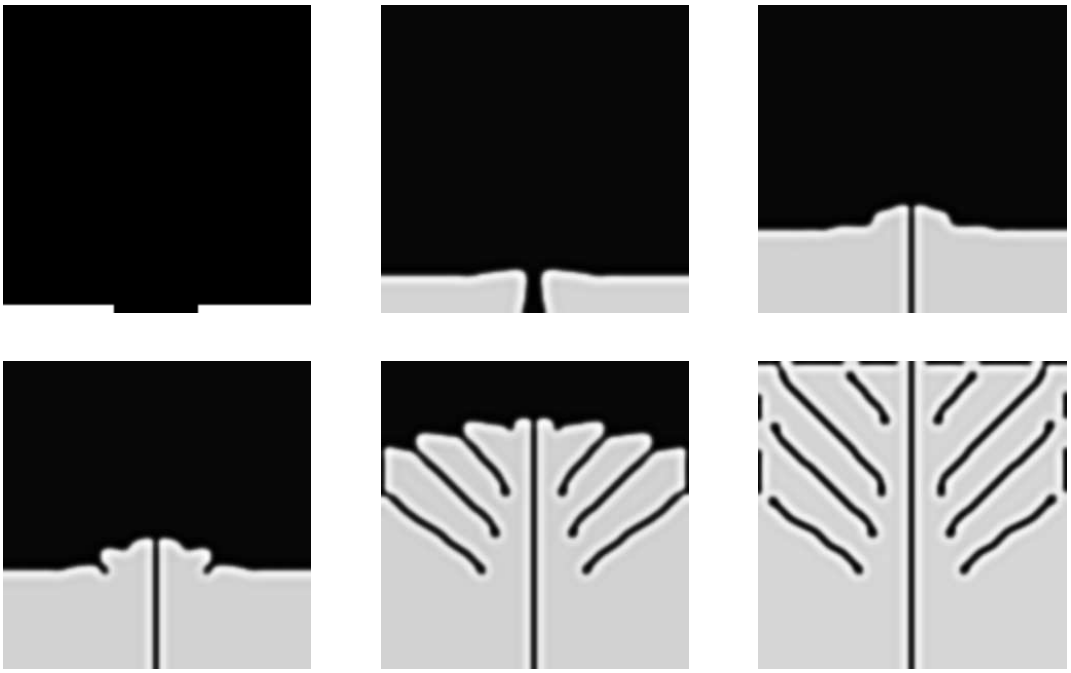

Figure 8.10: The evolution of two fronts in 2D, induced at the lower boundary of the grid. The upper left figure shows the initial state and the succesive figures on the right and in the lower row illustrate the emerging mophological instabilities and the remaining stable domains of the initial state (black) at different times.

8.3.5 Localized Structures

When a front stops to move, the structure becomes stationary and the pattern is called a localized structure. In the simulations of the reduced EOE-model this effect seems to be very common. It might be due to the fact that the Turing destabilized branch, which in our investigations is the middle homogeneously unstable branch, lies in between two stable and Turing stable branches that emerged out of the saddle node, and not because of any subcritical Turing bifurcation. The front velocity approaches zero as some non-adiabatic effects start to have influence on the dynamics. This effect is called intrinsic pinning. The weakly nonlinear theory of amplitude equations does not contain any explanation of the pinning effect.

A typical localized structure is shown in fig. 8.11. The pattern is started at the unstable middle branch and there was made a perturbation at one pixel in the middle of the grid. The evolution in time results in the successive development of concentric rings with a definite wavelenght. The number of rings depend on the size of perturbation. If the perturbation is small the effect is small and the number of rings is small, and if the perturbation is large, the concentric fronts which develop out can fill the whole space.

The same scenario appears when the simulation is initiated at for instance the

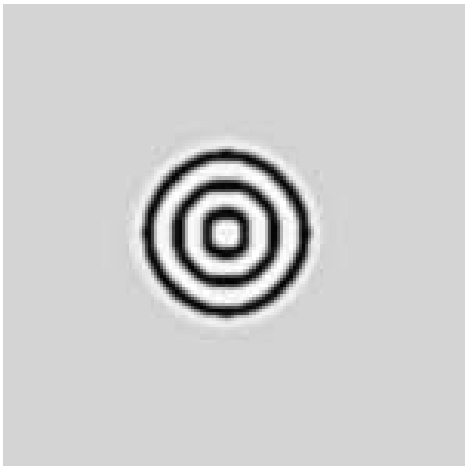

Figure 8.11: A localized structure which is initiated by a perturbation in the middle of the grid. The (more or less) concentric rings a stable and do not break up. The number of rings depends on the size of the perturbation. The parameters are: $a = 17, b = 1, F = 7.65, D_1 = 0.005, D_2 = 0.0036$ and the initial state is $u_0 = 5.1251545, v_0 = 2.5248455$.

lower stable branch, and the perturbation in the middle of the grid hits the region between the two higher states. Then the spatially unstable modes again create stable succesive rings of the lower vs. higher state, and the final pattern is the same as fig. 8.11. As it is the case of the one-dimensional simulations in chapter 4, or even more, it is very important to note the crucial dependence of the initial conditions and the size of the perturbation. Together with the intrinsic wavelenght chosen by the system, the final pinned structure relies fundamentally on these aspects. In this context one can imagine that it is possible to obtain an indefinite number of different pattern which all are stabilized by the effects discussed above. See fig. 8.12.

Figure 8.12: Self portrait. An intrinsic piece of art, started with appropriate initial perturbations. The structure is stable and the parameters are as before.

Appendix A

Ginzburg-Landau Parameters for the Selkov Model

Here we will shortly outline how to derive the parameters for the Ginzburg-Landau equation for a specific example. We want to derive a small amplitude equation near a Hopf bifurcation point for the Selkov model, and determine whether it is a super- or a subcritical Hopf bifurcation. The way to progress is similar as in [42], wherein references and the theoretical background is to be found.

We express the reaction-diffusion equation in terms of $\mathbf{u}(\mathbf{r}, t)$ and the deviation from the uniform steady state as

$$\frac{\partial \mathbf{u}}{\partial t} = (\mathbf{L} + \mathbf{D}\nabla^2)\mathbf{u} + \mathbf{Muu} + \mathbf{Nuuu} + ... \tag{A.1}$$

where $\mathbf{L}$ is the Jacobian matrix and $\mathbf{M}$ and $\mathbf{N}$ are tensors whose ith components are given as

$$(\mathbf{Muu})_i = \sum_{j,k} \frac{1}{2!} \frac{\partial^2 F_i(X_0)}{\partial X_{0j} \partial X_{0k}} u_j u_k, \tag{A.2}$$

$$(\mathbf{Nuuu})_i = \sum_{j,k,l} \frac{1}{3!} \frac{\partial^3 F_i(X_0)}{\partial X_{0j} \partial X_{0k} \partial X_{0l}} u_j u_k u_l \tag{A.3}$$

We can define a small positive parameter ϵ by $\epsilon^2 \chi = \mu$, where χ is equal to the sign of μ and ϵ is regarded as a measure for the amplitude to lower order. We also introduce a scaled time τ by $\tau = \epsilon^2 t$ and a scaled space coordinate s by $s = \epsilon r$. The time and space differentiations are thus transformed to

$$\frac{d}{dt} \to \frac{\partial}{\partial t} + \epsilon^2 \frac{\partial}{\partial \tau}, \tag{A.4}$$

$$\nabla \to \epsilon \nabla_s \tag{A.5}$$

Together with the transformations (A.4, A.5) and the expansion coefficients

$$\mathbf{L} = \mathbf{L}_0 + \epsilon^2\chi\mathbf{L}_1 + \epsilon^4\mathbf{L}_2 + ... \quad (A.6)$$
$$\mathbf{M} = \mathbf{M}_0 + \epsilon^2\chi\mathbf{M}_1 + \epsilon^4\mathbf{M}_2 + ... \quad (A.7)$$
$$\mathbf{L} = \mathbf{N}_0 + \epsilon^2\chi\mathbf{N}_1 + \epsilon^4\mathbf{N}_2 + ... \quad (A.8)$$

we can substitute all together in (A.1) and obtain a set of balance equations in the form

$$\left(\frac{\partial}{\partial t} - \mathbf{L}_0\right)\mathbf{u}_v = \mathbf{B}_v, \qquad v = 1, 2, ... \quad (A.9)$$

where

$$\mathbf{B}_1 = 0, \quad (A.10)$$
$$\mathbf{B}_2 = \mathbf{M}_0\mathbf{u}_1\mathbf{u}_1, \quad (A.11)$$
$$\mathbf{B}_3 = -\left(\frac{\partial}{\partial t} - \chi\mathbf{L}_1 - \mathbf{D}\nabla_s^2\right)\mathbf{u}_1 + 2\mathbf{M}_0\mathbf{u}_1\mathbf{u}_2 + \mathbf{N}_0\mathbf{u}_1\mathbf{u}_1\mathbf{u}_1 \quad (A.12)$$

etc. Using the solvability condition (see ref. [42]) in the form

$$\mathbf{U}^*\mathbf{B}_v^{(1)}(\tau, s) = 0 \quad (A.13)$$

one can recursively obtain solutions of $\mathbf{u}_n$ as a function of $\mathbf{u}_{n-1}, ...\mathbf{u}_1$ starting at $n = 1$. The neutral solution for $\mathbf{u}_1$ is

$$\mathbf{u}_1(t, \tau, s) = A(\tau, s)\mathbf{U}e^{i\omega_0 t} + c.c. \quad (A.14)$$

where *c.c* stands for the complex conjugated. For $v = 3$ one obtains the *Ginzburg-Landau equation*

$$\frac{\partial A}{\partial \tau} = \chi\lambda_1 A + d\nabla_s^2 A - g \mid A \mid^2 A \quad (A.15)$$

where

$$d = d^{'} + id^{''} = \mathbf{U}^*\mathbf{D}\mathbf{U} \quad (A.16)$$
$$\lambda_1 = \mathbf{U}^*\mathbf{L}_0\mathbf{U} = \sigma_1 + i\omega_1 \quad (A.17)$$
$$g = g^{'} + ig^{''} = -2\mathbf{U}^*\mathbf{M}_0\mathbf{U}\mathbf{V}_0 - 2\mathbf{u}^*\mathbf{M}_0\bar{\mathbf{U}}\mathbf{V}_+ - 3\mathbf{U}^*\mathbf{N}_0\mathbf{U}\mathbf{U}\bar{\mathbf{U}} \quad (A.18)$$

Let us turn to an explicit example. The scaled Selkov model consists of the two coupled differential equations

$$\frac{dx}{dt} = 1 - xy^\gamma$$
$$\frac{dy}{dt} = \alpha(xy^\gamma - y) \quad (A.19)$$

The steady state is $x = 1, y = 1$ and thus the Jacobian of the reference state is

$$\mathbf{J}_s = \begin{pmatrix} -1 & -\gamma \\ \alpha & \alpha(\gamma - 1) \end{pmatrix} \tag{A.20}$$

We want to expand around the vicinity of the Hopf-bifurcation point, and the appropriate parameter is chosen to be

$$\alpha_c = \frac{1}{\gamma - 1} \tag{A.21}$$

which is evaluated for $Tr = 0$. Inserting this in A.20 results in the matrix

$$\mathbf{L}_0 = \begin{pmatrix} -1 & -\gamma \\ \frac{1}{\gamma-1} & 1 \end{pmatrix} \tag{A.22}$$

If we call our expansion parameter μ and expand our bifurcation parameter α at criticality as $\alpha = \alpha_c + \mu\alpha_c$ and also the matrix $\mathbf{L}$ as $\mathbf{L} = \mathbf{L}_0 + \mu\mathbf{L}_1$ we obtain after differentiation with μ

$$\mathbf{L}_1 = \begin{pmatrix} 0 & 0 \\ \frac{1}{\gamma-1} & 1 \end{pmatrix} \tag{A.23}$$

The right ($\mathbf{U}$) and left ($\mathbf{U}^*$) eigenvectors of $\mathbf{L}_0$ are given as

$$\mathbf{U} = \begin{pmatrix} -\gamma + 1 + i\sqrt{\gamma - 1} \\ 1 \end{pmatrix} \tag{A.24}$$

$$\mathbf{U}^* = \begin{pmatrix} -\frac{i}{2\sqrt{\gamma - 1}} & \frac{1}{2} - \frac{i}{\sqrt{\gamma - 1}} \end{pmatrix} \tag{A.25}$$

These are normalized as $\mathbf{U}^*\mathbf{U} = \bar{\mathbf{U}}^*\bar{\mathbf{U}} = 1$,where $\bar{\mathbf{U}}$ is the complex conjugated of $\mathbf{U}$. The eigenvalues λ are also expanded as a power series

$$\lambda = \lambda_0 + \mu\lambda_1 + \mu^2\lambda_2 + .. \tag{A.26}$$

and the first two are then expressed as

$$\lambda_0 = \mathbf{U}^*\mathbf{L}_0\mathbf{U} = i\omega_0 = i\frac{1}{\sqrt{\gamma - 1}} \tag{A.27}$$

$$\lambda_1 = \mathbf{U}^*\mathbf{L}_1\mathbf{U} = \sigma_1 + i\omega_1 = \frac{1}{2}\left(1 + i\sqrt{\gamma - 1}\right) \tag{A.28}$$

Other important quantities for the calculation of d and g are

$$\begin{aligned}
\mathbf{D} &= \begin{bmatrix} D_x & 0 \\ 0 & D_y \end{bmatrix} \\
\mathbf{V}_+ &= \frac{1}{\gamma-5}\begin{bmatrix} 2\sqrt{\gamma-1}\gamma(\gamma-1)+\frac{\gamma-1}{2}-i(\sqrt{\gamma-1}\gamma(\gamma-1)-\gamma+1) \\ -2\gamma\sqrt{\gamma-1}-i(\gamma^2-\gamma) \end{bmatrix} \\
\mathbf{V}_0 &= \begin{bmatrix} \gamma(\gamma-1) \\ 0 \end{bmatrix}
\end{aligned} \tag{A.29}$$

Thus, d and g are given as

$$d = \frac{1}{2}\left[(D_x+D_y)+i(D_x-D_y)\sqrt{\gamma-1}\right] \tag{A.30}$$

$$Re(g) = \frac{-\gamma}{4(\gamma-5)}\left[-2\gamma^3+19\gamma^2-46\gamma+2\gamma\sqrt{\gamma-1}+25\right] \tag{A.31}$$

$$Im(g) = \frac{-i\gamma}{4(\gamma-5)}\left[\sqrt{\gamma-1}(\gamma^3-10\gamma^2+30\gamma-35)+2\gamma^2+2\gamma\right] \tag{A.32}$$

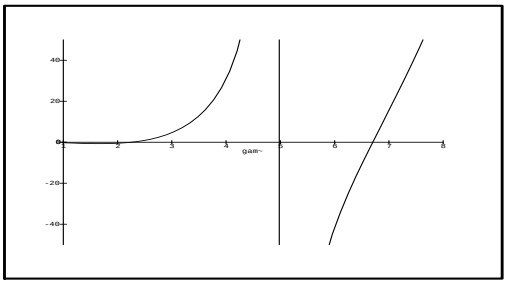

Figure A.1: $Re(g)$ as a function of γ. g changes sign at $\gamma \simeq 2.255$ $\gamma = 5$ and $\gamma \simeq 6.7$. In these points the parameters of the Ginzburg-Landau equation are not valid.

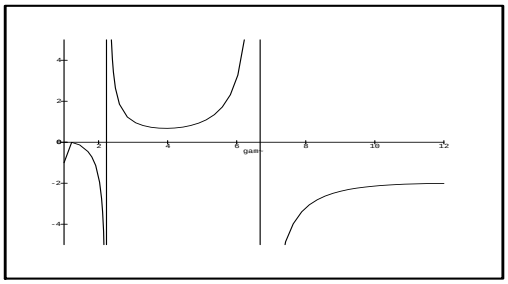

Figure A.2: $c2 = Im(g)/Reg$ as a function of γ. At the vertical lines the parameter $c2$ diverges and one needs higher order terms for a valid the description of the amplitude.

From figure A.1 we see that the system has a subcritical Hopf-bifurcation for $\gamma < 2.255\ldots$ which is given by the condition $g < 0$. A supercritical Hopf-bifurcation exists for $2.255\ldots < \gamma < 5$, and at $\gamma = 5$ g diverges. At $\gamma = 6.7\ldots$ there is again a transition from sub- to supercriticality. At the transition point between a sub- and supercritical bifurcation, the saturated amplitude diverges and therefore has no physical meaning. This can be explained by the fact that in this case one needs to include dominant higher order terms in the Ginzburg-Landau equation. The parameters in the Ginzburg-Landau equation are also only valid for cases of small amplitude oscillations, and hence in supercritical regions.

Appendix B

B.1 Scaling of the Reduced EOE-Model

In most textbooks the scaling of a reaction diffusion model is already performed, whereas the verification of the resultant equations is leaved to the student by reinserting the parameters in the scaled equations. This is of course not the correct procedure and we therefore here sortly want to derive the scaled equations for the reduced nonoscillatory EOE-model from section (8.3). By doing so one sees that there are many different equally good scaling choices for the parameters in the model. Our starting point is equation (8.8)

$$\begin{aligned} \frac{dX}{dt} &= -k_3XY^2 + k_2AY - (k_{-2} + k_4)X + D_x\nabla_\chi^2 X \\ \frac{dY}{dt} &= k_3XY^2 - (k_5 + k_2A)Y + k_{-2}X + k_1 + D_y\nabla_\chi^2 Y \end{aligned} \tag{B.1}$$

In order to make the reaction-diffusion system consisting of two variables dimensionless, we use four variable shifts: two for the two variables, one for time and one for the one-dimensional Laplacian $\nabla_\chi^2 = \frac{\partial^2}{\partial\chi^2}$

$$u = \frac{x}{x_0}, \qquad v = \frac{y}{y_0}, \qquad \tau = \frac{t}{t_0}, \qquad , s = \frac{\chi}{\chi_0} \tag{B.2}$$

and via the chain rule we get

$$\frac{du}{d\tau} = \frac{\partial u}{\partial x}\frac{\partial x}{\partial t}\frac{\partial t}{\partial \tau} = \frac{t_0}{x_0}\frac{dx}{dt} \tag{B.3}$$

$$\tag{B.4}$$

$$\frac{dv}{d\tau} = \frac{\partial v}{\partial y}\frac{\partial y}{\partial t}\frac{\partial t}{\partial \tau} = \frac{t_0}{y_0}\frac{dy}{dt} \tag{B.5}$$

$$\tag{B.6}$$

$$\nabla_s^2 u = \frac{\partial^2 u}{\partial s^2} = \frac{\partial}{\partial s}\left(\frac{\partial u}{\partial x}\frac{\partial x}{\partial \chi}\frac{\partial \chi}{\partial s}\right) = \frac{\partial}{\partial s}\left(\frac{\chi_0}{x_0}\frac{dx}{d\chi}\right) \tag{B.7}$$

$$= \frac{\chi_0}{x_0}\frac{\partial}{\partial\chi}\left(\frac{\partial x}{\partial s}\right) = \frac{\chi^2}{x_0}\nabla^2_\chi x \tag{B.8}$$

$$\tag{B.9}$$

$$\nabla^2_s v = \frac{\chi^2}{y_0}\nabla^2_\chi y \tag{B.10}$$

Now we can try to start inserting for the y-component

$$\frac{dv}{d\tau} = \frac{t_0}{y_0}\left(k_3 x_0 y_0^2 uv^2 - k_5 y_0 v - k_2 A y_0 v + k_{-2} x_0 u + k_1\right) + \frac{t_0 y_0 D_y}{\chi_0^2 y_0}\nabla^2_s v \tag{B.11}$$

As a start we can set $t_0 = \frac{\chi_0^2}{D_y}$ and remove all the constants in front of the cubic term

$$\frac{dv}{d\tau} = \frac{\chi_0^2 k_3 x_0 y_0}{D_y}\left(uv^2 - \frac{k_5}{k_3 x_0 y_0}v - \frac{k_2 A}{k_3 x_0 y_0}v + \frac{k_{-2}}{k_3 y_0^2}u + \frac{k_1}{k_3 x_0 y_0^2}\right) + \nabla^2_s v \tag{B.12}$$

and setting $y_0^2 = \frac{k_{-2}}{k_3}$ one obtains

$$\frac{dv}{d\tau} = \frac{\chi_0^2 k_3 x_0\sqrt{\frac{k_{-2}}{k_3}}}{D_y}\left(uv^2 + u - \frac{k_5}{k_3 x_0\sqrt{\frac{k_{-2}}{k_3}}}v - \frac{k_2 A}{k_3 x_0\sqrt{\frac{k_{-2}}{k_3}}}v + \frac{k_1}{x_0 k_{-2}}\right) + \nabla^2_s v \tag{B.13}$$

setting

$$x_0 = \frac{k_5}{k_3\sqrt{\frac{k_{-2}}{k_3}}} \tag{B.14}$$

the equation becomes

$$\frac{dv}{d\tau} = \frac{\chi_0^2 k_5}{D_y}\left(uv^2 + u - v - \frac{k_2 A}{k_5}v + \frac{k_1 k_3\sqrt{\frac{k_{-2}}{k_3}}}{k_{-2}k_5}\right) + \nabla^2_s v \tag{B.15}$$

where the last constants can be set to

$$\frac{k_2 A}{k_5} = a, \qquad \frac{k_1 k_3\sqrt{\frac{k_{-2}}{k_3}}}{k_{-2}k_5} = F \tag{B.16}$$

leading to

$$\frac{dv}{d\tau} = \frac{\chi_0^2 k_5}{D_y}\left(uv^2 + u - (1+a)v + F\right) + \nabla^2_s v \tag{B.17}$$

Before we determine χ_0^2 we turn to the x-component. Here the equation reads

$$\frac{du}{d\tau} = \frac{t_0}{x_0}\left(-k_3 x_0 y_0^2 u v^2 + k_2 A y_0 v - k_{-2} x_0 u - k_4 x_0 u\right) + \frac{t_0 D_x}{\chi_0^2}\nabla_s^2 u \tag{B.18}$$

We set $\frac{D_x}{D_y} = D$ and insert the already chosen constants

$$\frac{dv}{d\tau} = \frac{\chi_0^2 k_3\sqrt{\frac{k_{-2}}{k_3}}}{D_y k_5}\left(-\frac{k_5 k_{-2}}{k_3\sqrt{\frac{k_{-2}}{k_3}}}uv^2 + k_2 A\sqrt{\frac{k_{-2}}{k_3}}v - \frac{(k_{-2}+k_4)k_5}{k_3\sqrt{\frac{k_{-2}}{k_3}}}u\right) + D\nabla_s^2 u \tag{B.19}$$

which lead to

$$\frac{dv}{d\tau} = \frac{\chi_0^2 k_{-2}}{D_y}\left(-uv^2 + av - u - \frac{k_4}{k_{-2}}u\right) + D\nabla_s^2 u \tag{B.20}$$

Thus, setting $\frac{k_4}{k_{-2}} = b$ and chosing

$$\chi_0^2 = \frac{D_y}{\sqrt{k_5 k_{-2}}} \tag{B.21}$$

we finally obtain the scaled equations

$$\begin{aligned}
\frac{du}{d\tau} &= c\left[-uv^2 + av - (1+b)u\right] + D\nabla_s^2 u \\
\frac{dv}{d\tau} &= c^{-1}\left[uv^2 - (1+a)v + u + F\right] + \nabla_s^2 v
\end{aligned} \tag{B.22}$$

where

$$\left(\frac{\chi_0^2 k_{-2}}{D_y}\right)\left(\frac{\chi_0^2 k_5}{D_y}\right) = 1 = cc^{-1} \tag{B.23}$$

B.2 The Routh-Hurwitz Condition

When we perform linear stability analysis of ODE's emerging from reaction kinetics, we usually need to determine the roots of a polynomial. If the system is of n'th order, the characteristic polynomial associated to the eigenvalues λ has the general form

$$P(\lambda) = \lambda^n + a_1\lambda^{n-1} + ... + a_n = 0 \tag{B.24}$$

where the coefficients $a_i, i = 1, 2, ..., n$ are real. We also assume that $a_n \neq 0$, since otherwise $\lambda = 0$ would be a solution and the order of the polynomial would then decrease by one. Now we want to require the conditions on the a_i such that the roots of $P(\lambda)$ have $Re\lambda < 0$. The necessary and sufficient conditions for this to hold are the *Routh-Hurwitz conditions*. They read:

$$
\begin{aligned}
\triangle_1 &= a_1 > 0 \\
\triangle_2 &= \begin{vmatrix} a_1 & a_3 \\ 1 & a_2 \end{vmatrix} > 0 \\
\triangle_3 &= \begin{vmatrix} a_1 & a_3 & a_5 \\ 1 & a_2 & a_4 \\ 0 & a_1 & a_3 \end{vmatrix} > 0 \\
&\vdots \\
&\vdots \\
\triangle_k &= \begin{vmatrix} a_1 & a_3 & . & . & . & . \\ 1 & a_2 & a_4 & . & . & . \\ 0 & a_1 & a_3 & . & . & . \\ 0 & 1 & a_2 & . & . & . \\ . & . & . & . & . & . \\ 0 & 0 & . & . & . & a_k \end{vmatrix} > 0, \qquad k = 1, 2, ..., n
\end{aligned}
\tag{B.25}
$$

If we for instance have a cubic polynomial

$$\lambda^3 + a_1\lambda^2 + a_2\lambda + a_3 = 0 \tag{B.26}$$

the conditions for $Re(\lambda) < 0$ are

$$a_1 > 0, \qquad a_3 > 0, \qquad a_1 a_2 - a_3 > 0 \tag{B.27}$$

B.3 Descartes' Rule of Signs

Consider the polynomial (B.24) and take $a_n > 0$. If N is the number of sign changes in the sequence of coefficients $a_n, a_{n-1}, ..., 0$ Descartes' rule of signs says that there are at most N roots which are real and positive, and further, that there are either N or $N-2$ or $N-4$ or... real positive roots. That means, if there for instance are two sign changes in the sequence of coefficients in a polynomial, then there are either 2 or 0 real positive roots.

Appendix C

Publications

Early Biological Morphogenesis and Nonlinear Dynamics
Hunding, A., Engelhardt, R.
Submitted for publication.

A New Pattern Forming Mechanism in Bistable Chemical Systems
Engelhardt, R., Dewel, G., Métens, S., Borckmans, P.
Paper is still in editorial process.

Pattern Formation in Bistable Chemical Systems
Dewel, G., Engelhardt, R., Métens, S., Borckmans, P.
To appear in the proceedings of the IMACS third International Conference Copenhagen. August (1994), Copenhagen.

Bibliography

[1] Turing, A.M.
On the Chemical Basis of Morphogenesis,
Phil.Trans.Roy.Soc. London, Ser.B. **237**, 37-72 (1952)

[2] *Morphogenesis, Collected works of A.M. Turing*
Ed. P.T. Saunders, North-Holland (1992)

[3] Hunding, A
Reaction-Diffusion Prepatterns (Turing Structures): Supercomputer simulation of cytokinesis, mitosis and early drosophila morphogenesis, in: Complexity, Chaos and Biological Evolution, ed. by E. and L.Mosekilde, Plenum Press, New York (1991)

[4] Murray, J.D.
Mathematical Biology
Springer Verlag, 2.ed (1993)

[5] Harrison, L.G.
What is the Status of Reaction-Diffusion Theory Thirty-four Years After Turing?
J.theor.Biol., **125**, 369-384 (1987)

[6] Murray, J.D.
Turings Theory of Morphogenesis - its Influence on Modelling Biological Pattern and Form
Bull.Math.Biol., **52**,119-152 (1990)

[7] Goodwin, B.C., Kauffman, S., Murray, J.D.
Is Morphogenesis an Intrinsically Robust Process?
J.theor.Biol., **163**, 135-144 (1993)

[8] Lacalli, T.C.
In *Experimemtal and Theoretical Advances in Biological Pattern Formation*
Ed. H.G. Othmer et.al., Plenum Press, NY (1993)

[9] Wolpert, L.
Positional information and prepattern in the development of pattern
In *Cell to Cell signalling: From experiments to Theoretical Models*
Ed. Goldbeter, A., 133-145, Academic Press, London.

[10] Murray, J.D., Maini, P.K.
Pattern formation mechanisms - a comparison of reaction diffusion and mechanical models. In *Cell to Cell signalling: From experiments to Theoretical Models*
Ed. Goldbeter, A., 159-170, Academic Press, London.

[11] Kauffman, S.A.
em The Origins of Order
Oxford University Press (1993)

[12] Mosekilde, E.
Private communication.

[13] Gray, P., Scott, S.K.
A new model for oscillatory behaviour in closed systems: the autocatalotor.,
Ber. Bunsenges. Phys. Chem. **90**, 985-996 (1986).

[14] Hunding, A., Engelhardt, R.
Early Biological Morphogenesis and nonlinear Dynamics,
Submitted for publication.

[15] Guckenheimer, J., Holmes, P.
Nonlinear Oscillations, Dynamical Systems, and Bifurcations of Vector Fields,
Springer-Verlag, (1983)

[16] Hirsch, M.W., Smale, S.
Differential Equations, Dynamical Systems and Linear Algebra,
Academic Press, New York (1974)

[17] Nicolis, G., Prigogine, I.
Self-Organization in Nonequilibrium Systems,
Wiley and Sons, New York (1977)

[18] Nicolis, G.
Dissipative Structures with Applications to Chemical Reactions,
in *Cooperative Effects*, Progress in Synergetics,
ed. Haken, H., North-Holland (1974)

[19] Nicolis, G and Prigogine, I.
Exploring Complexity,
Piper,Munich, 1989.

[20] Lee, K.J., McCormick, W.D., Ouyang, Q., Swinney, H.L.
Pattern Formation by Interacting Chemical Fronts,
Science, **261**, 192 (1993)

[21] Lee, K.J., McCormick, W.D., Pearson, J.E., Swinney, H.L.
Experimental Observation of Self-replicating Spots in a reaction-Diffusion System,
Nature, **369**, 215-218 (1994)

[22] Hunding, A. and Sørensen, P.G.
Size adaptation of Turing prepatterns,
J.Math.Biol.(1988)**26**, 27-39.

[23] Lengyel, I. and Epstein, I.R.
Modeling of Turing Structures in the CIMA-Starch Reaction System,
Science (1991) **251**, 650-652.

[24] Landolt, H.
Ber. Dtsch. Chem. Ges., **19**, 1317 (1886)

[25] Castets, V., Dulos, E., Biossonade, J., De Kepper, P.
Phys. Rev. Lett., **64**, 2953 (1990)

[26] Meinhardt, H.
Bildung geordneter Strukturen bei der Entwicklung höherer Organismen,
Ordnung aus dem Chaos, ed.Bernd-Olaf Küppers, Piper, München,1987.

[27] Murray, J.D.
How the Leopard Gets Its Spots,
Sci.Amer. **258**(3), 80-87 (1988)

[28] Murray, J.D.
Parameter Space for Turing Instability in Reaction Diffusion Mechanisms: A Comparison of Models,
J. theor. Biol. (1982), **98**, 143-163.

[29] Pearson, J.E.,
Science, **261**, 189 (1993)

[30] Engelhardt, R., Dewel, G., Métens, S., Borchmans, P.
A New Pattern Forming Mechanism in Bistable Chemical Systems,
Paper in editorial process.

[31] Misbah, C., Valance, A.
Secondary instabilities in the stabilized Kuramoto-Sivashinksy equation
Phys. Rev. E, **49**, 166-83, (jan. 1994)

[32] Gaspar, V., Showalter, K.,
J. Phys. Chem. **94**, 4973 (1990)

[33] Hagberg, A., Meron, E.
From Labyrinthine Patterns to Spiral Turbulence,
Forthcoming Paper.

[34] Ganapathisubramanian, N., Showalter, K.
Critical Slowing Down in the Bistable Iodate-Arsenic(III) Reaction,
J. Phys. Chem. 1983, **87**, p.1098-1099

[35] Edblom, E.C., Orban, M., Epstein, I.R.,
J. Am. Chem. Soc., **108**, 2826 (1986)

[36] Gáspár, V., Showalter, K.,
J. Am. Chem. Soc., **109**, 4869 (1987)

[37] Gáspár, V., Showalter, K.,
J. Phys. Chem. **94**, 4973 (1990)

[38] Peng, B., Gáspár, V., Showalter, K.
False bifurcations in chemical systems: canards,
Phil. Trans. R. Soc. Lond. A (1991), **337**, 275-289

[39] Jensen, O., Pannbacker, V.O.
Pattern formation in reaction-diffusion systems
Master Thesis, The System Dynamics Group, Pysics Dept., Technical University of Denmark (1993)

[40] Showalter, K.
Private communication.

[41] Mikhailov, A.S., Davydov, V.A., Zykov, V.S.
Complex dynamics of spiral waves and motion of curves
Physica D, **70**, 1-39 (1994)

[42] Kuramoto, Y.,
Chemical Oscillations, Waves and Turbulence,
Springer-Verlag, Berlin, (1984)